INFORMATION TO USERS

This manuscript has been reproduced from the microfilm master. UMI films the text directly from the original or copy submitted. Thus, some thesis and dissertation copies are in typewriter face, while others may be from any type of computer printer.

The quality of this reproduction is dependent upon the quality of the copy submitted. Broken or indistinct print, colored or poor quality illustrations and photographs, print bleedthrough, substandard margins, and improper alignment can adversely affect reproduction.

In the unlikely event that the author did not send UMI a complete manuscript and there are missing pages, these will be noted. Also, if unauthorized copyright material had to be removed, a note will indicate the deletion.

Oversize materials (e.g., maps, drawings, charts) are reproduced by sectioning the original, beginning at the upper left-hand corner and continuing from left to right in equal sections with small overlaps. Each original is also photographed in one exposure and is included in reduced form at the back of the book.

Photographs included in the original manuscript have been reproduced xerographically in this copy. Higher quality 6" x 9" black and white photographic prints are available for any photographs or illustrations appearing in this copy for an additional charge. Contact UMI directly to order.

UMI

A Bell & Howell Information Company
300 North Zeeb Road, Ann Arbor MI 48106-1346 USA
313/761-4700 800/521-0600

The Climatic Effects and Requirements of Arctic Clouds

by

John A. Beesley

A dissertation submitted in partial fulfillment
of the requirements for the degree of

Doctor of Philosophy

University of Washington

1997

Approved by _____
(Chairperson of Supervisory Committee)

Program Authorized
to Offer Degree Department of Atmospheric Sciences

Date 18 Dec. 1997

In presenting this dissertation in partial fulfillment of the requirements for a Doctoral degree at the University of Washington, I agree that the Library shall make its copies freely available for inspection. I further agree that extensive copying of this dissertation is allowable only for scholarly purposes, consistent with "fair use" as prescribed in the U.S. Copyright Law. Requests for copying or reproduction of this dissertation may be referred to University Microfilms, 1490 Eisenhower Place, P.O. Box 975, Ann Arbor, MI 48106, to whom the author has granted "the right to reproduce and sell (a) copies of the transcript in microform and/or (b) printed copies of the manuscript made from microform."

Signature J. Anthony Beasley

Date 14 Dec. 1997

University of Washington

Abstract

The Climatic Effects and Requirements of Arctic Clouds

by John A. Beesley

Chairperson of the Supervisory Committee
Associate Professor David S. Battisti
Department of Atmospheric Sciences

The climatic effect and requirements of clouds over the Arctic Ocean are examined using a pair of one-dimensional models. A coupled ice-atmosphere column model with prescribed cloud properties is used to examine the effect of clouds on the central arctic climate. When forced with boundary conditions representative of the Central Arctic, the model produces a realistic simulation of the seasonal cycle of arctic air temperature, ice thickness, and radiative fluxes. Unlike previous studies, the results suggest that the annual net effect of clouds is to increase ice thickness slightly. This can be attributed to the fact that previous studies have not accounted for the effect of clouds on the atmospheric temperature profile, which is an internally-computed model variable in the present study. The results indicate that the response of sea ice thickness to a perturbation in clouds can be predicted by estimating how the cloud perturbation affects the radiative budget at the top of the atmosphere.

The annual cycle of low-cloud amount over the Arctic Ocean is examined using climatological data and a time-dependent atmospheric column model. Three hypotheses for the annual cycle are formulated, compared with climatological data for consistency, and then tested using a numerical model. The model, which includes a turbulence-closure cloud scheme and ice-phase microphysical processes, simulates the summer and winter cloud regimes when forced with the boundary conditions corresponding to those seasons. Results from the model experiments suggest that the main factor in determining the annual cycle of low cloud amount is the effectiveness of ice processes in eliminating liquid water clouds and preventing the water vapor mixing ratio in clear air from reaching saturation with respect to liquid. It is shown that, among general circulation models participating in the Atmospheric Model Intercomparison Project, those including ice microphysics produce qualitatively more realistic simulations of the mean annual cycle of cloud amount over the Arctic Ocean than models without atmospheric ice processes. The results suggest that the duration of the summertime cloudy season should be longer when the Arctic Ocean climate is warmer, and shorter when it is cooler.

TABLE OF CONTENTS

LIST OF FIGURES

LIST OF TABLES

ACKNOWLEDGMENTS

I would like to thank my advisors, R. Moritz and D. Battisti, for their valuable guidance during the course of my graduate studies. C. Bretherton's advice on cloud modelling was essential for the research described in Chapter 3, and his comments on the rest of the manuscript are also appreciated. Discussions with and comments from G. Maykut and S.Warren were also of great value.

This work was supported by the Arctic System Science Program, under grants DPP9113851 and OPP 9505093 from the National Science Foundation.

The completion of this work would not have been possible without the encouragement and companionship of my wife Sabina.

Chapter 1:

Introduction

A leading problem in atmospheric science is to predict how the global climate will respond to changes in climatic parameters such as increasing concentrations of carbon dioxide associated with combustion of fossil fuels. The general circulation model (GCM) has emerged as a promising tool for addressing this problem. GCM simulations of climate with enhanced carbon dioxide concentration suggest that climatic change in the Arctic may be greater than the global average (Houghton et al. 1990). However, simulations of fundamental climatic variables in the Arctic such as surface temperature and ice thickness vary widely among GCM's, suggesting that the factors controlling arctic climate are not well known. Clouds affect the arctic climate by absorbing and emitting in longwave (terrestrial) radiation and by absorbing and reflecting shortwave (solar) radiation. The mean thickness of arctic sea ice simulated by thermodynamic sea ice models is very sensitive to downward irradiance at the surface (e.g. Maykut and Untersteiner 1971; Ebert and Curry 1993), which suggests that clouds may be an important factor in shaping the arctic climate. Understanding the factors that control cloudiness is a prerequisite to predicting the sensitivity of the Arctic system to perturbations in external climatic parameters, since small changes in cloud amount can produce substantially larger radiative effects than the perturbations typically considered. The problem of understanding the role of clouds in the arctic climate sensitivity can be bro-

ken down into two parts: (1) understanding the dependence of arctic climate on the properties of clouds, and (2) understanding the factors that control the cloud properties.

The estimation of the climatic effect of arctic clouds is addressed in Chapter 2. The effect of clouds on arctic climate has been studied using surface observations and numerical models. The relationship between cloudiness and surface meteorological data in Arctic regions has been examined by Ambach (1974) and Herman (1980). Both studies found that increased cloudiness is associated with larger downward radiative fluxes at the surface. Modeling studies of the effect of arctic clouds on the surface energy budget have been performed by Shine and Crane (1984), Curry and Ebert (1992), Curry et al. (1993), and Zhang et al. (1996). These studies all concluded that clouds warm the surface of the Arctic by increasing downward radiative fluxes. The effect of clouds on atmospheric temperature was not incorporated in the preceding observational and modeling studies. The instantaneous effect of clouds on the vertical radiative fluxes at the top of the atmosphere and the surface was estimated using a radiative model by Curry and Ebert (1992). They found that, on average, clouds cool the atmosphere by increasing the upward radiative flux at the top of the atmosphere and increasing the downward radiative flux at the surface. Clouds must assert an indirect effect the surface energy budget through their influence on the atmosphere, since turbulent and radiative fluxes at the surface depend strongly on the vertical profile of atmospheric temperature. To understand how clouds effect arctic climate, it is necessary to evaluate both the direct and indirect effects of clouds on the surface energy budget. The present study of the climatic effect of clouds employs a one-dimensional, coupled ice-atmosphere model that computes atmospheric temperature prognostically on the basis of energy conservation, which fulfills the above requirement. The results are related to a simulated diagnostic variable that quantifies the effect of cloud on the radiative budgets at the surface and the top of the atmosphere -- cloud radiative forcing. In

addition. an attempt is made to use estimates of cloud radiative forcing in the present arctic climate to predict how changes in clouds affect climate.

A sensible way to improve the prediction of changes in cloud properties, such as average cloud amount*, condensate path, and condensate phase, is to explain variations of cloud properties observed in present climate. A well-observed and climatically important property is the mean annual cycle in cloud amount, which has a minimum of about 50% in the winter and a maximum of about 85% in the summer (e.g. Warren et al. 1988). Modeling studies of summertime stratus have been performed by Herman and Goody (1976), McInnes and Curry (1995), and Smith and Kao (1996). However, none of these explanations of the annual cycle of cloudiness has been examined quantitatively using observations or models.The cause of the annual cycle is examined in Chapter 3. Two different controlling factors have been suggested previously in the literature: (1) atmospheric moisture advection into the Arctic from lower latitudes, and (2) the evaporative flux at the arctic surface. Bjerknes (1925) and Petterssen (1956) describe cloud formation as an adjustment of warm, relatively humid air as it passes over the melting sea ice. According to this explanation, the onset of the summertime cloudy season occurs when the surface temperature of the land surrounding the Arctic exceeds freezing. Herman and Goody (1976) suggest that cloudiness is limited during the winter by an insufficient moisture flux from the surface, since the surface specific humidity in winter is strongly limited by temperature. In addition to these explanations, I examine whether ice microphysical processes could produce the annual cycle in cloud amount by limiting the longevity of clouds during the winter. In Chapter 3, these explanations are compared to relevant climatological datasets and tested using a cloud model that is capable of simulating both winter and summer cloud regimes in the Arctic.

---

* Cloud amount is defined as the frequency of observation of cloud (or a specific cloud type) multiplied by the fraction of the sky it covers when present.

In Chapter 4, the conclusions of Chapters 2 and 3 are used to predict how arctic cloudiness might respond a uniform increase in air temperature, and how this response affects the climate. Specific research goals are suggested to improve understanding of the role of clouds in the arctic climate.

Chapter 2:

Estimating the Climatic Effect of Arctic Clouds

2.1 Background

Manabe and Wetherald (1967) examined the effect of clouds on the global climate using a radiative-convective atmospheric column model. Their results suggest that the surface of the earth is warmed by high clouds and cooled by low clouds, and that the net effect of all types of cloud is to make the global climate cooler. These conclusions are supported by analyses of satellite data obtained during the Earth Radiation Budget Experiment (Harrison et al. 1990; Hartmann et al. 1992). In these studies, the warming or cooling effect of clouds was determined from their impact on the net radiative budget as measured by satellite at the top of the atmosphere. Low clouds cool the earth since they reflect incoming shortwave radiation yet emit longwave radiation at about the same temperature as the surface. High clouds tend to be less reflective than low clouds and emit longwave radiation at a substantially lower temperature which reduces radiative loss to space and warms the surface. The radiative budget at the top of the atmosphere is known with the same accuracy over the Arctic as over the rest of the globe, but satellite estimates of the radiative effect of clouds cannot be made with certainty until there is a proven method of identifying clouds unambiguously from ice and snow. However, this may soon become possible with improvements in retrieval algorithms and in the spatial and spectral resolution of satellite instruments.

The first detailed study of the effect of clouds on arctic sea ice was made by Shine and Crane (1984) using a one-dimensional thermodynamic sea ice model forced by prescribed turbulent sur-

face fluxes and downward fluxes of radiation. The contribution of clouds to downward radiative fluxes was computed using a parameterization formulated specifically for arctic conditions which permitted the radiative effect of clouds to be examined. The annual average ice thickness produced by the model decreased when an increase in the annual mean cloudiness was prescribed. A positive perturbation in prescribed monthly average cloud amount during any month except July or August decreased the mean ice thickness. The results of Shine and Crane also illustrated how the surface albedo feedback can enhance the impact of a change in cloudiness. Curry and Ebert (1992) and Curry et al. (1993) examined how radiative fluxes at the surface and at the top of the atmosphere depend on a number of cloud properties, including height, amount, and condensate particle size. Radiative fluxes were computed using a detailed radiative transfer model for prescribed, seasonally-varying atmospheric conditions, and surface temperature and albedo were computed interactively using the one-dimensional sea ice model of Ebert and Curry (1993). Curry and Ebert (1992) estimated the radiative effect of arctic clouds by integrating the model through an annual cycle with and without clouds. They concluded that, climatologically, clouds warm the surface of the Arctic by increasing net downward radiative fluxes, which is in contrast to the global effect of clouds mentioned above. Curry et al. (1993) integrated the same model for several decades to examine the relationship between equilibrium ice thickness and annual average cloud amount. These results showed a strong increase in ice thickness in response to reductions in annual mean cloud amount (Curry et al. 1993).

The effect of clouds on atmospheric temperature is not incorporated within the modeling frameworks employed in the preceding studies. However, Cess and Potter (1987) have shown that the effect of clouds on the surface energy budget changes as the surface and atmosphere adjust in response to the radiative effect of clouds. Cess and Potter noted that the impact of clouds on the surface energy budget after the adjustment of the surface and atmosphere is complete (the equilib-

rium effect) can be quite different from the instantaneous radiative effect of clouds (the direct effect). This was demonstrated by simulating the evolution of a column of atmosphere, initially in cloud-free equilibrium, after introducing an upper-level cloud. The direct effect of the cloud on the surface energy budget was to reduce the downward shortwave radiation by a larger amount than the increase in downward longwave radiation. As the atmosphere in Cess and Potter's model warmed in response to the radiative effect of the cloud layer, downward fluxes of longwave radiation and turbulent energy at the surface increased significantly, reaching an equilibrium surface energy budget quite different that immediately after the cloud was introduced. A relevant question is, how important is the atmospheric adjustment for the turbulent and radiative fluxes at the arctic surface, and does the adjustment, which is neglected in the previous studies, qualitatively affect the response of sea ice to changes in cloud amount?

First, we consider how atmospheric adjustment affects surface radiative fluxes in the Arctic. The results of Curry and Ebert (1992) indicate that arctic clouds increase outgoing irradiance at the top of the atmosphere and increase downward irradiance at the surface, which implies that clouds produce a net radiative divergence from the atmosphere which must cool the atmosphere. In Cess and Potter's experiment the cloud had a warming effect on the atmosphere which produced an increase in downward longwave radiation as the atmosphere reached equilibrium. If clouds tend to cool the arctic atmosphere, then downward longwave radiation at the surface should decrease as the atmosphere adjusts to the radiative effects of clouds, all other factors being equal.

The results of Curry and Ebert (1992) also indicate that the direct effect of arctic clouds is to warm the surface. If net effect of clouds is to decrease atmospheric temperature and to increase surface temperature, then they must increase the net upward turbulent flux at the surface. Among cloud types, this is especially true of low clouds since the direct warming of the surface is greatest (Curry et al. 1993) and the destabilizing effect of cloud top cooling can rapidly reach the surface.

The sea ice model of Ebert and Curry (1993) exhibited a strong sensitivity to perturbations in the prescribed air temperature above the ice, such that a 1 C decrease in surface air temperature increased equilibrium ice thickness from about 3 to 6 m. This suggests that there may be a systematic relationship between cloudiness and upward turbulent fluxes at the surface that acts to offset the direct effect of clouds on the surface.

The goal of the research described in this chapter is to understand how changes in cloudiness affect the arctic climate and to relate this effect to a diagnostic quantity describing the direct effect of clouds in the present climate, namely cloud radiative forcing. When addressing this problem, it is necessary to consider how the surface and atmosphere adjust as a coupled system, since the this adjustment occurs on a much shorter timescale than that characterizing arctic climate. Previous studies suggest a perturbation in clouds has an indirect effect on the surface energy budget through its effect on the atmosphere, and that this indirect effect has the opposite sign from the initial (direct) radiative effect produced by that perturbation. This study employs a one-dimensional, coupled ice-atmosphere model that is designed to allow the climate system to respond in a natural way to changes in cloud. The present arctic climate is simulated using the model, and experiments are conducted to examine the dependence of ice thickness on clouds. The model is an idealized representation of the actual three-dimensional arctic climate system and can simulate only a limited number of feedback processes. However, this approach is promising for two reasons. The first is that, qualitatively, almost all of the conclusions reached by Manabe and Wetherald (1967), based on an idealized one-dimensional model of the global climate system, still stand after subsequent research into the details that were omitted from their model. The second is that, in contrast to the lower latitudes, the atmospheric circulation in the arctic is relatively weak and does not exhibit strong vertical circulation structures on subregional scales that significantly weaken the assumption of one-dimensionality (Vowinckel and Orvig 1970).

2.2 Model

The model domain extends from the top of the atmosphere to the lower surface of the oceanic mixed layer in the perennially ice-covered portion of the Arctic Ocean (Figure 2.2). The atmospheric component of the model includes turbulent and radiative energy transfer processes, and a detailed representation of the radiative properties of liquid and ice clouds. The vertical distribution and bulk properties of clouds are prescribed from observational data. Incoming solar radiation and poleward energy flux convergence are prescribed boundary conditions which are described in the Section 2.3. Pack ice is represented by a simple one-dimensional, thermodynamic sea ice model with a prescribed amount of open water. The accumulation rate of snow, the heat flux from the deep ocean into the mixed layer, and the divergence of sea ice velocity are also prescribed. The atmospheric component of the model has 15 levels, with a grid spacing of 60 mb through most of the lower troposphere and narrower layers near the surface. The sea ice model has four layers plus a layer of snow.

2.2.1 Atmosphere

The time dependent evolution of atmospheric temperature (T) is computed prognostically based on the conservation of enthalpy. Specific humidity (q) is computed diagnostically as the product of relative humidity (r) and the local saturation specific humidity (q_{sat}), $q = r\, q_{sat}(T,p)$, where p is atmospheric pressure. Relative humidity is assumed to be proportional to atmospheric pressure following Manabe and Wetherald (1967): $r = r^* p/p_s$, where p_s is surface pressure. The relative humidly near the arctic surface (r^*) is set to 85% based on Peixoto and Oort (1992). The conservation of enthalpy in the atmosphere is given by,

$$\rho C_p \left(\frac{\partial T}{\partial t}\right) = -(1/\rho)\frac{\partial F_{rad}}{\partial z} - (T/\theta)\,(1/\rho)\frac{\partial}{\partial z}(\rho w'\theta') + \dot{T}_{wall} \quad , \qquad (2.1)$$

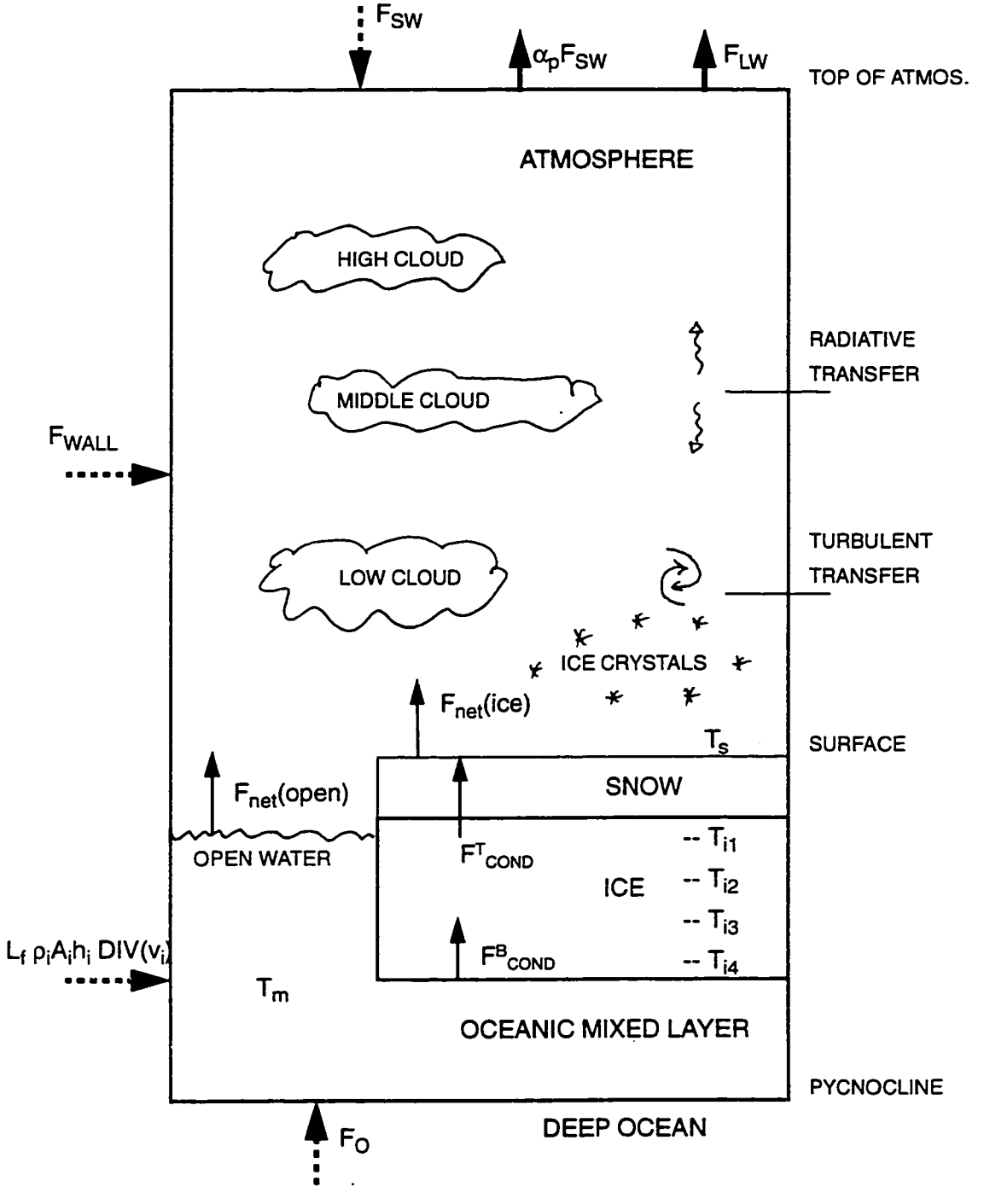

Figure 2.1: Schematic diagram of coupled ice-atmosphere column model.

where ρ, C_p^*, t, z, and θ are air density, effective heat capacity of air, time, geometric height, and potential temperature, respectively. Equation (2.1) states that the rate of change of enthalpy is affected by the convergence of radiative energy flux (F_{rad}), the convergence of turbulent eddy flux ($\rho w'\theta'$), and poleward energy flux convergence ($\dot{T}_{wall}$). The contribution of adiabatic heating produced by large-scale subsidence to the energy budget is included in the term T_{wall}. This ensures that the annual cycle of poleward energy flux convergence in the column can be prescribed exactly, which permits the effects of clouds to be examined more clearly. As an alternative, one could remove the contribution of geopotential flux convergence from $\dot{T}_{wall}$, prescribe large-scale vertical velocity ($\overline{w}$), and add an adiabatic heating term of the form $\left(-\overline{w}\frac{\partial\theta}{\partial z}\right)$ to (2.1). The storage and release of latent heat with changing air temperature -- at fixed relative humidity -- is accounted for using an effective heat capacity, given by $C_p^* = C_p + L\,r\frac{\partial q_{sat}}{\partial T}$, following Manabe and Wetherald (1967).

Radiative transfer is modeled in the same manner as described in Chapter 3, which is based on the radiative scheme from the second version of the NCAR Community Climate Model (CCM2) (Hack et al. 1993). Cloud radiative properties are computed as a function of cloud water path and cloud particle effective radius, using the parameterization of Slingo (1989) for liquid clouds and that of Ebert and Curry (1992) for ice clouds. The effective radius of all ice particles is 25 μm, and liquid droplets have radii of 7 μm. For mixed-phase clouds, the radiative properties of ice and liquid condensate are combined using Eq. (14) of Rockel et al. (1991). The bulk properties of clouds (condensate path, phase, and fraction) are prescribed as described in Section 2.2.4. The radiative interaction of multiple cloud layers is modelled using a random overlap scheme, as described by Hack et al. (1993).

Vertical energy fluxes by turbulent eddies are modeled using the 'local' first-order diffusive scheme described in Section 3(a) of Holtslag and Boville (1993). Vertical energy flux by turbulent eddies is approximated as $w'\theta' = -K\frac{\partial\theta}{\partial z}$, where the eddy diffusivity K is computed as a function of the vertical temperature gradient, wind shear, and a prescribed length scale. A fixed wind shear of 1 m s^{-1} km^{-1} is assumed in the present application. The contribution of poleward energy flux by large scale atmospheric circulation $\dot{T}_{wall}$ is described in Section 2.3.

2.2.2 Surface energy budget

The atmosphere and pack ice are coupled thermodynamically by the surface energy budget, given by

$$F_{net} = F^{\downarrow}_{LW} - F^{\uparrow}_{LW} + (1-\alpha) F^{\downarrow}_{SW} - F^{\uparrow}_{SH} - F^{\uparrow}_{LH} + F^{T}_{COND}, \qquad (2.2)$$

where $F^{\uparrow}$ and $F^{\downarrow}$ denote upward and downward fluxes of longwave (LW) and shortwave (SW) radiation, sensible heat (SH), latent heat (LH), and F^{T}_{COND} is heat conduction towards the surface of the ice or snow. F_{net} is the convergence of energy at the upper surface of ice, snow, or water; it is computed independently over open water and ice-covered areas. The energy budget over open water is computed using a surface temperature of T_m= -1.9 C (freezing temperature of seawater)* and F^{T}_{COND} = 0. The surface temperature of the ice-covered region is computed as the solution to the case where F_{net} =0. If this yields $T_s > 0$ C (melting), then F_{net} is computed with T_s= 0 C and excess energy (F_{net}) is used to melt the surface.

---

* In principle, the oceanic mixed layer temperature can exceed freezing when the sea ice has melted completely, but this case is not addressed in this study.

The upward longwave radiative flux ($F_{LW}^{\uparrow}$) is given by σT_s^4 using the Stefan-Boltzmann Law, and downward radiative fluxes, $F_{SW}^{\downarrow}$ and $F_{LW}^{\downarrow}$, are provided by the atmospheric component of the model. Surface albedo α is determined diagnostically as a function of surface type, snow depth, and temperature. The albedos of non-melting snow, bare sea ice, and open water are 0.80, 0.60, and 0.10, respectively. The prescribed sea ice albedos are within ~3% of satellite-based estimates by Lindsay and Rothrock (1994). The albedo of melting snow is 0.75 when snow depth (h_s) is greater than 10 cm, and it decreases linearly to the bare ice value when $h_s < 10$ cm.

Turbulent surface fluxes of sensible and latent heat, given by $F_{SH}^{\uparrow} = \rho C_p (w'\theta')_0$ and $F_{LH}^{\uparrow} = \rho L_v (w'q')_0$, are modeled following Holtslag and Boville (1993). Surface eddy fluxes of θ and q are parameterized as follows: $(w'\phi')_0 = U_1 C_\phi (\phi_0 - \phi_1)$, where ϕ represents θ or q, U is windspeed, and the subscripts 0 and 1 refer to values at the surface and at the lowest model level of the atmosphere, respectively. The surface-layer exchange coefficients C_θ and C_q depend on the stability of the lowest layer of the model atmosphere and surface roughness, as described by Holtslag and Boville (1993). The windspeed at the at the middle of the lowest model level (~40 m) is assumed to be 7 m s^{-1}. The upward conductive flux at the upper surface of the ice-covered area is given by $F_{COND}^{\uparrow} = k(T_{i1} - T_s)$, where T_{i1} is the midpoint temperature of the uppermost model layer of the sea ice. The factor k is the effective conductance of the upper half of the top ice layer and the overlying snow. It is given by $k = k_i k_s \left(k_i h_s + k_s h^* \right)^{-1}$, where k_i and k_s are the respective thermal conductivities of ice and snow, h* is half the thickness of the top layer of ice, and h_s is snow depth. Note that $k = k_i/h^*$ in the absence of snow.

2.2.3 Pack ice

The distribution of sea ice thickness is represented by a specified fraction of open water ($1-A_i$) and a single layer of ice that may accumulate snow. Open water within the ice pack is assumed to be part of the mixed layer that is exposed to the atmosphere. The temperature of open water is held at the freezing point of seawater (T_m) when ice is present, and net heat exchange between open water and the atmosphere is immediately applied to the growth or decay of the sea ice layer. Sea ice is modeled using a one-dimensional thermodynamic model based on Maykut and Untersteiner (1971). Ice temperature (T_i) is governed by the conservation of internal energy, given by $\rho_i C_i \frac{\partial T_i}{\partial t} = \frac{\partial F_{COND}}{\partial z}$. The density and specific heat of ice are given by ρ_i and C_i, respectively, and conduction through the ice is given by $F_{COND} = -k_i \frac{\partial T_i}{\partial z}$. The rate of change of snow depth is given by $\frac{\partial h_s}{\partial z} = \frac{H(h_s)F_{net}}{\rho_s L_f} + \dot{h}_{acc}$, where ρ_s is snow density, L_f is the latent heat of fusion of ice, and $H(h_s)$ is the unit step function that is defined to be 1 when $h_s>0$ and 0 when $h_s=0$. Snowmelt occurs when snow is present and $F_{net}(snow) > 0$; and snow accumulation ($\dot{h}_{acc}$) is permitted when $T_s < 0$ C. The snowfall rate is 3 cm/month from November to mid-May and 8 cm/month from July to September, with transitions in between, based on Walsh et al. (1994).

Ice thickness is governed by the conservation of ice mass per unit area ($A_i h_i$), given by

$$\frac{\partial}{\partial t}(A_i h_i) + \mathrm{div}(\vec{\nabla}_i A_i h_i) = \left[\frac{d}{dt}(A_i h_i)\right]_{\text{thermodynamics}}, \qquad (2.3)$$

where $\vec{\nabla}_i$ is the ice drift velocity. Advective terms can be ignored since the model represents the entire perennially ice-covered Arctic Ocean, and (2.3) can be rewritten as,

$$A_i\frac{\partial h_i}{\partial t} + h_i\frac{\partial A_i}{\partial t} + A_i h_i \mathrm{div}(\vec{\nabla}_i) =$$

$$(\rho_i L_f)^{-1}\{-A_i[1-H(h_s)]F_{net}(\mathrm{ice}) + A_i F^B_{COND} - F_o - (1-A_i)F_{net}(\mathrm{open})\}. \qquad (2.4)$$

Thermodynamic terms affecting ice mass include (from the left within the braces): melting at the upper surface of the ice (when snow is absent and $F_{net} > 0$), heat conduction at the bottom surface of the ice F^B_{COND}, heat flux from the deep ocean into the mixed layer (F_o), and heat exchange between the atmosphere and open water within the pack. The last three thermodynamic terms (multiplied by -1) are the heat budget of the oceanic mixed layer. An imbalance in this budget contributes directly to the formation and melting of ice since the oceanic mixed layer does not store energy when ice is present in the model. Rearranging (2.4) yields the following expression governing the thickness of sea ice:

$$\frac{\partial h_i}{\partial t} =$$

$$(\rho_i L_f)^{-1}\{-[1-H(h_s)]F_{net}(\mathrm{ice}) + F^B_{COND} - \frac{F_o}{A_i} - \frac{(1-A_i)}{A_i}F_{net}(\mathrm{open})\} - h_i \mathrm{div}(\vec{\nabla}_i) - \frac{h_i}{A_i}\frac{\partial A_i}{\partial t}. \qquad (2.5)$$

The last two terms of (2.5) are effects of ice velocity divergence and the prescribed evolution of ice concentration. The prescribed annual cycle of ice concentration shown in Figure 2.2 is based on the analysis of Gloersen et al. (1992) with slight modification. Ice concentration estimated by Gloersen et al. is about 97% in the winter and 80% in the summer. Since melt ponds are included in this estimate of open water, it is assumed that, during summer, melt ponds occupy 10% of the total area and ice concentration is 90%. The estimated wintertime ice concentration by Gloersen et al. is lower than previous estimates, which are >99% (e.g. Maykut 1978), so an intermediate value of 98% is used in this study.

2.2.4 Cloud Specification

Three height classes of cloud and low-level ice crystal precipitation are prescribed using the parameters listed in Table 2.1. The properties of each cloud type include frequency of occurrence (f_{type}), amount-when-present, cloud water path, and cloud phase. It is noted that 'cloud amount', such as in Figure 3.1, is the product of f_{type} and amount-when-present. The presence and position of cloud at each height range is determined stochastically every 9 hours as described in Table 2.2. The procedure is performed for one of the height categories at a time, so that the presence of cloud is determined for one height class every 3 hours. Up to three different cloud layers can be present at a given time. However, low cloud and ice crystal precipitation (ICP) are treated as mutually

Table 2.1: Parameters for clouds and ice crystal precipitation

cloud type	*frequency of occurrence (%)*	*amount when present (%)*	*water path ($g\ m^{-2}$)*	*phase*
high cloud	50	50	8	frozen
middle cloud	45	75	12	mixed[a]
low cloud	19-68[b]	88	30	liquid
ice crystal pre-cipitation	0 -25[c]	100	3- 40[d]	frozen

a. The ice fraction of middle clouds increases with height from 0% at 770 mb to 100% at 530 mb.
b. The probability of low cloud is 68% from May 20 to 15 Sept. and 19% from Nov. 1 to May 1; transitions between these periods are linear with time.
c. The probability of ice crystal precipitation is 25% from Nov. 1 to April 15 and 0% from June 1 to Sept. 15, with linear transitions between these periods.
d. The water path of ICP in a given model layer is the product of the model layer depth and a specified ice water content of 0.02 g m^{-3}. The total water path of the surface-based ICP layer depends on its depth, which is determined by a random process described in Table 2.2. Possible values of total depth range from about 150m (lowest model layer only) to 2000m.

exclusive entities, based on observations (Curry and Ebert 1992; Hoff and Leaitch 1989). Individual clouds occupy one model level at a time, and ICP occupies between one and five model layers extending from the surface to as high as 2 km (see footnote in Table 2.1).

The frequency of occurrence and the amount-when-present of low, middle, and high clouds are based on the cloud climatology of Warren et al. (1988). Warren et al. detected artificial diurnal cycles in the frequency of middle and high-level stratiform clouds which result because of insufficient illumination during the night. At high latitudes, this may produce a *seasonal* bias in the estimated cloud amounts (Hahn et al. 1995), and this calls into question whether the wintertime minima in middle and upper cloud amount are real. In the present study, the frequency of these clouds is held at their summertime values throughout the year. The summer and winter frequencies

Table 2.2: Algorithm for determining the presence and position of cloud or ICP

Determine if cloud type is present.

1. Choose a random number x from a uniform distribution between 0 and 100.
2. If $x < f_{type}$, cloud is present. Proceed to 3.
   If not, cloud is not present[a]. End of procedure.

Determine model level with cloud.

3. Choose a random number x from a uniform distribution between 0 and 1.
4. Select pressure level of cloud p_{cloud} from within the range of atmospheric pressure[b] that defines the given height class: $p_{cloud} = p_{top} + x\,(p_{bottom} - p_{top})$. Find the model layer that includes p_{cloud}.
5. Using information from Table 2.1, assign cloud fraction, ice water path, and liquid water path for the chosen model layer[c].

a. For low-level clouds, repeat step 2 using $f_{type} = f_{low} + f_{icp}$. Ice crystal precipitation is present if $f_{low} < x < f_{low} + f_{icp}$.
b. p_{bottom} and p_{top} refer to the lower and upper pressure surfaces of each height class. (p_{bottom},p_{top}) assume the following values (in mb): (1000,770) for low; (770,530) for middle; and (530,225) for high.
c. For ice crystal precipitation, repeat step 5 for all model layers between p_{cloud} and the surface.

of low clouds are based on the seasonal averages of low stratiform cloud presented in Warren et al. (1988), and the monthly cloud climatology of Huschke (1969) is used to determine the period of transition between summer and winter regimes. The amount-when-present of each cloud type is approximately constant throughout the year for the types of cloud found in the Arctic (Warren et al.).

Typical values of cloud water path are not well known for arctic clouds, especially those at greater altitudes. The values listed in Table 2.1 are best estimates based on a variety of measurements reported for clouds in the arctic and upper-level clouds in other regions. Tsay and Jayaweera (1984) and Curry and Herman (1985) reported water paths in the range of 9 - 116 g m^{-2} for low clouds and 5 - 15 g m^{-2} for middle clouds based on data from the Arctic Stratus Experiment of 1980. Heymsfield (1977) observed ice water concentrations between ~10^{-4} and 10^{-1} g m^{-3} in cirrus clouds at temperatures between -30 and -60 C. Choosing from the middle of this range and assuming a cloud thickness of 2 km gives an ice water path in the range of ~2 - 20 g m^{-2}. There are very few published measurements of the mass concentration and thickness of arctic ice crystal precipitation (Curry et al. 1990). With an assumed ice water concentration of 0.02 g kg^{-1}, the ice water path of ICP in the model ranges between 3 and 40 g m^{-2} depending on the depth of the layer. The upper bound of this range is comparable to that used by Curry and Ebert (1992). The prescription of cloud phase in Table 2.1 is consistent with general characteristics of cloud types presented by Houze (1993) and similar to that assumed in the study of Curry and Ebert (1992). They sensitivity of the model to uncertainties in these cloud properties is examined in the Section 2.4.2.

2.3 Forcing

The daily average influx of solar radiation at the top of the atmosphere is prescribed for 80 N as shown in Figure 2.2. The divergence of sea-ice drift ($\mathrm{div}(V_i)$) is assumed to have a constant value of $(6\ \mathrm{yr.})^{-1}$, based on the analysis of Colony and Thorndike (1985). An oceanic heat flux of 1 W m^{-2} is used based on Maykut and Untersteiner (1971) and the energy budget analysis of Nakamura and Oort (1988).

The effect of large-scale circulation on the atmospheric heating rate is represented by $\dot{T}_{wall}$ in (2.1). The vertically integrated energy input associated with this term is the atmospheric poleward energy flux convergence (F_{wall}) depicted in Figure 2.2. The time-dependent heating profile is given by $T_{wall}(p, t) = F_{wall}(t)\xi(p)$, where ξ is a unit heating profile with a vertically integrated energy input of 1 W m^{-2}. The profile ξ is the weighted average of summer and winter unit heating profiles (ξ_s and ξ_w), which are based on normalized profiles of energy flux across 70 N, as analyzed by Overland and Turet (1994). The weights associated with the summer and winter profiles vary through the year such that $\xi = \xi_w$ during the winter, $\xi = \xi_s$ during the summer, and ξ is a blend of ξ_s and ξ_w during the spring and fall. Summer and winter profiles of T_{wall} are shown in Figure 2.3. The annual cycle of F_{wall} (Figure 2.2(c)) for the central Arctic is estimated based on monthly estimates of F_{wall} for the region north of 70 N by Overland and Turet (1994) and the latitude-dependent, annual radiative budget at the top of the atmosphere presented in Hartmann (1994).

(a)

(b)

(c)

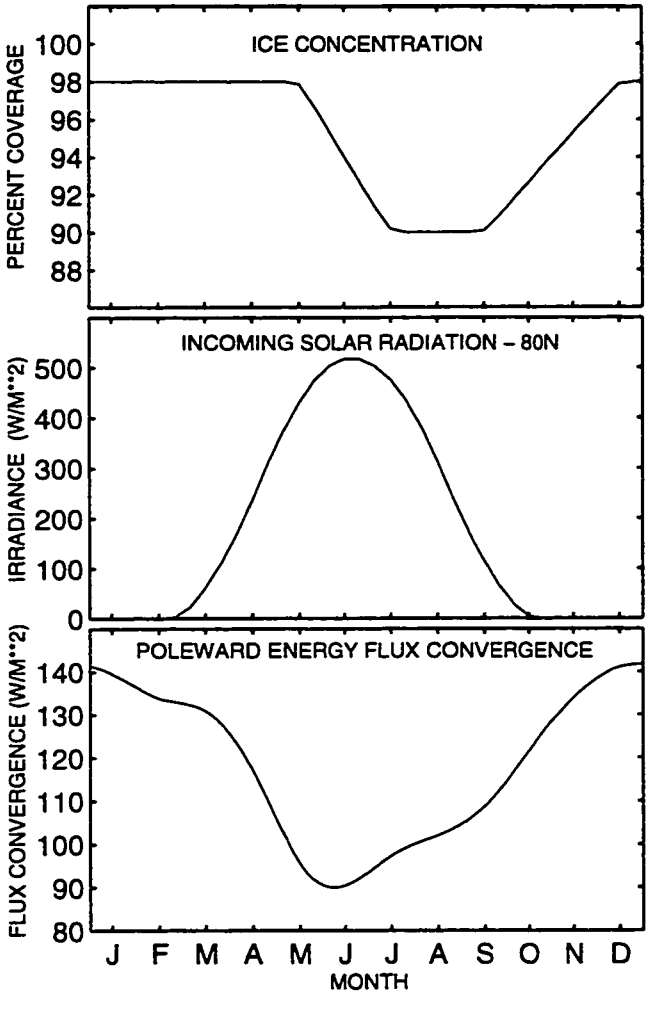

Figure 2.2: Prescribed annual cycles of (a) ice concentration, (b) incoming solar radiation, and (c) poleward energy flux convergence in the atmosphere.

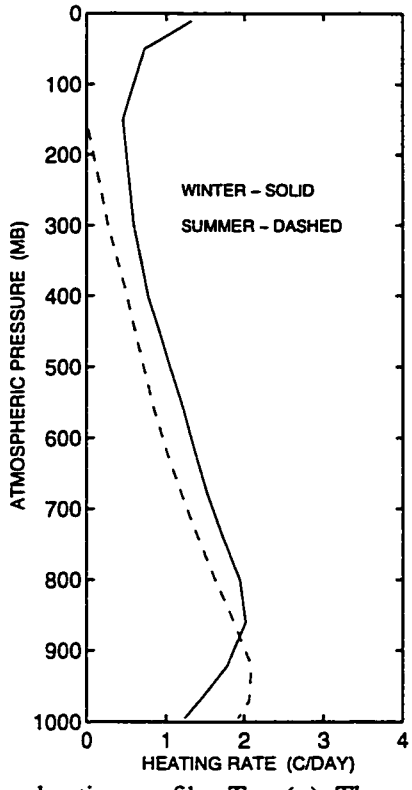

Figure 2.3: Winter and summer heating profiles $T_{wall}(p)$. The winter profile is (135 W m^{-2}) x ξ_w, and the summer profile is (100 W m^{-2}) x ξ_s. The profiles ξ_w and ξ_w are described in the text.

2.4 Simulation of present arctic climate system

The model is integrated for 20 years using the annually recurrent forcing* described in the previous section. The equilibrium state of the simulated ice-atmosphere climate system is based on the last decade of the integration. Equilibrium ice thickness changes by more than a meter in some of the experiments described below, but the absolute value of the trend in ice thickness is never greater than 2 cm/yr. during the averaging period.

* Although the probability of cloud occurrence follows the same cycle every year, the presence and height of each cloud is determined by a random, non-repeating process.

2.4.1 Present climate

The model output variables include ice thickness, snow depth, ice temperature, air temperature, turbulent and radiative fluxes at the surface, and radiative fluxes at the top of the atmosphere. The mean annual cycles of ice thickness, snow depth, and surface temperature in the standard model simulation are shown in Figure 2.4. The annual march of ice thickness shown in Figure 2.4 is typical of the central arctic, with melting between early June and late August and steady growth through the rest of the year (e.g. Untersteiner 1961). However, the mean ice thickness is about half a meter less than observed by Untersteiner and the annual range in ice thickness (1.25 m) is larger than observed (0.4 m) since the model uses a lower ice albedo to account for regions of thin ice

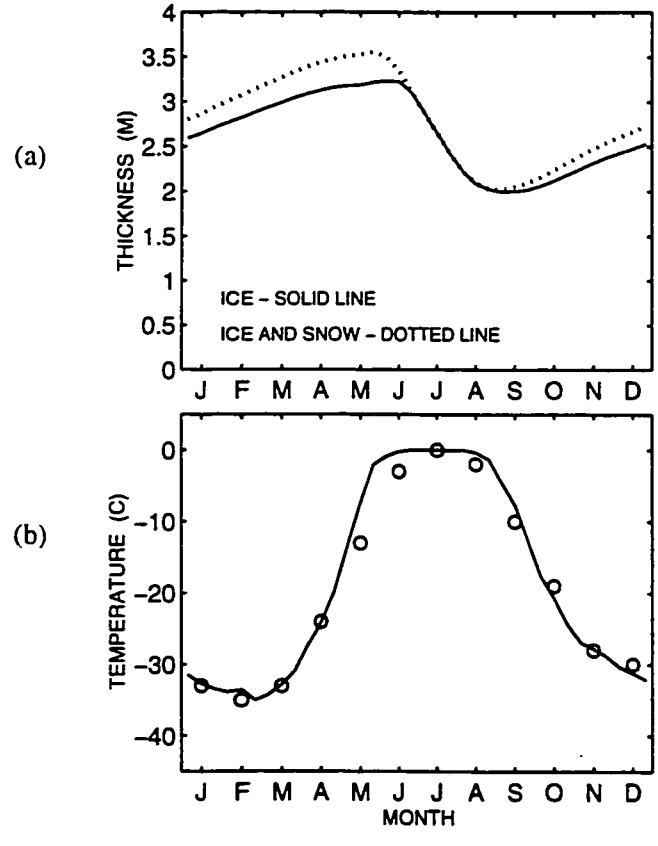

Figure 2.4: (a) Ice and snow thickness and (b) sea ice skin temperature from the simulation of present climate. Circles indicate surface air temperature in the central Arctic from Gorshkov (1983).

and melt ponds. Another factor contributing to the large range of ice thickness simulated by the model is that all meltwater is assumed to drain from the ice instead of possibly being stored in brine pockets or meltponds (this process is included in the Maykut and Untersteiner model). The annual cycle of surface skin temperature is consistent with observations of surface air temperature in the Central Arctic. Snow begins to melt in early June and has melted completely by the beginning of July. The surface freezes and begins to accumulate snow again in mid August.

Temperature profiles from January and July are generally close to observations as shown in Figure 2.5. A surface-based inversion is present in the mean temperature profile for January but is not as strong as observed. A possible explanation is that the observations were obtained at a large

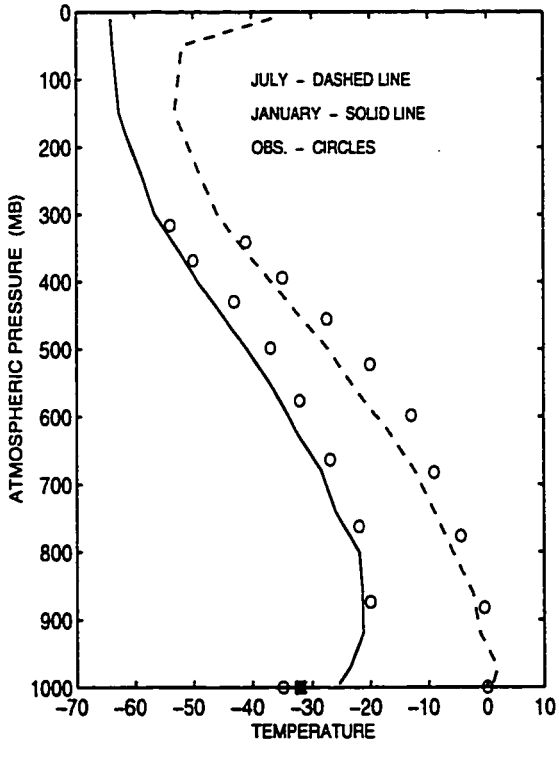

Figure 2.5: January and July temperature profiles from simulation of present climate.The winter surface skin temperature is indicated by an 'x'. Observed temperature profiles (1952-53) are from Hare and Orvig (1958)

ice island where the warming effect of open water was probably smaller than simulated in the model.

Downward longwave radiation at the surface (Figure 2.6) ranges from about 165 Wm^{-2} in the winter to 280 Wm^{-2} in summer; downward shortwave flux peaks at about 290 Wm^{-2} in early June. The modeled mean annual cycles of both terms are within the uncertainty of observations. The net radiative flux at the surface is upward during the winter and downward during the summer, when the surface temperature is fixed at the melting point and shortwave absorption is largest. The area-averaged turbulent surface flux is upward during all seasons in the simulation, including winter when large upward fluxes over open water areas outweigh downward fluxes over the ice. Seasonal variations in the surface energy balance are dominated by the radiative components. There is an annually-averaged net upward flux of 3 Wm^{-2}, which is balanced by the oceanic heat flux (F_o) and latent heat import associated with the divergence of sea ice, $\rho_i L_f h_i \, div(V_i)$.

The mean annual cycle of radiative fluxes at the top of the atmosphere is presented in Figure 2.7. Outgoing longwave radiation ranges from about 160 Wm^{-2} in the winter to 220 Wm^{-2} in the summer, which is in close agreement with satellite-based observations. Net downward solar radiation is less than longwave emission to space throughout the year except for a period during June when net incoming shortwave radiation reaches a peak value of about 225 Wm^{-2}. Planetary albedo, which is less sensitive to latitude than net downward shortwave radiation, also agrees well with observations (Figure 2.7). It should be noted that the specified cloud water paths were chosen (from a plausible range of values) to maximize the agreement of the simulated and observed radiative fluxes at the TOA. However, the ability to fine-tune TOA radiation in this manner is very limited since the water path of each cloud type is constant throughout the year.

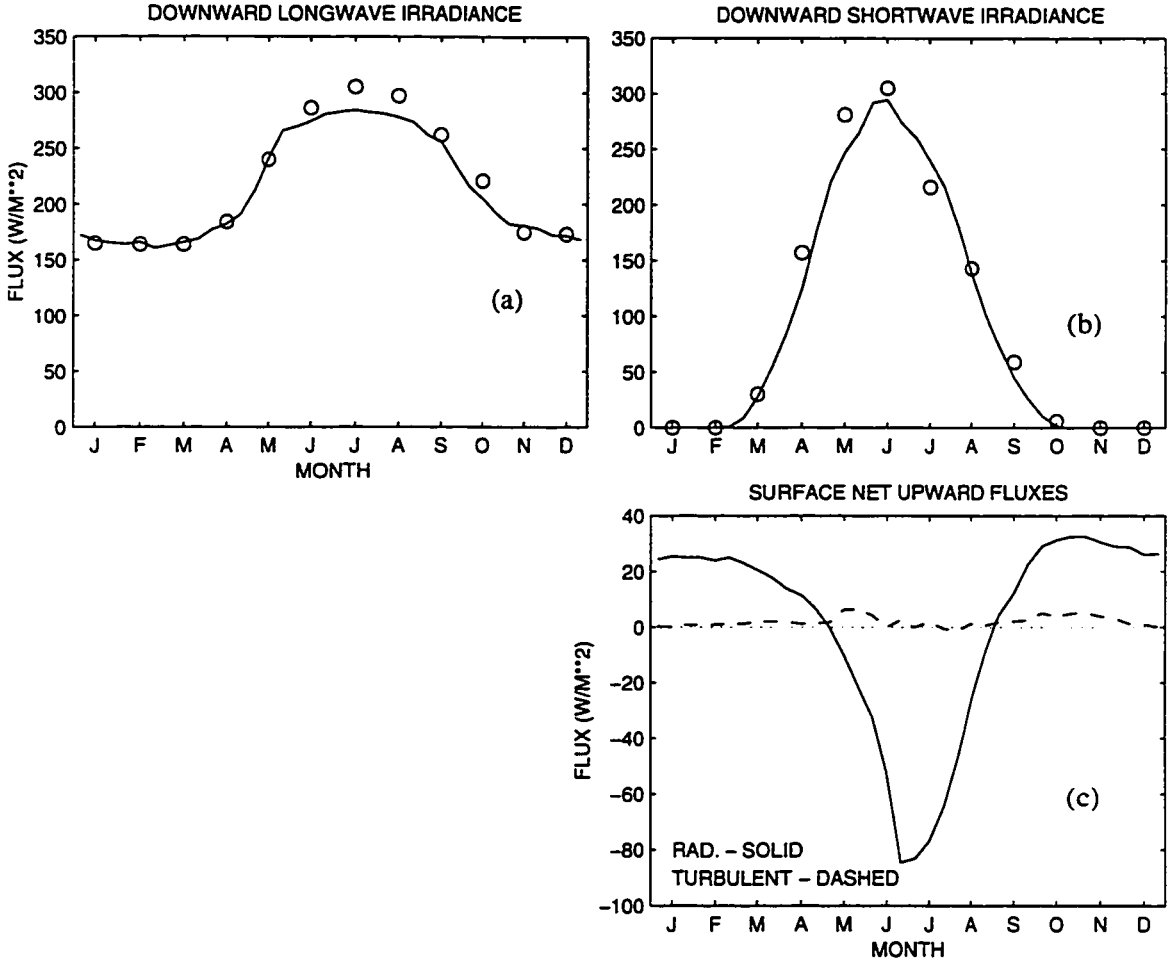

Figure 2.6: (a) and (b) Annual cycles of downward longwave and shortwave radiation at the surface. Circles denote mean monthly values observed at drifting ice stations compiled by Fletcher (1965). (c) Net upward radiative and turbulent fluxes at the surface.

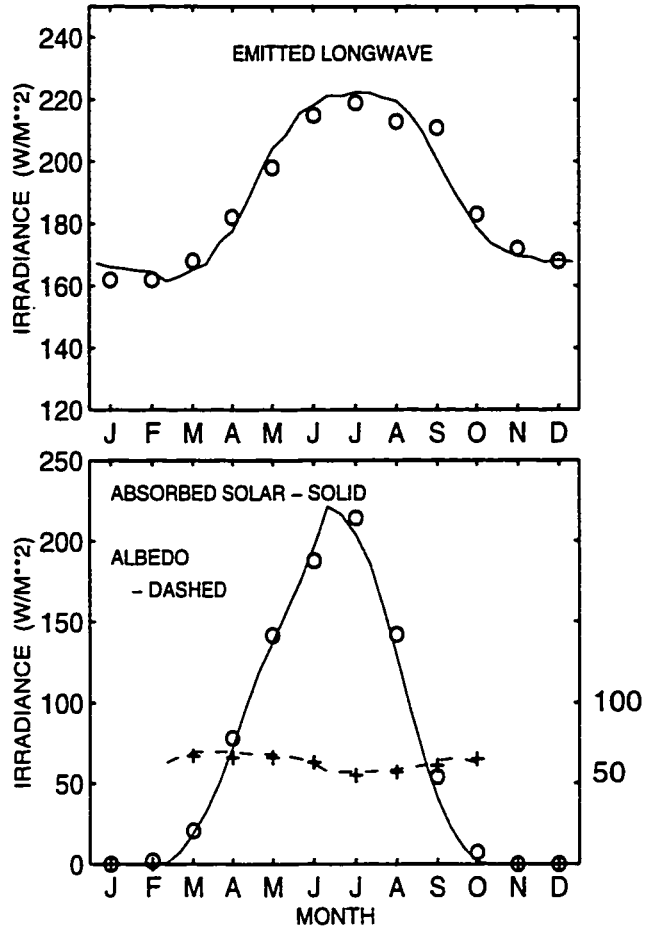

Figure 2.7: Energy fluxes at the top of the atmosphere from the simulation of the present climate. Observed monthly average fluxes are indicated by circles (scale on left) and planetary albedo is indicated by crosses (in percent, scale on right). Data are from the Earth Radiation Budget Experiment (1985-86) for 80 N (Hartmann and Michelsen, personal communication).

The direct effect of clouds on the radiative budget at a given level of the atmosphere can be quantified by calculating cloud radiative forcing (CRF), which is defined by Harrison et al. (1990) as

$$CRF = F_{rad}(total) - F_{rad}(clear), \quad (2.6)$$

where F_{rad} is the net downward radiative flux. The longwave and shortwave components of CRF at the surface from the model are shown in Figure 2.8(a). The direct effect of clouds is to increase

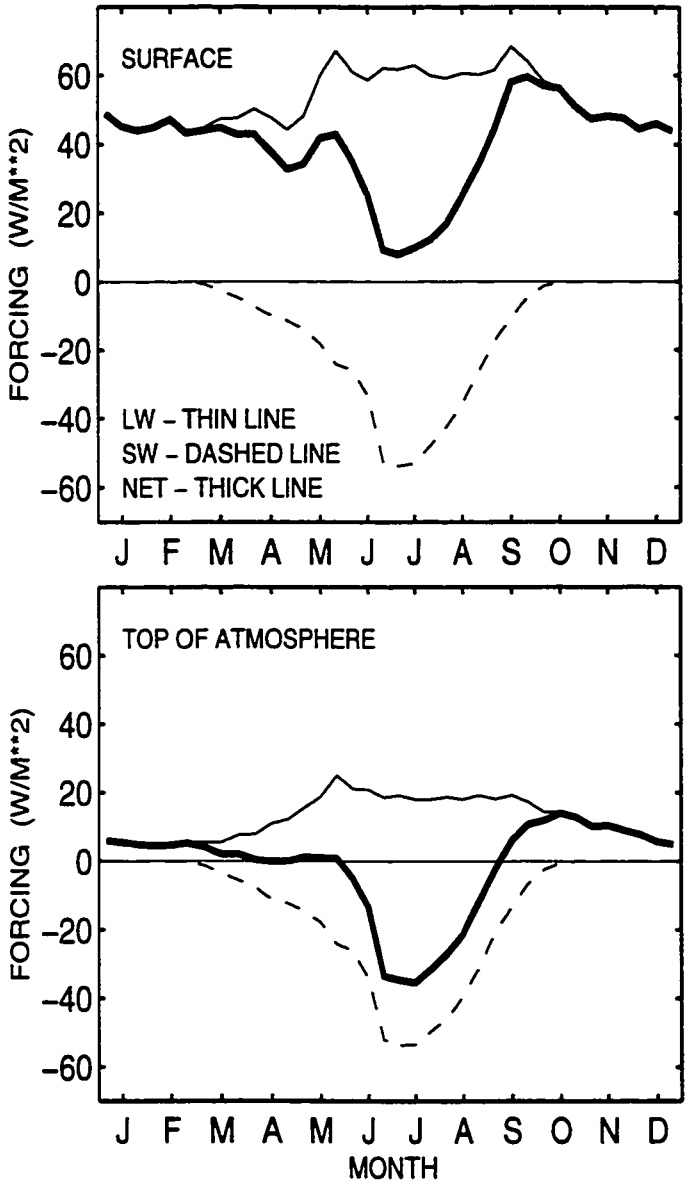

Figure 2.8: Cloud radiative forcing at (a) the surface and (b) the top of the atmosphere from the simulation of the present climate.

downward longwave radiation by about 50-60 Wm^{-2} and to decrease shortwave absorption by as much as 50 Wm^{-2} in the summer. The annual averaged net CRF at the surface is 39 Wm^{-2}.The annual variation of CRF at the TOA is similar to that at the surface, except that the longwave effect is smaller in magnitude. At -1.9 Wm^{-2}, the modeled annual average CRF at the top of the arctic atmosphere is of the same sign but substantially smaller than the observed global average of -17 Wm^{-2} (Harrison et al. 1990). Annually-averaged, the direct effect of all cloud types in the model is to increase the loss of energy from the arctic climate system, but to a lesser extent than the global climate system. Since clouds increase the upward energy flux at the top of the atmosphere and increase the downward flux at the surface, the direct effect of clouds is to remove energy from the atmosphere, as noted by Curry and Ebert (1992).

Cloud radiative forcing by a single cloud type was computed in a similar manner as the CRF by all types, except that only the cloud type in question was removed when evaluating the latter term on the right hand side of (2.6). Figure 2.9 shows the annual cycles of CRF at the surface and top of the atmosphere for high, middle, and low clouds, and ICP. Surface cloud radiative forcing depends on the amount, height, and radiative properties of clouds. These factors combine such that the wintertime values of surface CRF by low cloud, middle cloud, and ICP are approximately the same; which is probably a coincidence considering the uncertainty in the parameters that control cloud radiative properties. Surface CRF by low clouds increases in summer due to increases in temperature and low cloud amount, but shortwave reflection by low clouds produces a local minimum in CRF during mid-summer (when incoming solar radiation is greatest). The summertime minimum in surface CRF by middle clouds is also caused by increased shortwave reflection. Surface CRF by ICP decreases to zero during the summer when it is not present. The annual cycle of surface CRF by high clouds is similar to that to middle cloud, except smaller in magnitude.

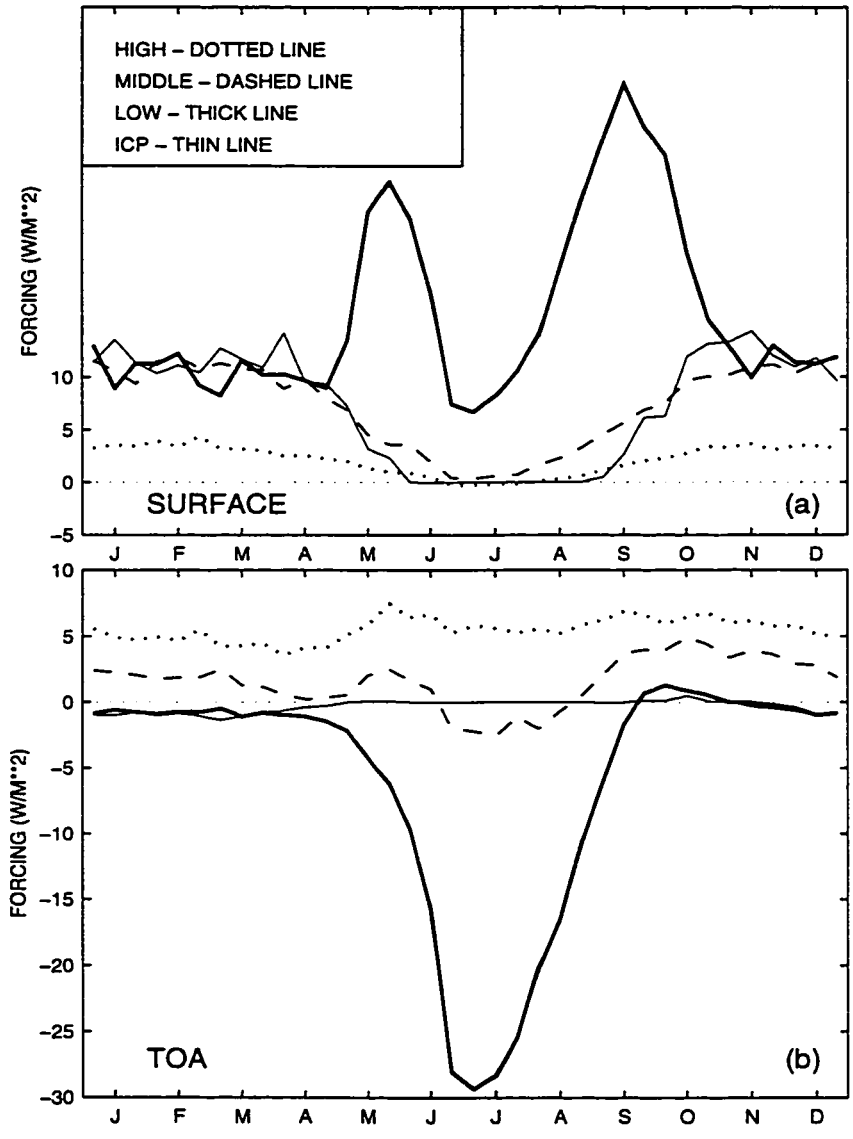

Figure 2.9: The annual cycle of cloud radiative forcing by individual cloud types at (a) the surface and (b) the top of the atmosphere.

At the top of the atmosphere, CRF by low clouds and ice crystal precipitation is small and negative during the winter months. Since these types of cloud typically are warmer than the surface, they actually increase the loss of longwave radiation to space. TOA CRF by low clouds reaches a pronounced minimum in the summer due to the reflection of incoming sunlight. Middle clouds reduce the loss of radiation to space during all months except July and August. High clouds consistently warm the arctic climate throughout the year.

The annually-averaged radiative forcing of the four cloud types is summarized in Table 2.3. The sum of CRF by each cloud type does not equal the total CRF by all clouds due to the overlapping of clouds when more than one type is present. It is interesting to note that, among the four types, CRF by low clouds is most positive at the surface and the most negative at the top of the atmosphere; and the opposite is true of high clouds. Estimates of the terms in Table 2.3 from observations are not possible due to the inadequate data base. The model estimates are qualitatively similar to model estimates of total CRF by Curry and Ebert (1992) and of surface CRF by cloud type by Curry et al. (1993); however, the magnitudes in the present study tend to be smaller than the previous estimates.

Table 2.3: Annual average cloud radiative forcing, by cloud type (in W m^{-2})

	Height of Computation	
cloud type	*surface*	*top of atmosphere*
high	2.2	5.5
middle	7.4	1.6
low (liquid)	15.9	-5.9
low (ICP)	7.3	-0.4
all clouds	39	-1.9

2.4.2 Model sensitivity to forcing and parameters

The simulated arctic climate is an internally consistent solution of the model equations subject to realistic forcing for the central Arctic. The results presented above indicate that the solution agrees well with observations of the arctic climate system. However, there is considerable uncertainty in many of the model parameters and forcing terms. The sensitivity of the simulated equilibrium ice thickness to plausible perturbations of these specified terms is shown in Table 2.4. The discussion of these results is kept brief, as they are not directly related to the goal of the study.

2.4.2.1 Cloud properties

The amount and radiative properties of clouds are essential factors in determining the effect of clouds on the arctic climate. The dependence of the simulated climate on the frequency of occurrence of clouds is examined in detail in Section 2.5. The radiative properties of clouds can be modeled as a function of bulk microphysical quantities -- water path, phase, and effective particle radius -- as discussed by Slingo (1989), Ebert and Curry (1992), and Curry and Ebert (1992). However, realistic values for these microphysical parameters in the Arctic are uncertain (Curry and Ebert 1992). The first eight experiments show the effect of multiplying the water path of each type of cloud or ice crystal precipitation by factors of 0.5 and 2.0. These perturbations correspond approximately to the uncertainty in condensate path. Increasing the water path of high and middle clouds reduces the ice thickness. This suggests that, for a given change in water path, the greenhouse effect of these clouds changes to a greater degree than the albedo effect, which is consistent with the traditional climatic interpretation of TOA CRF (e.g. Harrison et al 1990). The opposite must be true for low clouds since ice thickness increases with low cloud water path. Ice thickness is relatively insensitive to changes in the water path of ice crystal precipitation, as anticipated from TOA CRF. Possible reasons for this insensitivity are discussed below. For a given cloud water

Table 2.4: Sensitivity of simulated equilibrium ice thickness to prescribed terms

Term changed	Standard value (with units)	Experimental value	Equilibrium Ice Thickness (in m) (standard = 2.64)
high cloud water path	8 g m^{-2}	4	3.37
"	"	16	1.85
middle cloud water path	12 g m^{-2}	6	3.25
"	"	24	2.17
low cloud water path	30 g m^{-2}	15	2.19
"	"	60	3.78
ICP mass concentration	0.02 g m^{-2}	0.01	2.72
"	"	0.04	2.57
ice particle effective radius[a]	25 μm	50	3.59
liquid droplet effective radius[a]	7 μm	10	2.05
cloud ice fraction	see Table 2.1	100%	1.44
"	"	0%	2.78
winter sea ice concentration	98%	97	2.98
summer seas ice concentration	90%	89	2.63
windspeed at lowest model level	7 m s^{-1}	5	2.15
bare ice albedo	0.60	0.58	2.39
F_{wall}	118 W m^{-2}	123	1.60
F_o	1 W m^{-2}	2	2.22
latitude of incoming F_{SW}	80 N	70	1.44
sea ice velocity divergence	(6 yr.)$^{-1}$	(10 yr.)$^{-1}$	3.67

a. The particle radius is used in computation of radiative properties (see section 2.2.2).

path, cloud albedo and emissivity decrease as the effective radius of cloud particles increases (Slingo 1989; Ebert and Curry 1992). Doubling the effective particle radius of ice clouds and ICP increases ice thickness, apparently by reducing the greenhouse effect of upper clouds. Increasing the radius of liquid cloud particles reduces the emissivity and albedo of low and middle-level clouds, producing a drop in ice thickness which suggests that the effect on albedo is stronger. The sensitivity of the model to condensate phase is examined by assuming that all condensate is either frozen or liquid (which of course are unrealistically large perturbations). When all clouds are assumed to be 100% ice, the albedo and emissivity of the (formerly liquid) lower clouds decreases; the net effect is a decrease in ice thickness. The albedo and emissivity of (formerly frozen) upper clouds and ICP are greater if all condensate is assumed to be 100% liquid. The net effect of these competing effects is to create slightly thicker ice.

2.4.2.2 Ice concentration and albedo

The minimum and maximum values of ice concentration are not known with great precision due to the limited accuracy of satellite observations and limited sampling of more accurate techniques such as visual observation and upward looking sonar. Decreasing the ice concentration (i.e. increasing open water fraction) during the winter and spring increases ice thickness since open water regions produce ice very rapidly during the cold season. Decreasing ice concentration in the summer and autumn increases summertime ice melt due to more solar absorption by leads. However, much of that loss is made up by extra ice growth in open water during the autumn, and the net effect is a only slight decrease in ice thickness. Reducing the albedo of snow-free ice in the model increases solar absorption and decreases mean ice thickness.

2.4.2.3 Other parameters

The efficiency of turbulent energy transfer at the surface depends on windspeed at the lowest model level (~40 m). Typical windspeeds at 2-m in the Arctic are around 4 m s^{-1} (Untersteiner 1961) so a value of U_1 =7 m s^{-1} was chosen as the 40-m windspeed. Decreasing U_1 reduces mean ice thickness, mainly by reducing wintertime upward turbulent fluxes (and ice growth) over open water. Ice thickness decreases when more energy is imported across the boundaries of the modelled arctic climate system. For example, equilibrium ice thickness decreases with larger values of F_{wall}, F_o, and incoming solar radiation; and ice thickness is greater when ice export (latent heat import) is smaller.

The model is most sensitive to perturbations in poleward energy flux convergence and surface albedo. Aside from these two parameters, the results indicate that plausible variations in specified quantities can change the simulated mean ice thickness by up to a meter. Therefore, it is possible that the model could produce an equally realistic simulation using a different yet plausible combination of parameters.

2.5 Experiments

2.5.1 Cloud-free arctic climate

To examine the total effect of clouds on the arctic climate system, the model is integrated without clouds or ICP. Surface temperature (Figure 2.10) is lower throughout the winter in the absence of clouds, but it increases rapidly with increasing sunlight to produce a slightly longer melt season. The annual cycle of ice thickness has a larger amplitude in the absence of clouds which is consistent with clouds reducing the energy loss from the arctic climate system during the

winter and reducing energy absorption during the summer. Even though the direct effect of clouds is to increase the amount of energy absorbed by the surface, the equilibrium ice thickness in the standard simulation is 48 cm greater than in the cloud-free simulation. This suggests that, in the present arctic climate, clouds have affected the atmosphere in a way that increases the net upward heat flux from the surface. We expect that atmosphere should be cooler in the present climate than in the absence of clouds since the clouds promote radiative energy loss from the atmosphere. Indeed, the mean temperature profiles shown in Figure 2.11 suggest that the present atmosphere is significantly cooler than it would be without clouds. The effect of atmospheric adjustment in response to clouds on the annually averaged equilibrium surface energy budget is summarized in

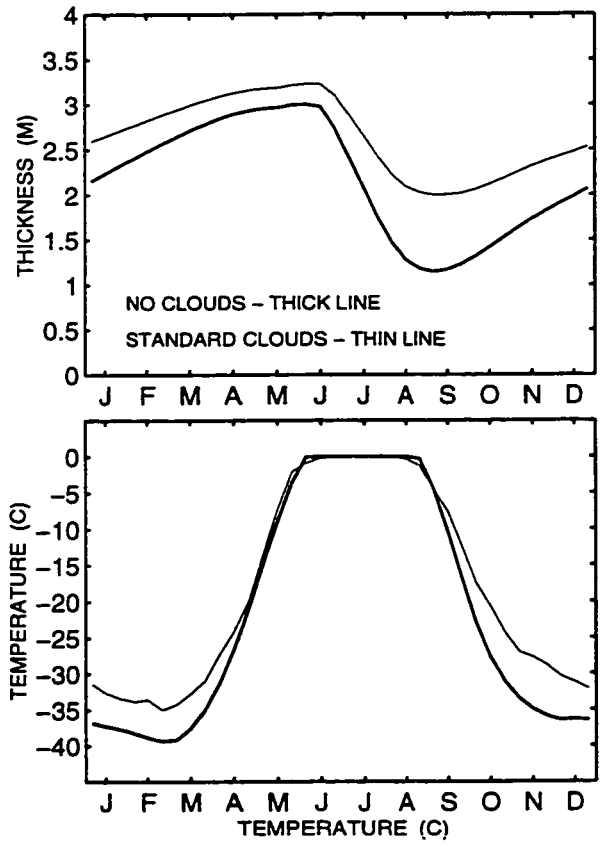

Figure 2.10: Ice thickness and surface temperature from the cloud-free simulation. Results from the standard simulation are also shown.

Table 2.5. Although the direct effect of clouds, as defined by surface CRF, is to increase downward longwave irradiance at the surface by 53.2 Wm^{-2}, the equilibrium effect of clouds on the surface radiative budget is only a third of this. Downward longwave irradiance from clear sky in the standard simulation is 25.3 Wm^{-2} less in than in the cloud-free simulation because the atmosphere is cooler in the presence of clouds. Enhanced emission associated with the difference in surface temperature between the standard and cloud-free simulations (Figure 2.10) carves another 10.5 Wm^{-2} from the direct longwave effect of clouds on the surface. Since shortwave radiative transfer in clear air does not depend strongly on atmospheric temperature, the equilibrium effect of clouds on absorbed shortwave energy at the surface is very close to the direct effect (shortwave CRF at the

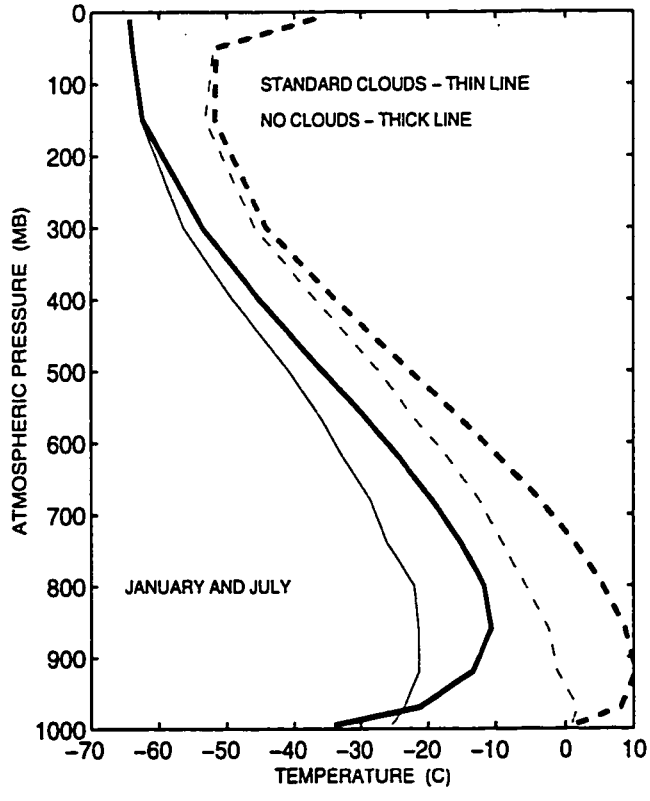

Figure 2.11: Temperature profiles from the cloud-free case. Dashed lines are for July and solid lines are for January.

surface). Finally, the upward turbulent flux is 5.8 Wm^{-2} greater in the simulation of present climate than in the cloud free climate as a result of the dramatic effect of clouds on boundary layer structure. In equilibrium, the net upward surface flux in the presence of clouds is 1 W m^{-2} greater than in the cloud-free case. The extra watt of energy loss at the surface in the standard simulation is balanced by additional latent heat import associated with the export of thicker ice.

The results indicate that the equilibrium effect of clouds on the surface energy budget is opposite from the direct effect. This suggests that the thermodynamic coupling between the pack ice and atmosphere is an essential element in understanding the effect of clouds on the arctic climate. The increase in the net upward surface energy flux associated with clouds in the present arctic climate is consistent with the fact that clouds tend to increase the energy loss to space (CRF < 0 at the TOA).

Table 2.5: Surface energy budget terms in the standard and cloud-free simulations

Flux	*Standard Simulation*	*Cloud-Free Simulation*	*Direct Effect of Clouds*[a]	*Equilibrium Effect of Clouds*[b]
net upward longwave	32.1[c]	49.5	-53.2	-17.4
absorbed shortwave	31.1	43.7	-13.7	-12.6
upward turbulent	2.0	-3.8	0	5.8
total net upward	3.1	2.0	-39.4	1.0

a. Surface cloud radiative forcing.
b. Cloud-free climate subtracted from standard simulation.
c. All values are in W m^{-2}.

2.5.2 Variations in frequency of all clouds (including ICP)

To gain more information about the relationships among cloud radiative forcing, radiative and turbulent energy budgets at the surface, and equilibrium ice thickness, a series of experiments are performed in which the frequency of occurrence of all cloud types is multiplied by a factor γ. Experimental values of γ range from 0 (cloud-free) to 1.4 (almost 100% chance of low clouds in summer). The dependence of simulated ice thickness, net surface fluxes, and cloud radiative forcing on γ is presented in Figure 2.12. Ice thickness reaches a maximum value when $\gamma \sim 0.6$ and is about 1 m less than the standard case when $\gamma=1.4$*. With increasing values of γ, there is a monotonic increase in the upward turbulent flux and a corresponding decrease in the net upward radiative flux at the surface. This suggests a systematic relationship between clouds and these types of surface fluxes. However, ice thickness depends on the total net upward flux at the surface, which does not bear an obvious relationship to γ. Increasing proportionately with γ, surface CRF increases does not appear to be related with mean ice thickness. CRF measured at the top of the atmosphere has a minimum value at $\gamma \sim 0.6$ and appears to have a significant negative correlation with ice thickness.

These results suggest that CRF measured at the top of the atmosphere may offer more valuable information about the climatic effect of clouds on the arctic than CRF measured at the surface. Although TOA CRF appears to be systematically related to ice thickness, these experiments do not indicate how measurements of its present average value may be used to predict how a change in clouds will affect arctic climate. For example, TOA CRF indicates how the simulated ice thickness

---

* This does not necessarily indicate that ice thickness will decrease with an increase in total cloud amount as observed at the surface. Changes in total cloud amount may indicate a change in the amount of only one cloud type. For example, the annual cycle of cloudiness over the Arctic (Figure 2.1) is almost entirely attributable to variations in low cloud amount. The dependence of ice thickness on cloud frequency not uniform among cloud types, as shown in Section 2.5.3.

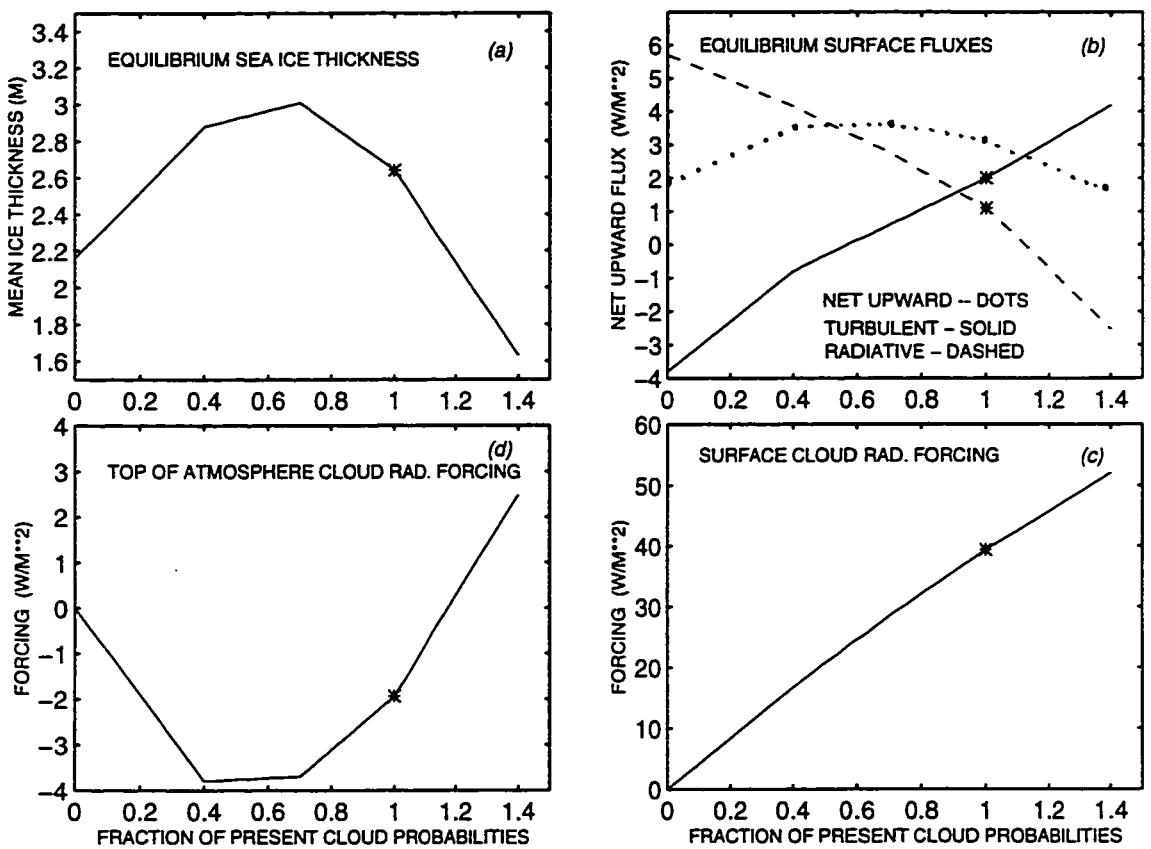

Figure 2.12: Variations of climatic quantities with cloud frequency: (a) ice thickness, (b) surface energy budget, (c) surface cloud radiative forcing, and (d) top of the atmosphere cloud radiative forcing. Stars indicate values from the standard simulation.

would change if there were no clouds but not how it would change with a 10% change in γ. Uniformly changing the frequency of occurrence of all cloud types provides added information about the relationship between CRF and ice thickness in the climate system of the model, but it is not particularly realistic since clouds are not likely to change in this manner in nature. For this, an understanding of the relationship between TOA CRF and specific information about clouds is required. The dependence of ice thickness on cloud height and time of year are discussed in the next two sections.

2.5.3 Variations in cloud by height class (low, middle, high)

The dependence of climate on cloud height was examined in the same manner as Manabe and Wetherald (1967). In this study the effect of clouds on the arctic surface energy budget is diagnosed in terms of ice thickness, whereas Manabe and Wetherald used global average surface temperature in their study of the global climatic effect of clouds. Three sets of experiments were performed in which the frequency of occurrence of cloud at one level is changed. In each of the low-cloud experiments, the frequency of occurrence of low liquid clouds is uniform through the year and the frequency of ice crystal precipitation is not changed from the standard simulation.

Estimates of cloud radiative forcing by each type of cloud in the present climate (Table 2.3) may provide a means of predicting how a change in a given cloud type affects equilibrium ice thickness. These experiments are an opportunity to formulate and test such predictions. The predicted dependence of ice thickness on cloud amount* is quite different depending on whether CRF is evaluated at the surface or the top of the atmosphere. Surface CRF suggests that an increase in

* Recall that cloud amount is the product of the frequency of occurrence, which is varied in these experiments, and the amount when present, which is constant for each cloud type (see Table 2.1).

cloud frequency at any level should decrease ice thickness, and that this dependence is strongest for low clouds whose CRF at the surface is most positive. Using TOA CRF, we reach a different set of predictions: a greater amount of middle or high cloud should decrease ice thickness and more low cloud should increase ice thickness.

The dependence of equilibrium ice thickness on the frequency of low, middle, and high clouds is shown in Figure 2.13. The results indicate that the effect of clouds depends strongly on the type of cloud in question: middle and high clouds reduce ice thickness and low clouds increase thickness. The results indicate that CRF at the top of the atmosphere is a much better basis than CRF at the surface for predicting the effect of changes in cloud frequency at different levels.

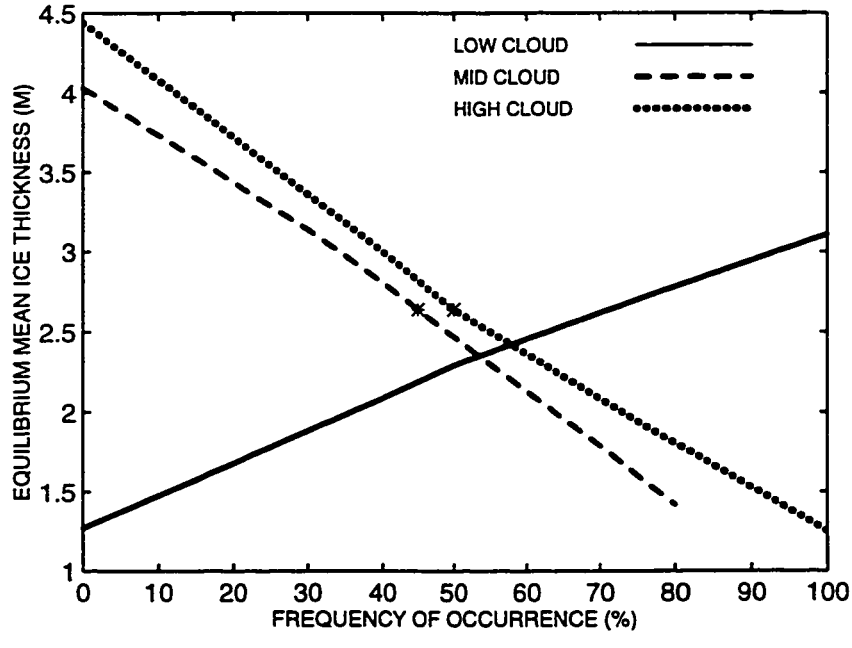

Figure 2.13: Dependence of equilibrium ice thickness on the frequency of low, middle, and high cloud. Stars indicate the frequencies of high and middle cloud in the present climate

The general tendency for higher clouds to decrease the net upward surface heat flux and for lower clouds to increase it is consistent with the results of Manabe and Wetherald (1967). However, this study suggests that middle clouds tend to reduce the upward heat flux at the surface (decreasing ice thickness), whereas Manabe and Wetherald found that, globally, these clouds increase surface heat loss and cool the global climate. This may be attributed to the fact that the amount of sunlight entering the top of the atmosphere in the polar regions is about half of the global average.

It is interesting to note that the equilibrium ice thickness is less than the standard simulation if the frequency of occurrence of low clouds is held at either the winter value (19%) or the summer value (68%) for the whole year. This indicates that in the present climate the ice-thickening effect of low clouds is greater than average when their frequency of occurrence is greater than average.

2.5.4 Dependence of ice thickness on the monthly presence of cloud

The strong seasonality of cloud radiative forcing in the simulation of the present arctic climate (Figure 2.8) suggests that the climatic effect of a change in clouds depends on when the change takes place. To see how the climatic effect of clouds varies by season, a series of experiments were performed in which all clouds are eliminated for a given month of the year. For example, the effect of clouds during January was examined by comparing the standard simulation to an experiment in which January was cloud-free during each year of the 20-year integration. Figure 2.14 (b) indicates that the presence of clouds during January reduces the equilibrium ice thickness.

Since there is negative correlation between TOA CRF and ice thickness (as shown in Figure 2.12), the equilibrium ice thickness should be larger than the standard simulation if clouds are removed during a month of positive CRF. The results (Figure 2.14) indicate that this prediction is valid for eight months, but there are significant discrepancies during April, May and June. The

removal of clouds in June increases ice thickness by more than 50 cm, even though clouds reduce the absorption of energy by the arctic climate system during this month in the present climate. Shine and Crane (1984) had the same result in their study which was explained was related to surface albedo feedback. To isolate the effect of the surface albedo feedback in the present model, the experiments were repeated using a prescribed annual cycle of surface albedo from the standard simulation to suppress the interactions between the albedo and other factors. The simulation of the present arctic climate in this case was almost identical to the standard case (equilibrium ice thickness is 2.68 m, versus 2.64 m in standard case). In these experiments, TOA CRF is a more reliable

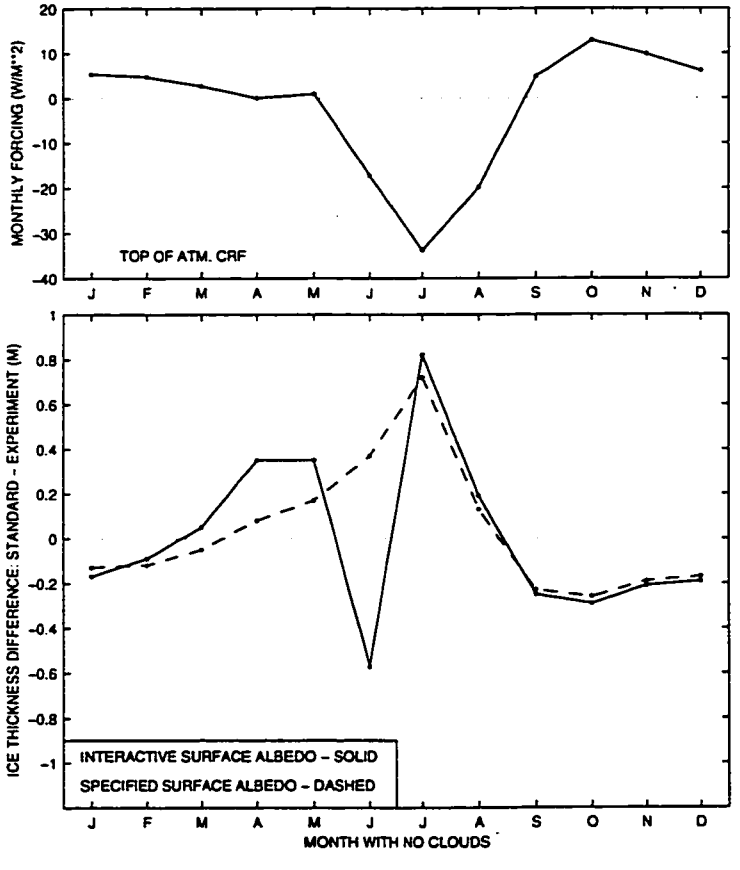

Figure 2.14: (a) Monthly mean cloud radiative forcing at the top of the atmosphere from the standard simulation. (b) The effect of cloudiness on mean ice thickness by month. Each value is the difference between the standard simulation and an experiment with no clouds during the month in question.

indicator of the effect of clouds on a monthly basis. CRF still fails to predict the change in ice thickness during April and May, but the discrepancy is much smaller with a non-interactive surface albedo.

The results indicate that the effect of clouds on the arctic climate varies significantly through the year and that CRF at the top of the atmosphere can be used to predict this effect of clouds on monthly timescales. However, the experiments demonstrate how a feedback mechanism -- in this case related to surface albedo -- can dramatically change the predictions based on the monthly value of CRF.

2.6 The interpretation of cloud radiative forcing in the central Arctic

The results show that the atmosphere responds to changes in clouds in a manner that opposes the direct radiative effect of clouds on the surface energy budget. Clouds cool the atmosphere relative to the surface, which significantly decreases their direct effect on downward longwave irradiance and increases upward turbulent energy fluxes from the surface. TOA CRF appears to be a good diagnostic indicator of the equilibrium effect of clouds on ice thickness, such that higher values of TOA CRF are associated with thinner ice. We would expect to see a relationship between equilibrium ice thickness and annually-averaged values of TOA CRF in the experiments described in Section 2.5, since the only prescribed parameters that differ among the experiments were those pertaining to clouds. Figures 2.15 (a, b) indicate that there is virtually no relationship between mean ice thickness and surface CRF, but there is a strong negative correlation between ice thickness and CRF at the top of the atmosphere.

TOA CRF is a measure of the effect of clouds on the radiative energy budget at the top of the atmosphere. On a regional scale such as the central Arctic, the annual radiation budget at the top of the atmosphere is balanced by energy fluxes across the lower or lateral boundaries of the domain.

These fluxes are held constant in the present model, except that the export of ice mass (latent heat influx) is computed as a function of ice thickness and prescribed ice velocity divergence (which produces an obvious negative feedback). On longer timescales the atmosphere cannot act as a source or sink of energy, which suggests that there should be a relationship between annually-averaged TOA CRF and net surface energy budget. Since there is a direct relationship between the net upward flux at the surface and ice growth, we expect greater equilibrium ice thickness to be associated with lower values of TOA CRF, as shown in Figure 2.15 (b).

Results also show how the surface albedo feedback can modify the effect of clouds predicted by TOA CRF. Figure 2.15 (c) shows the relationship between TOA CRF and ice thickness when all the experiments were run with prescribed (non-interactive) annual cycle of surface albedo. The main differences between this plot and Figure 2.15 (b) are that the correlation is stronger (-0.96 versus -0.86) and that the dependence of ice thickness on TOA CRF is weaker. The former feature demonstrates that removing the surface albedo feedback mechanism reduces the complexity of the system, bringing it closer to a zero-feedback system in which the effect of clouds is explained completely by TOA CRF. The latter feature suggests that the surface albedo feedback in the model increases the sensitivity of ice thickness to the effect of clouds or, in other words, the surface albedo feedback is positive.

2.7 Summary

Previous studies (Shine and Crane 1984; Curry and Ebert 1992; Curry et al. 1993) have examined the direct effect of clouds on the surface radiative budget in the Central Arctic. These studies were not designed to incorporate the response of the atmosphere to changes in clouds and thus could not examine their equilibrium effect that is relevant to climate. The present study is based on

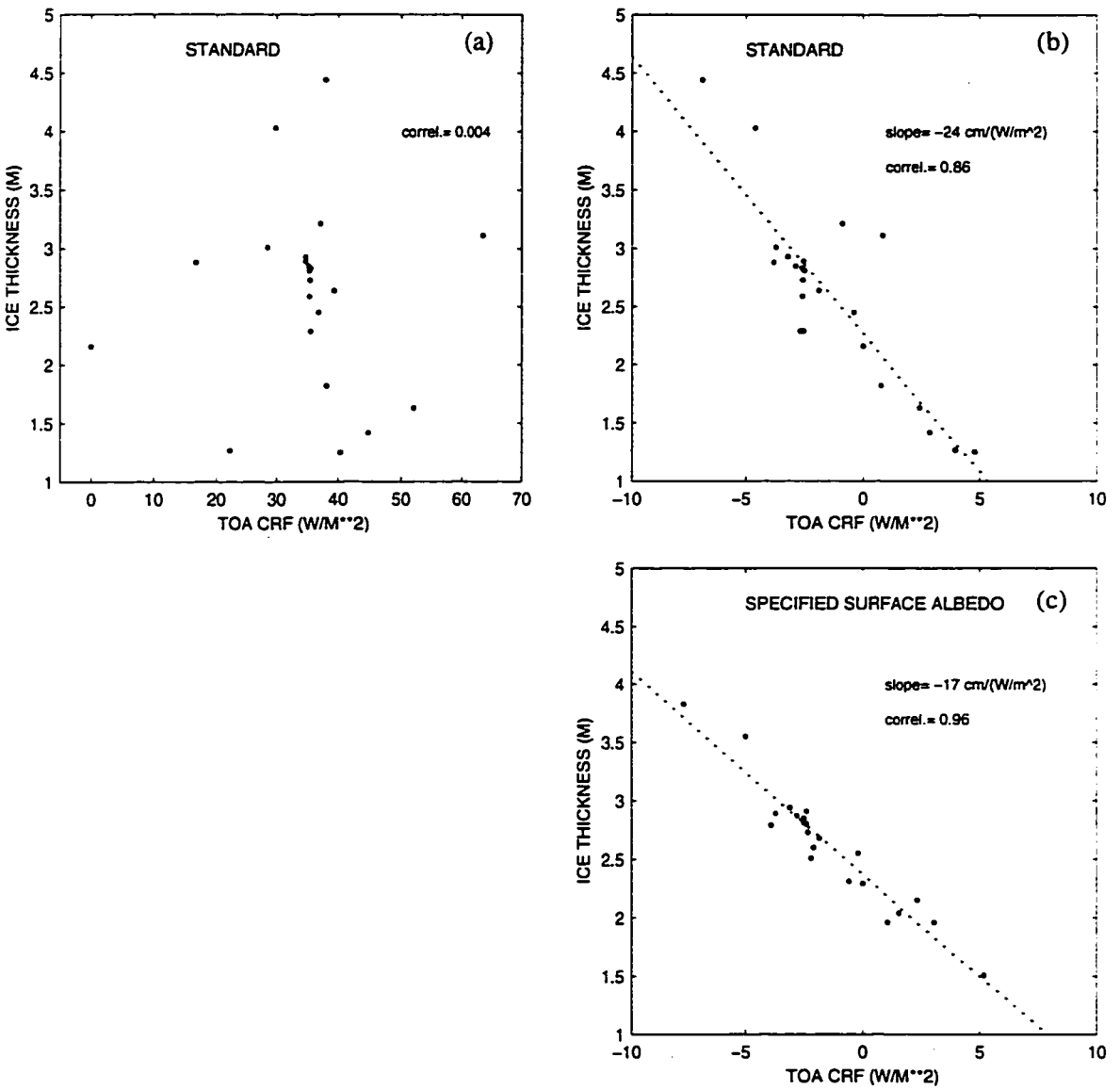

Figure 2.15: Relationship between equilibrium ice thickness and CRF at (a) the surface and (b) the top of the atmosphere. (c) is the same as (b) but surface albedo is specified in the experiments. The dotted line in (b) and (c) is a best fit.

a model that includes the essential physical processes needed to explicitly simulate the direct and equilibrium effects of clouds in the arctic.

The model used in this study produces a reasonable simulation of the present arctic climate system when realistic estimates of present forcing and parameters are applied. Model experiments suggest that clouds have a slight thickening effect on the arctic ice pack, which is opposite of previous conclusions. Despite the strong direct effect of clouds on the surface radiative budget (CRF at surface) and the immediacy of the surface energy budget to the thickness of ice, surface CRF does not provide information about the climatic effect of clouds on ice thickness. TOA CRF, on the other hand, is closely related to mean ice thickness in the model simulations. When evaluated on the basis of height or the time of year, TOA CRF from the present climate can be used to predict the effect of perturbations in cloudiness on ice thickness. The monthly sensitivity experiments and the height sensitivity experiments show that the effect of cloud is not constant through the year or by cloud type. This indicates that it is necessary, when assessing the effect of a cloud change, to consider the specific nature and time of year of the change. The following is a recipe for assessing effect of a change in cloudiness on ice thickness. First, identify and quantify the change in cloud (e.g., height, time of year, and bulk properties). Then, determine how the change in clouds affects the energy balance at the TOA. In the absence of strong feedbacks, ice thickness change will have the opposite sign from the change in TOA CRF. Finally, it is necessary to anticipate how this result might be modified by feedbacks, such as the surface albedo feedback.

Overall, the effect of clouds is essentially the same in the Arctic as for the global climate with two basic modifications. The amount by which arctic clouds increase the net loss of energy to space is less than the global average, since incoming sunlight at the top of the atmosphere in the central Arctic is about half of the global average. Seasonal variations in the impact of clouds are

larger in the Arctic due to large changes in incoming solar radiation at the top of the atmosphere and surface conditions.

The results of this study can be applied to future arctic climate research. The simulated sensitivity of the arctic climate to cloudiness is fundamentally different depending on whether the atmosphere and ice pack are thermodynamically coupled. This suggests that, in future modeling studies of the climatic effect of arctic clouds, it is necessary to permit these interactions in the modeling framework or be aware of the limitations of not doing so. The results indicate that TOA CRF measured in the present climate can be used to predict how sea ice thickness will change in response to changes in clouds. Therefore, it is desirable to have observational estimates of TOA CRF as functions of time of year and cloud height (or type). At lower latitudes, reliable estimates of TOA CRF have been made as a function of season by Harrison et al. (1990) and as a function of cloud type by Hartmann et al. (1992). The extension of these analyses to the Arctic, which hinges on the ability to identify clouds and cloud types, would provide valuable information for improving the understanding of the effect of clouds on the arctic climate.

Chapter 3:

Explaining the Annual Cycle of Arctic Stratus

3.1 Introduction

A prominent feature of the climate over the Arctic Ocean is the annual cycle of low cloud amount which ranges from ~20% in the winter to ~70% in the summer, as shown in Huschke's (1969) analysis* (Figure 3.1). Tao et al. (1996) examined the simulations of arctic climate by nineteen GCM's participating in the Atmospheric Model Intercomparison Project (AMIP). The 10-year mean annual cycles of total cloud amount varied widely among the models, and less than half were even qualitatively similar to surface-based climatological data (see Figure 8 of Tao et al.). This result casts doubt on the ability of typical GCM's to predict changes in cloud amount and associated changes in other elements of the arctic climate. The goal of the research described in this chapter is to identify the factors that control mean low cloud amount over the Arctic Ocean, as

* Huschke's (1969) study, based on 7.5 station-years of surface observations obtained at drifting ice stations during 1955-1960, is the most recently published source of mean *monthly* low cloud amount. The *seasonal* mean low-cloud amount for the summer and winter in the Huschke study are within a few percent of the 30-year averages computed by Warren et al. (1988). Hahn et al. (1995) estimate a negative bias of 5% for total cloud amount observed from the surface during the winter (December - February) at 80-90 N due to poor illumination. Evidence suggests that the illumination bias is substantially larger for upper-level clouds than for lower clouds (Hahn et al. 1995, Warren et al. 1988), which implies that the underestimation of mean low cloud amount during the winter due to the illumination bias is probably not more than 5% in the central Arctic. It is important to note that the monthly values of cloud amount shown in Figure 3.1 do not represent the annual cycle of all condensate in the lowest 2 km of the troposphere since ice crystal precipitation is not reported as 'cloud' by surface observers (Curry et al. 1996). Unfortunately, the climatology of ice crystal precipitation in the Arctic is not known as well as that of clouds since its occurrence has not been recorded consistently in the weather code of surface observations.

recorded by surface observers, by examining the cause of its annual cycle.

Klein and Hartmann (1993) examined the seasonal relationships between the amount of low stratus and other meteorological variables in maritime regions around the world. They found a significant positive correlation between stratus amount and the difference between the potential temperature at 700 mb and the sea surface temperature (SST). By this criterion, the lower troposphere over the Arctic Ocean should be cloudy throughout the year. However, there is much less Arctic stratus during the winter than the summer, despite the extreme stratification of the wintertime arctic lower troposphere. This suggests that the best approach to understanding the cause of the annual cycle of cloud amount is to explain the rarity of low clouds in the winter. An early treat-

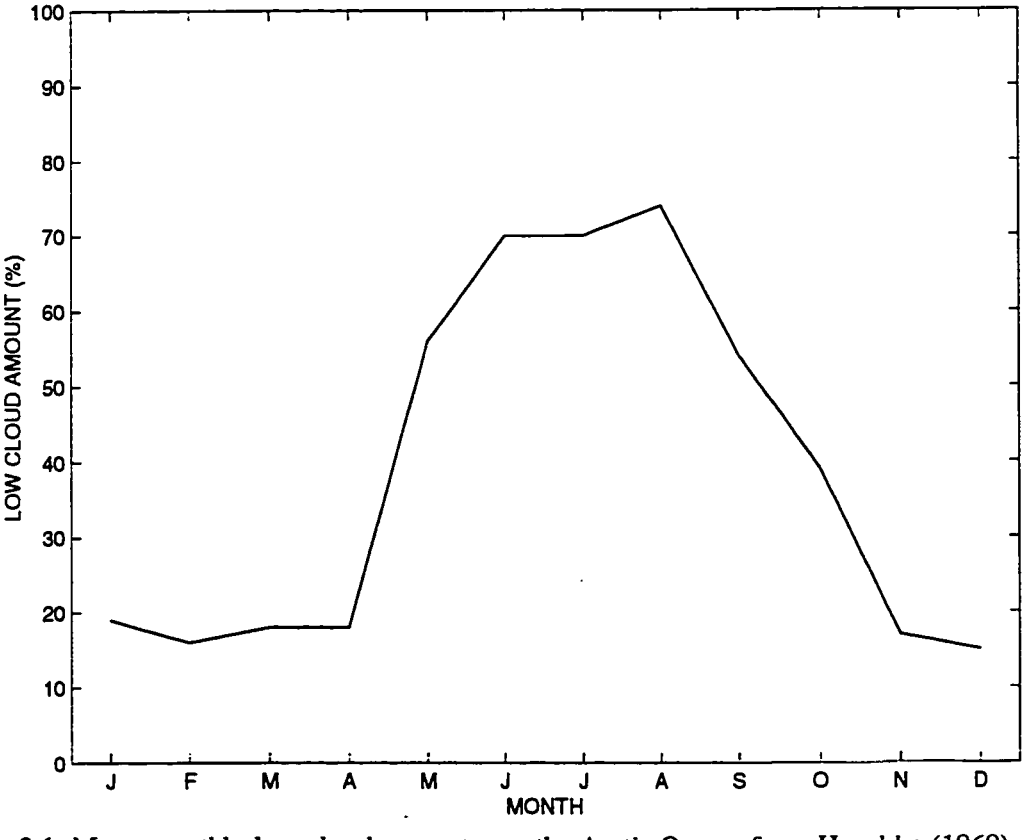

Figure 3.1: Mean monthly low cloud amount over the Arctic Ocean, from Huschke (1969).

ment of this topic was Bjerknes' (1925) explanation of the annual cycle of fog over the Arctic. Bjerknes attributed the formation of fog to the cooling of relatively warm and humid air of continental origin by contact with the polar ice pack. A similar explanation for both fog and stratus was offered by Petterssen (1956), who categorized stratus as an example of advection fog. According to Bjerknes, the onset of summertime fog occurs when the land surrounding the Arctic Ocean becomes warmer than the surface of the pack ice and thus allows the specific humidity of incoming air to exceed that at the surface of the ice pack. This implies that the low amount of fog and stratus in the winter may be explained by the fact that the continents surrounding the Arctic are not warmer than the surface of the ice pack. However, Herman and Goody (1976) suggested that stratus cloud could not persist in the winter due to an insufficient flux of water vapor from the surface of the ice pack. Herman and Goody mentioned two factors that could limit the surface vapor flux in winter: (1) the very low saturation specific humidity of the cold surface and (2) the suppression of turbulent mixing by the strongly stratified temperature profile.

Both of the explanations cited above are based on variations in the supply of water vapor to the lower arctic atmosphere and not on microphysical processes related to atmospheric condensate. Nevertheless, a change in these physics can improve the simulation of the annual cycle of low cloud amount in a GCM. For example, Smith (1990) noted an improvement in the simulation of wintertime cloud amount after introducing a new cloud and precipitation scheme to the GCM of the U.K. Meteorology Office. The former version of the model, which used a diagnostic cloud scheme with no representation of ice microphysical processes, simulated too much low cloud during the winter in the northern high latitudes. Smith attributed the improved simulation of wintertime low-cloud amount by the new version of the model to the more realistic representation of the formation and precipitation of frozen condensate. These results imply that physical processes related to atmospheric ice may be responsible for reducing cloudiness in the winter. If so, these

processes would be an essential part of the explanation of the annual cycle in the amount of low cloud.

In summary, the annual cycle of low-level cloud amount over the Arctic has been attributed to three different controlling factors: (1) the difference between the specific humidity of air entering the Arctic and the saturation humidity at the surface of the pack ice, (2) evaporative flux at the surface of the ice pack, and (3) microphysical processes related to atmospheric ice. None of these explanations has been examined using observations or numerical models, except as part of the study of Smith (1990). Herman and Goody (1976) developed a one dimensional radiative-turbulent cloud model to simulate the formation and evolution of Arctic stratus within an air mass of continental origin as it passes over the melting ice pack. Subsequent theoretical advancements in the representation of sub-grid scale condensation and turbulent mixing were incorporated into turbulence-closure cloud models developed by McInnes and Curry (1995) and Smith and Kao (1996), which were also used to study summertime Arctic stratus. The impact of ice formation on the wintertime atmosphere in arctic regions has been assessed in the modeling studies of Curry (1983) and Lynch et al. (1995). Curry (1983) examined the adjustment of an air mass in the arctic winter using a one dimensional radiative-diffusive model with prognostic condensate. This study demonstrated how the formation and precipitation of ice particles could produce a significant effect on the evolution of the air mass. For example, precipitating ice particles spread the longwave cooling over a deeper layer, instead of concentrating the cooling at the cloud top. Lynch et al. (1995) found that, during the winter, the inclusion of ice-phase microphysics produced an increase in precipitation and cooling through much of the atmosphere in their regional model.

The abundance of cloud condensation nuclei (CCN) is a fourth factor that might in principle control cloudiness in the Arctic. The simplest effect of CCN abundance is to control the size of cloud particles: more particles implies smaller cloud droplets for a fixed amount of condensate.

The fall speed depends on size, such that the characteristic residence time of a cloud particle increases with CCN abundance, all other factors being equal (Albrecht 1989). The abundance of CCN may be closely associated with the presence of pollutants that form arctic haze or biologically produced dimethyl sulfide. The observed frequency of arctic haze is greatest in late winter when the arctic atmosphere is most stable and aerosol removal processes are least active (Shaw 1995). The concentration of dimethylsulfide -- a natural precursor to sulfate aerosols that can act as CCN -- has a pronounced annual cycle in the lower atmosphere over the Arctic Ocean, apparently in response to marine productivity in open water areas (Aagaard et al. 1996). The possible effects of aerosol on arctic clouds are reviewed in Curry et al. (1996), who conclude that variations in CCN are probably important in determining variations in the optical and microphysical properties of arctic clouds. Nevertheless, it remains uncertain whether the wintertime concentrations of CCN are sufficiently small to exert primary control on the occurrence and persistence of low clouds, i.e. on mean cloudiness. In this paper, it is assumed that the concentration of CCN is sufficient throughout the year to produce non-precipitating cloud droplets in an environment supersaturated with respect to liquid water.

In the present study, the summer and winter cloud regimes are simulated using a one-dimensional radiative-turbulent cloud model that includes basic mixed-phase microphysical processes. The model is integrated in an Eulerian frame of reference for a period sufficient to produce a stationary climatic state that is purely a function of the boundary conditions and the representation of physical processes within the model. The chapter proceeds as follows. In Section 3.2, climatological data are discussed in the context of the three hypotheses. The modeling framework, model equations, and boundary conditions are described in Sections 3.3 and 3.4. In Sections 3.5 and 3.6, the simulations of the summer and winter climates are presented, along with experiments designed to test the hypotheses. In Section 3.7, the results are applied to the problem of simulating

the annual cycle of cloudiness over the Arctic using GCM's.

3.2 Review of climatological data

The essential features shown on Figure 3.1 are the large difference between winter and summer low cloudiness and the rapid transitions between these values. We wish to investigate whether these qualitative features can be explained by the annually periodic time dependencies of the following: (a) the specific humidity difference between arctic land and ocean regions, (b) the evaporative flux from the ice pack, and (c) ice-phase precipitation processes. As a first step, we review times series plots of the mean annual cycles of each factor, or of proxies that represent each factor.

3.2.1 Specific Humidity Difference between Land and Ocean

The explanation of Bjerknes (1925) and Petterssen (1956) implies that the difference in specific humidity between the land and the pack ice should be greater during the summer than during the winter, with transitions in October and May. The annual cycles of surface air specific humidity at 70 N and 80 N along longitudes of 120 E (Siberia) and 150 W (Alaska) shown in Figure 3.2 represent typical contrasts between land near the coast and the arctic pack ice. The plots show the humidity over Siberia dropping below that over neighboring ocean during the winter, when the land becomes colder than the ice pack. The difference in specific humidity at both locations is indeed greatest during the summer, when the land temperatures exceed freezing, and least during the winter. The transitions are not sharply defined but appear to be approximately concurrent with transitions in low cloud amount, except for the autumn transition in Siberia which occurs about a month early. These data do not indicate when the relatively warm and humid continental air is being carried over the pack ice, as is believed necessary for the formation of stratus. This

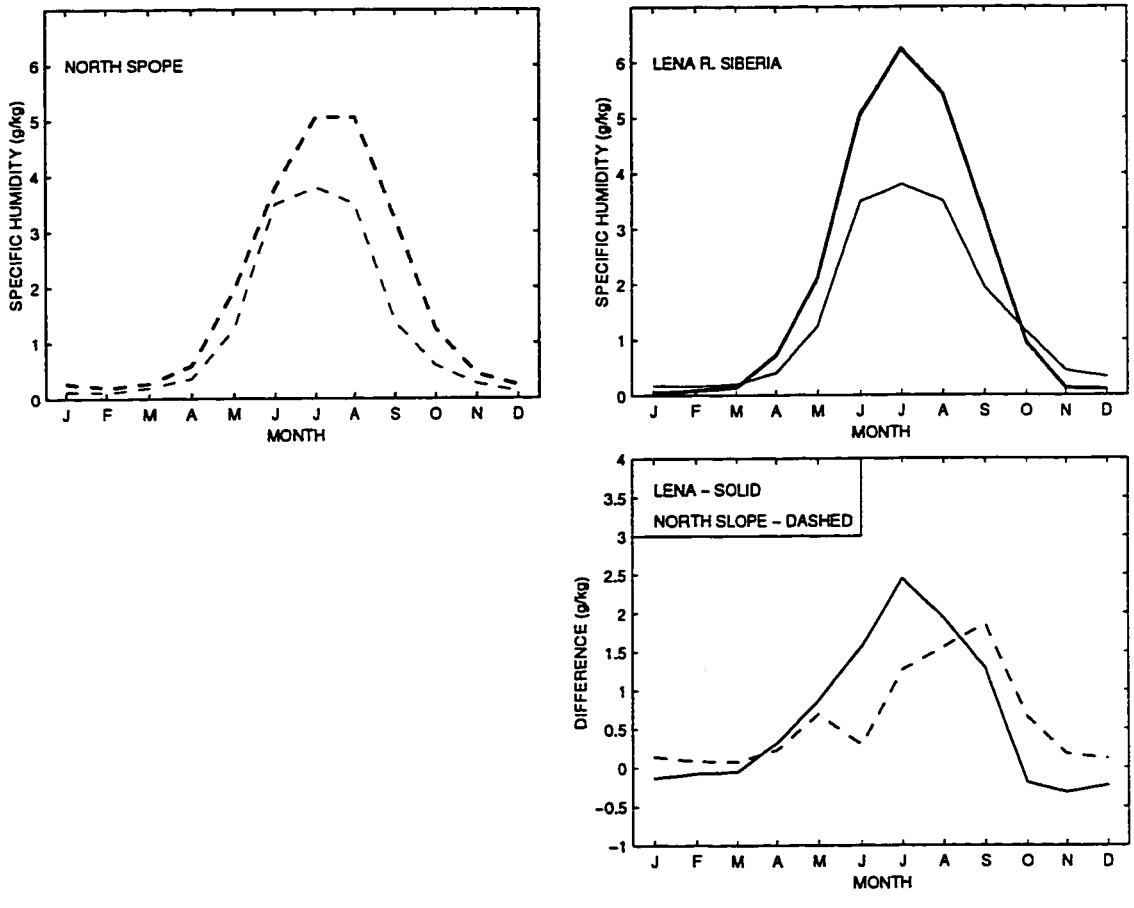

Figure 3.2: Surface air specific humidity at latitudes 70N (thick line) and 80 N (thin line) for (a) the North Slope of Alaska (150 W) and (b) the Lena River region of Siberia (120 E); (c) the difference in surface air specific humidity between 70 N and 80N. Data are from Crutcher and Meserve (1970). At both locations, 70 N is less than 200 km inland and 80 N is perennially ice-covered.

information is provided by measurements of the net moisture flux across the lateral boundaries of the Arctic. Walsh et al. (1994) have estimated this transport through the full depth of the atmosphere based on statistical analyses of rawinsonde data from stations surrounding the Arctic Ocean (Figure 3.3). Like the annual cycle of low cloud amount, the estimated time series exhibits a pronounced difference between winter and summer regimes of moisture advection, and fairly sharp transition seasons. It should be noted that the data are not consistent with the hypothesis that the spring transition in moisture advection causes the spring transition in low cloud amount, because the latter variable increases toward its summer plateau one month before the former.

The climatological data do not contradict Bjerknes' explanation of the annual cycle of low cloud amount. A time series of moisture flux into the Arctic in the lowest 1 or 2 km of the atmosphere would enable a more informative analysis of this explanation for low cloud amount.

3.2.2 Surface Evaporative Flux

Surface evaporation is a major source of water vapor for boundary layer stratiform clouds in subtropical oceanic regions of large scale subsidence. The basic features of these clouds are well-described by the mixed layer cloud model of Lilly (1968), in which evaporation at the surface is the only source of moisture. Aircraft observations of Arctic stratus by Tsay and Jayaweera (1984) include examples of surface based mixed layer clouds and others that are decoupled from the surface, suggesting that a mixed layer cloud model and surface evaporation may be relevant to some meteorological situations that occur in the Arctic. The subtropical low-level stratiform clouds simulated by the Lilly model would disappear if the surface evaporation were turned off, but this cannot occur over the relatively steady SST's in low latitudes. The surface conditions of the Arctic ice pack undergo substantial variations that may produce seasonal changes in cloud amount by controlling the evaporative flux. A rough estimate of the evaporative moisture flux over

the Arctic Ocean was obtained by Walsh et al. (1994) as a residual from other components of the moisture budget (Figure 3.3). The dotted line in Figure 3.3 is a direct estimate of the large scale surface evaporative flux based on the thermodynamic model of Maykut (1982) which resolves the thickness distribution of sea-ice, including open water. Both estimates reach a maximum in the summer and are approximately zero during the winter, with transitions at approximately the same time of year as that of low cloud amount. If the formation and persistence of Arctic stratus depend on surface evaporation as a source of moisture, then it is plausible that the small amount of stratus

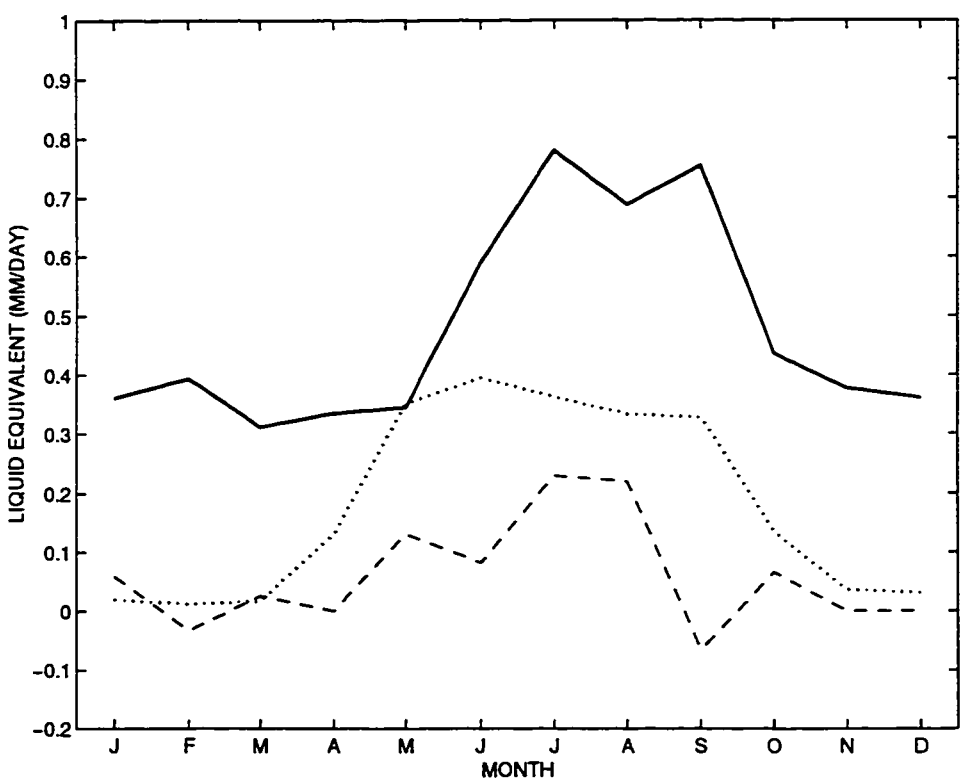

Figure 3.3: Mean monthly moisture flux convergence (solid) and evaporation (dashed) over the Arctic Ocean (in Kg m^{-2} d^{-1} or mm d^{-1} liquid equivalent) based on Walsh et al. (1994). Evaporation is computed as a residual from direct estimates of moisture flux convergence, precipitation, and vapor storage. Values are 18-year means for the region poleward of 70 N from 120 E eastward to 120 W and poleward of 80 N from 120 W eastward to 120 E. The dotted line is a model-derived estimate of large-scale evaporation by Maykut (1982).

during the winter is caused by an insufficient upward moisture flux at the surface.

3.2.3 Ice precipitation processes

The potential for atmospheric ice to influence the annual cycle of low-cloud amount is based on the following facts: (1) the latent heat of vaporization of ice is greater than that of liquid water and (2) the concentration of ice nuclei is several orders of magnitude smaller than that of cloud droplet condensation nuclei. A consequence of the former property is that the saturation vapor pressure over ice is lower than that over liquid water at temperatures below the triple point of water, which causes ice particles to grow by vapor deposition in an environment sub-saturated with respect to liquid water. Since the concentration of ice nuclei is much smaller than that cloud condensation nuclei (CCN), a given mass of condensate is distributed among a smaller number of larger particles if it is frozen as opposed to liquid. that grow rapidly to precipitable sizes in air that is supersaturated with respect to ice. The formation of atmospheric ice can affect the mean amount of low arctic clouds by favoring condensate with a short residence time (ice) over condensate with a long residence time (liquid droplets). The modeling study of Starr and Cox (1985) suggests that differences in the amount and vertical distribution of condensate between altostratus and cirrus cloud can be explained by the difference in fall speed between liquid droplets (altostratus) and ice particles (cirrus). The elimination of mid- and low-level stratiform clouds by ice phase microphysical processes in mid-latitudes has been observed and described by Hobbs and Rangno (1985). In summertime aircraft measurements of clouds over the Beaufort Sea, Hobbs and Rangno (1996) occasionally observed high concentrations of ice particles (tens per liter) and localized dissipation of cloud due to ice particles precipitating from above. The impact of atmospheric ice processes on the evolution of arctic clouds during winter has not been documented, but the observation of ice crystal precipitation during the cold months (e.g. Curry et al. 1990) suggests that ice phase pro-

cesses may be at work. In fact, the deposition of water vapor directly onto ice crystal precipitation may be viewed as the preemptive dissipation of stratus by keeping the humidity below saturation with respect to water.

The rate of water vapor deposition is determined by several factors, including the difference between the environmental vapor pressure and the saturation vapor pressure over ice and the concentration of ice nuclei or frozen precipitates that serve as deposition sites (see equation (3.5)). Although the concentration of ice particles is typically greater at lower temperatures (Fletcher 1966), the factors that control the concentration of ice nuclei are not known. Observations by Hobbs and Rangno (1985, 1996) and Heymsfield (1977) indicate ice particle concentration is not related simply to temperature. For a given population of ice particles in a saturated environment (with respect to liquid), the rate of vapor deposition onto ice particles increases with decreasing temperature. Therefore, one might expect that atmospheric ice deposition would cause a decrease in low cloud amount with decreasing temperature, and thus produce the annual cycle of low cloud over the Arctic Ocean, even if advection of moisture and surface evaporation were constant throughout the year. According to this hypothesis, the mean temperature of the lower troposphere should have approximately the same value during the spring and fall cloud transition periods. This "threshold" temperature can be estimated by comparing the annual cycles of low cloud amount (Figure 3.1) and lower tropospheric temperature, represented by the 850 mb temperature in Figure 3.4. Spring and fall transitions both occur when the 850 mb air temperature is about -13 C, which is consistent with this hypothesis. A better evaluation of the hypothesis could be obtained by analyzing simultaneous observations of low-cloud properties and lower tropospheric air temperature.

To summarize, inspection of climatological mean annual cycles of moisture advection, surface evaporation, and atmospheric temperature indicates that all three explanations are qualita-

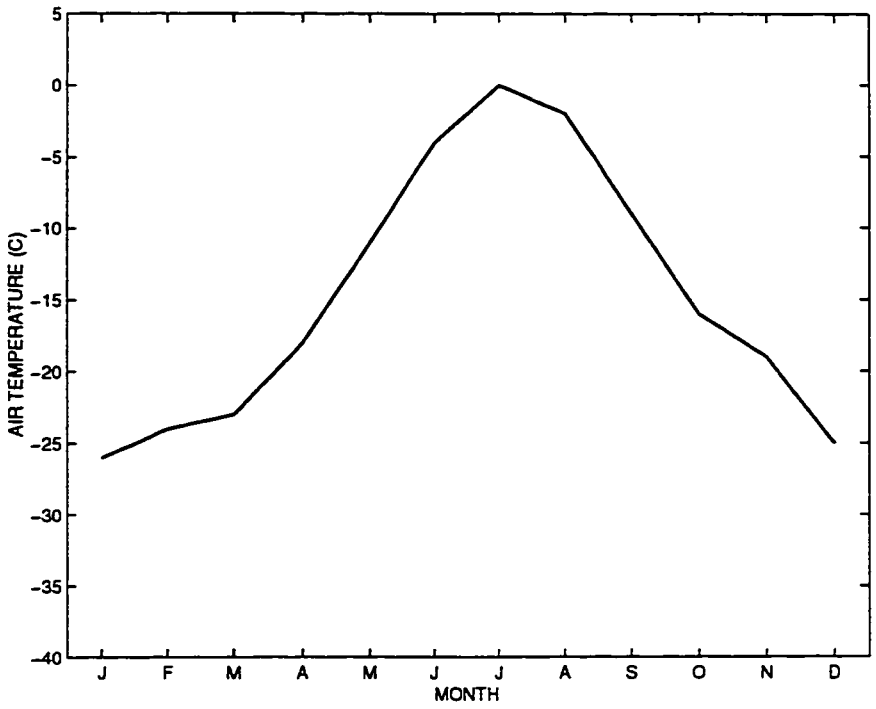

Figure 3.4: Mean monthly 850 mb air temperature near 80 N, 180 W from Crutcher and Meserve (1970).

tively viable. The assessment of these hypotheses is limited by the availability of analyzed data, although more information can be gained analyzing existing data archives. Nevertheless, it is possible to conduct a more thorough investigation that indicates how the *essential qualitative features* (small low-cloud amount in the winter, large low-cloud amount in winter) depend on *quantitative* prescriptions of water vapor advection, evaporation, and temperature-dependent ice-phase processes. This investigation is based on a physical model for the atmospheric column.

3.3 Model description

3.3.1 Modeling framework

The hypotheses are evaluated using a column model of the arctic atmosphere. The column extends vertically through the full depth of the atmosphere and covers an area of approximately $(100\ \text{km})^2$ over the perennially ice covered Arctic Ocean. The model is depicted schematically in Figure 3.5. Basic principles of conservation of energy, conservation of water substance, and conservation of momentum are applied to the column state variables to obtain a closed system of time-dependent equations similar to equations governing a single column in a GCM. In this framework, the state of the column, including a description of atmospheric condensate, evolves in response to prescribed time-dependent boundary conditions and to physical processes acting within the column. The boundary conditions are incoming solar radiation at the top of the atmosphere, vertical profiles of moisture advection, temperature advection and divergence at the lateral boundaries of the column, and open water fraction and sea-ice thickness at the bottom. The surface energy balance and surface temperature of the sea-ice are calculated internally as part of the model solution. Physical processes acting within the column include radiative transfer, vertical mixing by turbulent eddies, microphysical processes related to clouds and precipitation, and heat conduction through the sea-ice. By perturbing the prescribed vertical profile of moisture advection, the first hypothesis can be tested. By perturbing coefficients within the model, it is possible to artificially suppress or enhance surface evaporation and ice-phase precipitation physics to test the second and third hypotheses. These physical processes may be viewed as potentially necessary agents that translate the annual cycles of the boundary conditions into the annual cycle of low cloud amount.

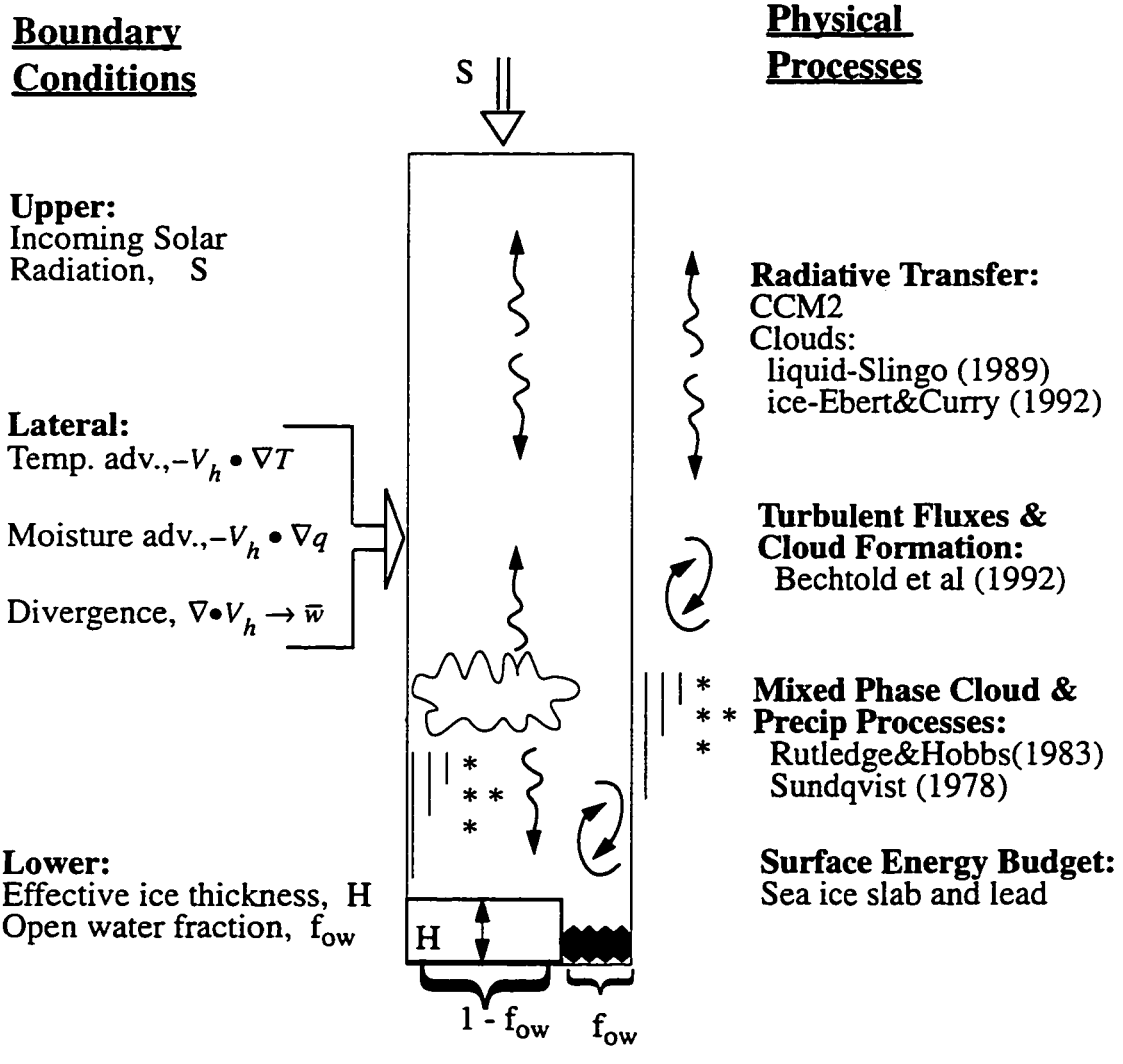

Figure 3.5: Schematic diagram of the arctic column model.

3.3.2 Atmosphere

The model atmosphere is governed by prognostic equations for liquid water potential temperature (θ_l), total (liquid plus vapor) water mixing ratio (q_w), ice mixing ratio (q_i), precipitating liquid water mixing ratio (q_r), horizontal winds, and turbulent kinetic energy. The variables and symbols are defined in the Appendix. Cloud liquid water (q_l), cloud fraction (f_c), and turbulent fluxes ($w'\theta_l'$ and $w'q_w'$) are computed diagnostically at each time step and each model level from the prognostic variables, using the 1.5-order turbulence-closure cloud model of Bechtold et al. (1992). For the purpose of comparing the model results to surface observations, instantaneous low-cloud amount is defined as the maximum value of f_c in the (39) model layers between the about 50 and 2000 m*. Mean low-cloud amount is the time average of instantaneous low cloud amount. In this definition, atmospheric ice is not recognized as a contributor to low cloud amount, which is consistent with the practice of not including ice crystal precipitation in the climatology of low cloud shown in Figure 3.1†. The vertical grid with a spacing of the atmospheric model (Δz) is 50 m through the lowest 3 km and becomes increasingly wide at greater altitudes. The model time step is 10 s, except for the computation of radiative fluxes and turbulent length scales which occur at intervals of 360 s and 60 s, respectively.

Prognostic equations pertinent to the present topic are the following:

$$C_p\frac{\partial\theta_l}{\partial t} = -C_p\frac{\theta}{\bar{T}}\bar{V}\cdot\nabla\bar{T} - C_p\bar{w}\frac{\partial\theta_l}{\partial z} - \frac{C_p}{\rho}\frac{\partial}{\partial z}\left(\rho\overline{w'\theta_l'}\right) - \frac{1}{\rho}\frac{\partial F_{rad}}{\partial z}$$
$$+\frac{\theta}{\bar{T}}L_v\left(C_l + A_l - E_r\right) + \frac{\theta}{\bar{T}}L_f\left(-M_i\right) + \frac{\theta}{\bar{T}}L_s\left(I_i - E_i\right), \qquad (3.1)$$

* This definition excludes the lowest model level so that the occurrence of steam fog over open water during winter does not affect the statistics of low cloud.

† The mass and phase of lower tropospheric condensate are also used when comparing model experiment.

$$\frac{\partial q_w}{\partial t} = -\vec{V}\cdot\nabla q_v - w\frac{\partial q_w}{\partial z} - \frac{1}{\rho}\frac{\partial}{\partial z}(\rho q_w' w') + E_r + E_i - C_l - A_l - I_i, \tag{3.2}$$

$$\frac{\partial q_i}{\partial z} = \frac{1}{\rho}\frac{\partial}{\partial z}(\rho q_i \bar{v}_i) + I_i - E_i - M_i, \tag{3.3}$$

$$\frac{\partial q_r}{\partial z} = \frac{1}{\rho}\frac{\partial}{\partial z}(\rho q_r \bar{v}_r) + C_l + A_l + M_i - E_r. \tag{3.4}$$

The equations for horizontal winds and turbulent kinetic energy (not reproduced here) are identical to Bechtold et al. (1992).

Processes affecting θ_l, on the right hand side of (3.1), are horizontal temperature advection, vertical temperature advection, turbulent heat flux, radiative transfer, and latent heat transfer associated with processes that convert water from one form to another. Processes affecting q_w in (3.2) are horizontal moisture advection, vertical moisture advection, turbulent moisture flux, the evaporation (E_r) of q_r, the evaporation (or deposition) (E_i) of q_i, the collection (C_l) of q_l by q_r, the autoconversion (A_l) of q_l to q_r, and the initiation (I_i) of q_i from vapor. The horizontal advection term in (3.2) is the prescribed boundary condition associated with the first hypothesis. Terms related to the horizontal advection of cloud liquid water q_l are ignored and are omitted from (3.1) and (3.2).

The rate of change of q_i in (3.3) is affected by the precipitation of q_i, and the initiation (I_i), evaporation (or deposition) (E_i), and melting (M_i) of q_i. The physical parameterization of the evaporation/deposition term (E_i) is associated with the third hypothesis. Processes affecting the rate of change of q_r in (3.4) are precipitation fallout, the collection (C_l) and autoconversion (A_l) of q_l, the melting (M_i) of q_i, and the evaporation (E_r) of q_r. Figure 3.6 illustrates the transformations between the various forms of water substance represented by the model. The bulk fall speeds of

ice and liquid precipitation are defined as positive downwards.

The autoconversion of cloud liquid water to precipitating liquid is modeled following Sundqvist (1978) and Smith (1990) as $A_l = c_l\{1 - \exp[-(q_l^*/q_{lo})^2]\}q_l$, where $c_l = 10^{-3}$ s^{-1}, $q_l^* = q_l/f_c$, and $q_{lo} = 0.4$ g kg^{-1}. The bulk fall velocity of liquid precipitation ($\overline{V}_r$) and the remaining microphysical processes pertaining to liquid condensate (C_l, E_r) are treated using the bulk moisture model of Rutledge and Hobbs (1983). When air is below freezing temperature and supersaturated with respect to ice, the initiation of atmospheric ice is computed as $I_i = c_i$ max (N_i m_{io} - q_i, 0), where $c_i = 0.01$ s^{-1}, m_{io} is the assumed mass of an ice particle when first nucleated (10^{-12} kg),

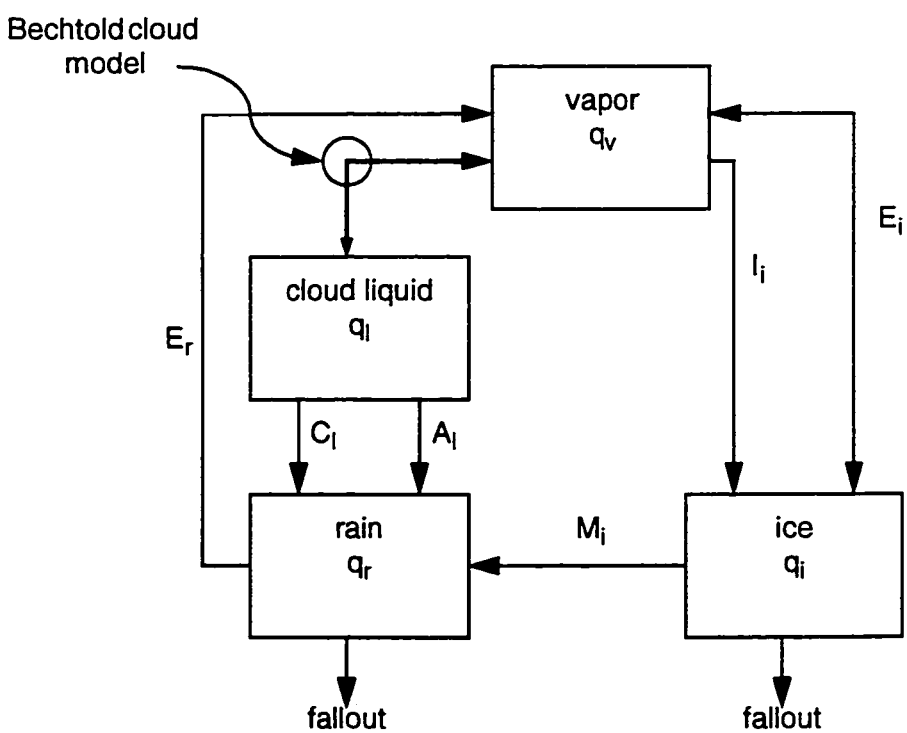

Figure 3.6: Conversions of water substance from one form to another.

and N_i is the specified number concentration of ice particles. N_i is 10 l^{-1} during the winter based on observations in cold environments by Curry et al. (1990) and Heymsfield (1977), and N_i= 1 l^{-1} during the summer based on Hobbs and Rangno (1996). The role of I_i is to produce ice particles in cold, supersaturated environments where there are no ice particles. Ice particle initiation can only occur in the model when the mixing ratio of atmospheric ice is very low (e.g., $q_i < 10^{-5}$ g kg^{-1} in winter); the evolution of q_i is controlled by other processes after ice particles are first introduced.

Evaporation and deposition at the surface of ice particles are modeled similarly to Rutledge and Hobbs (1983):

$$E_i = \frac{1}{\rho} \frac{4 D_i N_i F_v}{F_d + F_c} \frac{e_{si} - e}{e_{si}} , \tag{3.5}$$

where the ice particle diameter (D_i) is a function of q_i and N_i, the ventilation factor (F_v) is assumed to be 1, the factors F_d and F_c are related to the diffusivity and conductivity of water vapor, e is the environmental vapor pressure, and e_{si} is the saturation vapor pressure with respect to ice. Environmental vapor pressure is related to water vapor mixing ratio by the equation, $q_v = 0.622e/(p - 0.378e)$. The saturation vapor pressure with respect to ice can be computed as

$$e_{si}(T) = e_{si}(T_f) \exp\left[-\frac{L_s}{R_v}\left(\frac{1}{T} - \frac{1}{T_f}\right)\right] , \tag{3.6}$$

where T_f is the freezing point temperature of water, at which the saturation vapor pressure is the same over ice and water. Growth by deposition ($E_i < 0$) occurs when the water vapor mixing ratio of the environment exceeds saturation with respect to ice ($q_v > q_{si}$). The melting of ice particles into precipitating liquid is given by $M_i = c_i\, q_i$, when $T > T_f$. The bulk fall speed of ice particles is computed as a function of q_i based on the empirical relationship derived by Heymsfield (1977):

$$\bar{V}_i = 100\, (\rho\, q_i)^{0.17} \text{ cm/s}, \tag{3.7}$$

where (ρ q_i) is in g m^{-3}.

The convergence of radiative energy fluxes ($\frac{\partial F_{rad}}{\partial z}$) is computed using the radiative component from the second version of the NCAR Community Climate Model (CCM2), which employs a δ-Eddington approximation for shortwave bands and a broad band method for clear sky longwave radiation (Hack et al. 1993). For longwave radiation, liquid cloud is modeled as a grey body occupying a fraction (f_c) of a model layer with an emissivity of $\varepsilon_l = 1 - \exp(-k_l W_l)$, where k_l is the absorption coefficient and W_l the liquid water path. Shortwave optical properties of liquid cloud are computed as functions of W_l and effective cloud droplet radius (r_{el}) using the parameterization of Slingo (1989). The constants k_l and r_{el} are 0.1 $m^2 g^{-1}$ and 10 μm, as in the CCM2; and liquid water path is computed as $W_l = \rho\, q_l\, \Delta z / f_c$, where q_l and f_c are provided by the Bechtold cloud scheme.

The radiative properties of atmospheric ice are treated analogously to liquid clouds using the parameterization of Ebert and Curry (1992). The longwave absorption coefficient k_i is represented as a function of the ice particle effective radius (r_{ei}) and shortwave optical properties are functions of r_{ei} and ice water path, $W_i = \rho\, q_i\, \Delta z$. The two general classes of ice in the arctic atmosphere are cirriform cloud particles found in the upper troposphere and ice crystal precipitation and snow found mainly in the lower troposphere. The present one-dimensional model is intended for the study of stratus clouds and microphysical processes occurring in the lower troposphere, and does not include dynamical processes that are believed important for the formation and maintenance of cirriform clouds (see e.g. Starr and Cox 1985). Therefore, upper level cirrus clouds are prescribed at randomly chosen heights between 3 and 8 km. The frequency (50%) and amount-when-present (50%) of the cirrus clouds are based on the climatology of by Warren et al. (1988),

and W_i is set to 5 g m^{-2}. The ice water path of model-produced ice is tapered off to zero above 4 km since the radiative properties of ice in the upper troposphere are already represented by the prescribed cirrus clouds. The effective radius of ice particles is 14 μm for cirrus cloud and 40 μm for lower tropospheric precipitating ice, following Curry and Ebert (1992). When cloud liquid and ice coexist in a given model layer, the cloud fraction for radiative computations is set to f_c (when $q_l > q_i$) or 100% (when $q_i > q_l$), and the cloud radiative properties of ice and liquid clouds are combined using equation 14 of Rockel et al. (1991).

3.3.3 Surface fluxes

Upward radiative and turbulent fluxes at the lower surface of the atmosphere are computed independently over sea-ice and liquid water surfaces. Energy flux convergence near the surface of the ice is given by

$$F_{net} = F^{\downarrow}_{LW} - F^{\uparrow}_{LW} + (1-\alpha_s)F^{\downarrow}_{SW} - F^{\uparrow}_{LH} - F^{\uparrow}_{SH} + F_{CND}, \quad (3.8)$$

where $F^{\uparrow}$ and $F^{\downarrow}$ denote upward and downward fluxes of longwave radiation (LW), shortwave radiation (SW), sensible heat (SH), latent heat (LH), and conduction (CND), and α_s is the surface albedo. $F^{\uparrow}_{SH}$ and $F^{\uparrow}_{LH}$ are computed following Holtslag and Boville (1993). Conduction is computed as $F_{CND} = k_i (T_b - T_s)/H$, where T_b is the prescribed temperature at the bottom of the ice (-1.9 C), k_i is the thermal conductivity of sea-ice, and H is the prescribed ice thickness. Over the liquid water portion, which represent both leads and melt ponds, fluxes other than F_{CND} are computed using a prescribed surface temperature of 0 C and a surface albedo of 0.1. The fluxes over sea-ice are computed similarly except that a surface albedo of 0.7 is prescribed, and the surface temperature T_s is computed such that $F_{net} = 0$. When the computed sea-ice surface temperature exceeds the melting point, the surface is assumed to be melting and surface fluxes are computed using a sur-

face temperature of 0 C. The surface fluxes seen by the model atmosphere are the area-weighted averages over the liquid water and sea-ice portions.

The surface latent heat flux $F^{\uparrow}_{LH}$ provides the lower boundary condition on the turbulent flux term in (3.2). The second hypothesis can be addressed by changing the transfer coefficient in this surface flux term.

3.3.4 Appraisal of model components

The present application of the column model is to simulate the features that distinguish the summer and winter cloud regimes observed over the Arctic Ocean. The model includes processes that are necessary to describe the boundary layer stratiform clouds of lower latitudes, plus mixed-phase microphysical processes that probably play a role in the Arctic. The schemes used to represent the processes have been tested by the people who developed them, and most are used routinely in other models. Data from the Atlantic Stratocumulus Transition Experiment (ASTEX) may be used to test some components of the present model -- especially Bechtold's cloud and mixing scheme -- by comparing model output with the observed time evolution of a cloudy marine boundary layer (Bretherton and Pincus 1995; Bretherton et al. 1995). The model was integrated in a Lagrangian frame of reference using a lead fraction of 100% and prescribed time series of surface temperature, divergence, and upper air temperature and humidity, as observed at ASTEX. The height of the simulated cloud top closely tracked the observations of the cloud top as it rose from ~600 to ~1400 m during the 42-hours of observation. A comparison of simulated and observed profiles of potential temperature indicated that the model accurately captures the time at which the cloud-topped mixed layer decouples from the surface. The modeled precipitation also was in good agreement with observations. The results from the ASTEX simulation demonstrate, to the extent currently possible, the ability of the model to simulate cloudy mixed layers both when they are

well mixed down to the surface and when decoupled from the surface, as is often the case in the Arctic (e.g., Tsay and Jayaweera 1984).

It is important to test the role of ice phase microphysics in the model since these processes are not well observed in the Arctic and play an important role in the third hypothesis. Unfortunately, well constrained observations like the ASTEX data set are not available for mixed-phase boundary layer clouds, preventing us from performing a similar test of the model's representation of ice processes. Instead, we examine the sensitivity of the model to variations in parameters whose values are not well known in the Arctic. The sensitivity of the model to two key parameters -- ice particle fall speed and ice particle concentration -- is examined in the Section 3.5.3.

3.4 Forcing

Incoming solar radiation at the top of the atmosphere is computed as a function of time at a latitude of 80 N, resolving the diurnal variations. For the summertime we assume a fixed date of July 19. Open water fraction and sea-ice thickness at the bottom boundary are prescribed constants for each season. Sea-ice thickness of 4 m is prescribed in both summer and winter. This rather large value of ice thickness takes into account the thermal effect of snow, which is not treated explicitly in the model. Ice thickness is irrelevant during the summer since the melting surface is always at 0 C. Open water fraction within the ice is 3% in winter and 20% in summer, based on the satellite-derived climatology of Gloersen et al. (1992). With albedos of 0.7 for ice and 0.1 for open water, this produces an area-averaged surface albedo of 0.58 in summer. Integrating the model in an Eulerian reference frame requires that the profiles of water vapor advection ($-\vec{\nabla} \cdot \nabla q_v$), temperature advection ($-\vec{\nabla} \cdot \nabla T$), and divergence be prescribed at the lateral boundaries. The profile of large scale vertical motion (ω) (expressed in pressure coordinates) can be calculated from the pro-

file of divergence using the continuity equation.

Time-dependent profiles of advection and large scale vertical motion are available in the form of gridded fields produced by assimilating rawinsonde and surface observations into a general circulation model (e.g. Schubert et al. 1993). However, the accuracy of these data depends on the accuracy and density of rawinsonde and surface measurements and the ability of the host model to simulate the evolution of the weather in the region of question. Since very little information about the weather over the Arctic Ocean is available, reanalyses are influenced strongly by the physics of the host model in the Arctic. The direct use of advection and vertical motion terms from current gridded analyses may be inadvisable for the study of mean arctic climate. Nevertheless, these analyses do provide valuable statistical information about the variability in the these terms associated with large-scale cyclones and anticyclones, which most GCM's can simulate accurately. Furthermore, simulations forced by the full spectrum of natural variability may require long integrations to compile statistics that represent the steady state climate. Because the hypotheses are related to qualitative climatic features, we can test them in a clear fashion using idealized forcing that has the essential features of the climatological mean and natural variability.

Let the symbol $X_i(p,t)$ stand for the time dependent profile of any of the lateral forcing terms (i): moisture advection, temperature advection, or divergence. In the present study, X is expressed as the sum of mean and randomly varying components:

$$X_i(p,t) = \overline{X}_i(p) + z(t)\, X_i'(p), \tag{3.9}$$

where $\overline{X}_i(p)$ is a mean forcing profile, z(t) is a zero-mean random process, and $X_i'(p)$ is a time-independent perturbation profile. $\overline{X}_i(p)$ is obtained from climatological budget analyses and general circulation statistics. The frequency spectrum of z(t) and the vertical structure of $X_i'(p)$ are

estimated from an empirical orthogonal function (EOF) analysis of time-dependent profiles extracted from a gridded atmospheric reanalysis at grid points over the Arctic Ocean.

The mean component of the lateral forcing terms are shown in Figure 3.7. The non-dimensional profiles of vertical motion and water vapor advection can be scaled using information from Table 3.1. The mean profiles of large scale vertical motion used for the summer and winter simulations exhibit weak subsidence through the troposphere and maximum downward motion at

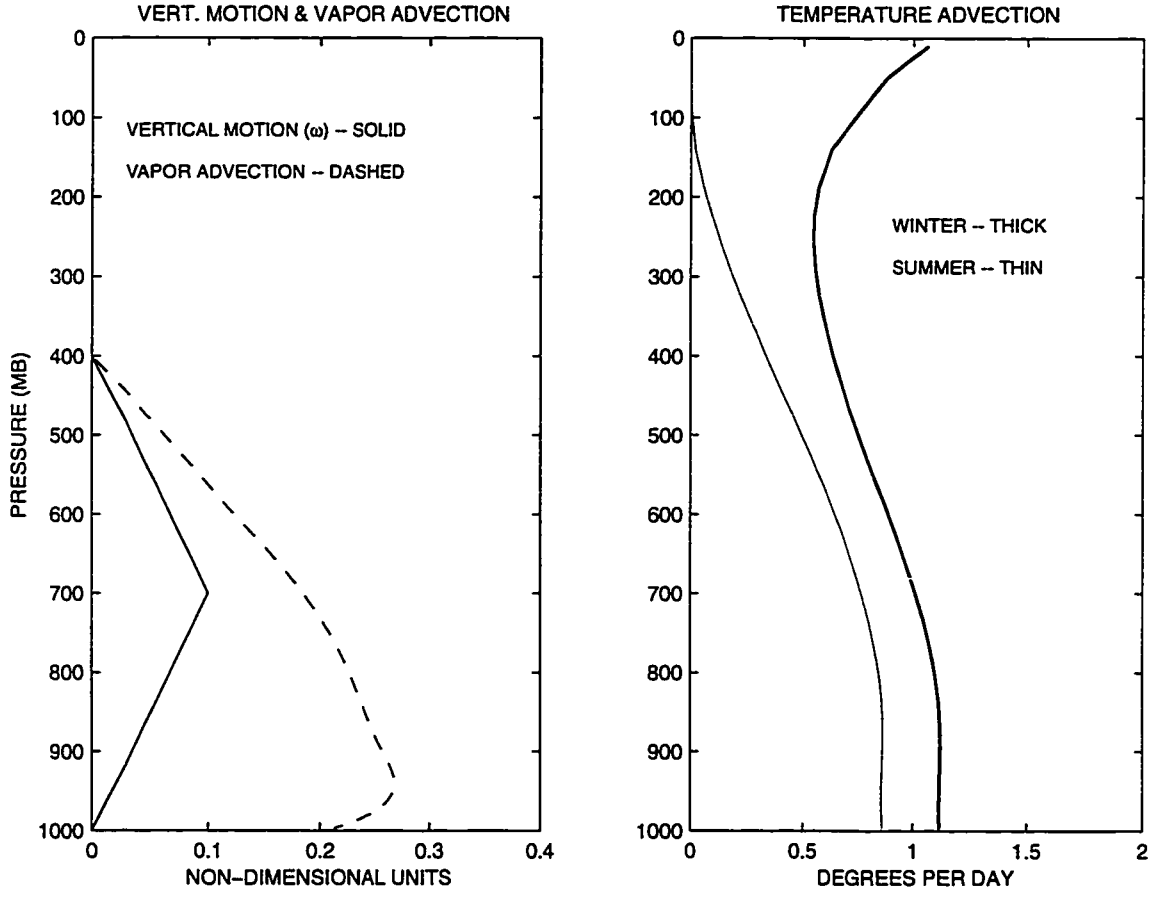

Figure 3.7: Profiles of $\overline{X}(p)$, the mean component of lateral forcing terms. (a) Non-dimensional profiles of large-scale downward vertical motion (ω) and water vapor advection $-\vec{\nabla} \cdot \nabla q_v$ that can be scaled using information in Table 3.1. (b) Mean temperature advection profiles for summer (thin line) and winter (thick line).

700mb, based on Figure 7.19 of Peixoto and Oort (1992). The mean profile of water vapor advection reaches a maximum near 950 mb and decreases with height, similar to the mean profile of water vapor flux across the boundary of the Arctic Ocean depicted in Figure 2 of Walsh et al. (1994). A normalized profile with this shape is scaled so the vertically integrated mean moisture advection, including the estimated effect of the mean meridional circulation, matches the seasonal average for summer or winter, as shown in Figure 3.3. The mean vertical profile of temperature advection in the stratosphere adjusted to balance the radiative cooling rate of the model when the observed mean temperature profile is prescribed (for each season)*. The mean component of temperature advection in the troposphere has a broad maximum centered at ~900 mb, similar to the mean profile of poleward energy flux shown in Figure 3a of Overland and Turet (1994). The magnitude of the lower atmospheric temperature advection is adjusted so that the total vertically-integrated convergence of moist static energy contributed by lateral forcing matches the seasonal averages estimated for the Arctic Ocean region (139 W m^{-2} in winter and 98 W m^{-2} in summer). These values are estimated using mean monthly estimates of poleward energy flux across 70 N by Overland and Turet (1994) and latitude-dependent estimates of the annual mean energy budget at the top of the atmosphere from Hartmann (1994).

The variable component of the lateral forcing terms (X_i', i= ω, $-\hat{\nabla} \cdot \nabla T$ and $-\hat{\nabla} \cdot \nabla q_v$) should represent the intraseasonal variability of a given term and its covariance with the other two terms. This was achieved by extracting time series of the three forcing profiles at Arctic grid points of the NASA/DAO Reanalysis (Schubert et al. 1993). Each time-dependent profile from the reanalysis consists of two months of 6-hourly realizations (240), interpolated to four equally

* The total energy flux convergence by large-scale circulation (including subsidence) is cast as temperature advection in the lateral forcing of the model stratosphere.

spaced pressure surfaces between the surface and 600mb. Normalized profiles ($\hat{X}_i$) were computed for each term using their mean and standard deviation (σ_i)*, and these were combined into a single 12-point vector with 240 realizations: $\bar{X} = \begin{bmatrix} \hat{X}_T \\ \hat{X}_q \\ \hat{X}_\omega \end{bmatrix}$. The first EOF vector ($E_1$) and corresponding expansion coefficient time series ($z_1(t)$) of $\bar{X}$ were then computed. This procedure was carried out at two different locations over the Arctic Ocean during the summer and winter, for a total of four cases. In each case, the first EOF explained about half ($f_1 = 50\%$) of the total variance. The patterns of the first EOF vectors were very similar among the four cases examined.

The first EOF vectors of the four cases are averaged into a single 12-point vector, $\langle E_1 \rangle$. This vector is divided into three vectors, each of which has four points corresponding to pressure surfaces in the lower atmosphere. Each of the three vectors is a normalized perturbation profile ($\xi_i(p)$) of one of the three forcing terms. The perturbation profiles are interpolated to model pressure levels as shown in Figure 3.8. The profiles indicate that positive perturbations in temperature advection in the lower troposphere are associated with positive perturbations in vapor advection and negative perturbations in omega (i.e. upward motion), which is consistent with the well-known fact that relatively warm, humid air is transported into the Arctic by cyclonic systems. The power spectra of the expansion coefficients ($z_1(t)$) corresponding to the first EOF's are similar to that of red noise for periods less than 30 days. To force the model, z(t) is represented as a unit-vari-

* The vertically averaged variances (σ_i^2) of temperature advection and vertical motion varied from one case to another but did not exhibit significant differences between summer and winter. By contrast, the variance in water vapor advection was about five times larger in summer than winter, which is probably explained by the fact that specific humidity is about an order of magnitude greater in summer than in winter.

ance Markov process with an autocorrelation time scale of 0.7 days and has no variability on timescales longer than 30 days.

In summary, the vertical profile of the variable component of each lateral forcing term is expressed as $X_i'(p) = f_l^{1/2} \sigma_i \xi_i(p)$. Temporal variability is obtained by multiplying this expression by z(t), which is the same for all three components of the lateral forcing. The total forcing is obtained by adding the variable component ($z(t)X_i'$) to the seasonal mean ($\overline{X}_i$). This representation of the lateral forcing takes advantage of information from available climatic data and gridded analyses in a simple manner, so that differences in lateral forcing between summer and winter can be investigated using a small number of parameters. Using only the first EOF is a good way to describe variability associated with large scale dynamic systems, but it neglects variability associ-

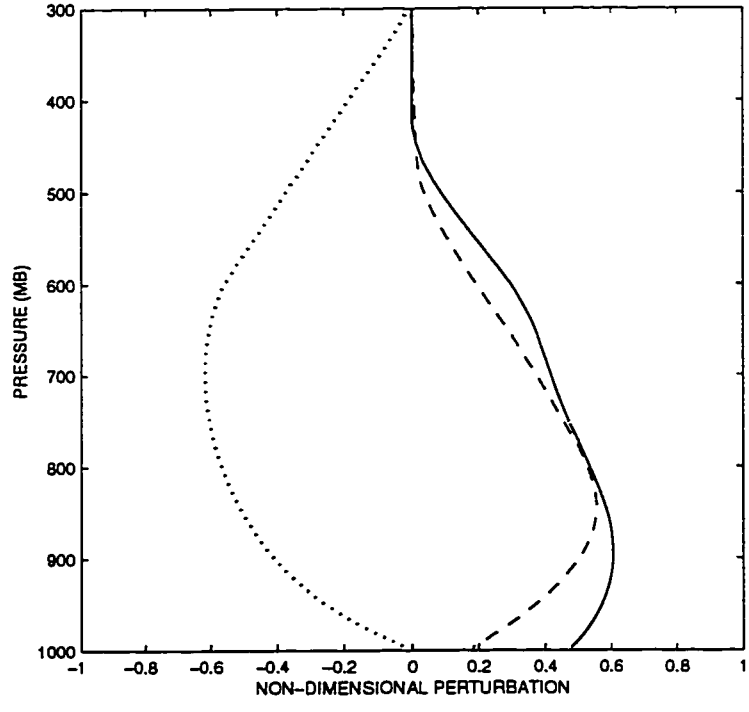

Figure 3.8: Perturbation patterns ($\xi_i(p)$) of the lateral forcing terms: temperature advection (solid), water vapor advection (dashed), and omega (dotted).

ated with smaller features. Results presented in Section 3.5.3 demonstrate that we would reach the same conclusions if the lateral forcing profiles were obtained directly from an atmospheric reanalysis. The boundary conditions are summarized in Table 3.1.

Table 3.1: Model boundary conditions

		winter		summer		
term	symbol	mean	standard dev.	mean	standard dev.	units
incoming solar radiation	S	0	0	461	153[a]	$W\ m^{-2}$
open water fraction	f_{ow}	3	0	20	0	%
ice thickness	H	4	0	4	0	m
temperature advection[b]	$-\vec{\nabla} \cdot \nabla T$	1.1	2.7	0.8	2.7	$C\ d^{-1}$
water vapor advection[a]	$-\vec{\nabla} \cdot \nabla q_v$	0.10	0.5	0.21	1.0	$g\ kg^{-1}\ d^{-1}$
large-scale vertical vel.[a]	ω	4.0	16.6	1.3	16.6	$mb\ d^{-1}$

a. This is the amplitude of the diurnal cycle.
b. Evaluated at 900 mb.

3.5 Simulation of summer and winter cloud regimes

The model is integrated for periods of thirty days to produce the standard simulations of winter and summer using representative boundary conditions The influence of the initial conditions is insignificant after about 5 days. The statistical description of each of the standard simulations is virtually the same whether it is based on days 10-20 or days 10-30, which permits shorter integrations for the experiments. The mean quantities presented in this section are based on days 10-20 unless otherwise stated.

3.5.1 Winter

The winter simulation is initiated with a surface air temperature of -5 C and relative humidity (over liquid) of 95%, with temperature and relative humidity decreasing aloft. These abnormally warm and humid conditions could occur with the incursion of a storm into the Arctic. A mixture of frozen and liquid condensate forms immediately in the rapidly cooling air (Figure 3.9). Starting with a height of 1.5 km, the upper surface of the condensate layer descends with time, leaving a thin layer of ice particles after about a day. For the rest of the integration the atmosphere is virtually free of liquid condensate except for the occasional formation of steam fog in the lowest 50 m-thick layer of the model, as seen in the time-averaged vertical profile of cloudiness ($\bar{f}_c(z)$) (Figure 3.10). The mean low cloud amount in the winter simulation is 0.3%, which is significantly less than the observed winter mean of ~20%. The deposition of moisture directly onto ice nuclei or other ice particles is so efficient that the water vapor mixing ratio rarely reaches saturation with respect to liquid. The amount of ice in the atmosphere (Figure 3.9) varies with time and is directly related to variations in the lateral forcing terms. The vertically integrated ice path in the lower troposphere (50- 2000 m) can reach as high as 100 g m^{-2} but has an average value of about 11 g m^{-2}. The mean temperature profile shown in Figure 3.10 has a surface based temperature

inversion of ~15 C and agrees well with observations, except that the temperature is slightly higher in the lowest 500 m. Mean values of downward longwave radiation and surface temperature shown in Table 3.3 agree well with observations.

The under-prediction of low-cloud amount by the model might be attributed to the fact that the variable component of the lateral boundary conditions best represents the passing of large scale atmospheric waves, whereas low level clouds in the Arctic winter are more likely produced by the stronger, short lived variations that accompany smaller features such as fronts and cyclones. These events can produce an anomalously warm environment such as the initial conditions of the simulation, in which liquid clouds formed. It may be that these more intense events account for most winter clouds, but the lateral forcing is too weak to reproduce recurrent transients of this magnitude.

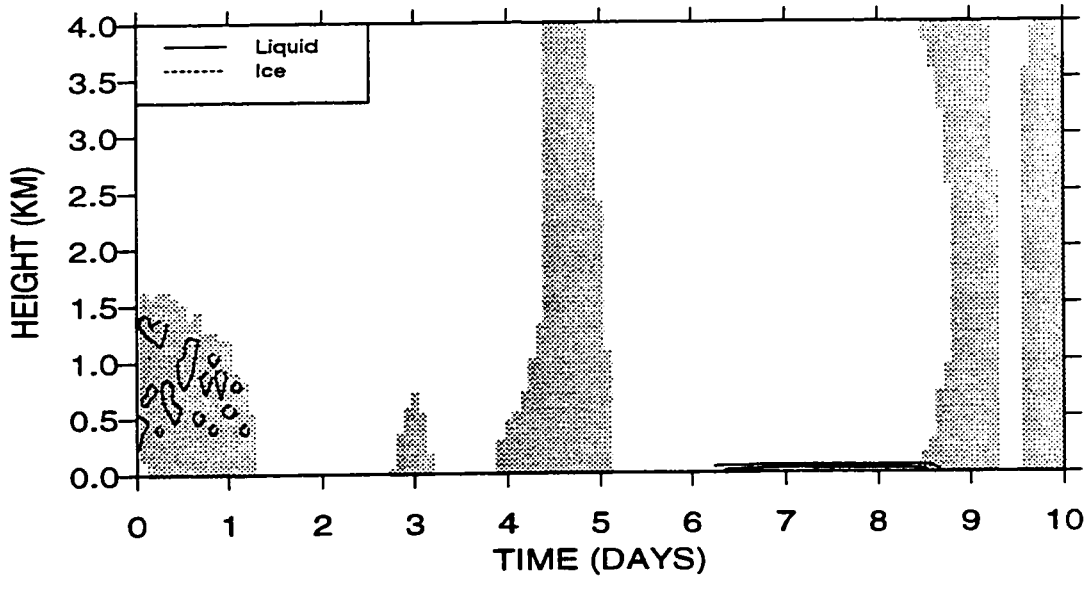

Figure 3.9: Time-height contours of liquid water mixing ratio for the first ten days of the standard winter simulation. The outer and inner contours are 0.01 and 0.10 g kg^{-1}, respectively. The 0.10 g kg^{-1} contour only appears near the surface on days 6.5 - 8.5 in this plot. Shading indicates the presence of ice (q_i > 0.005 g kg^{-1}).

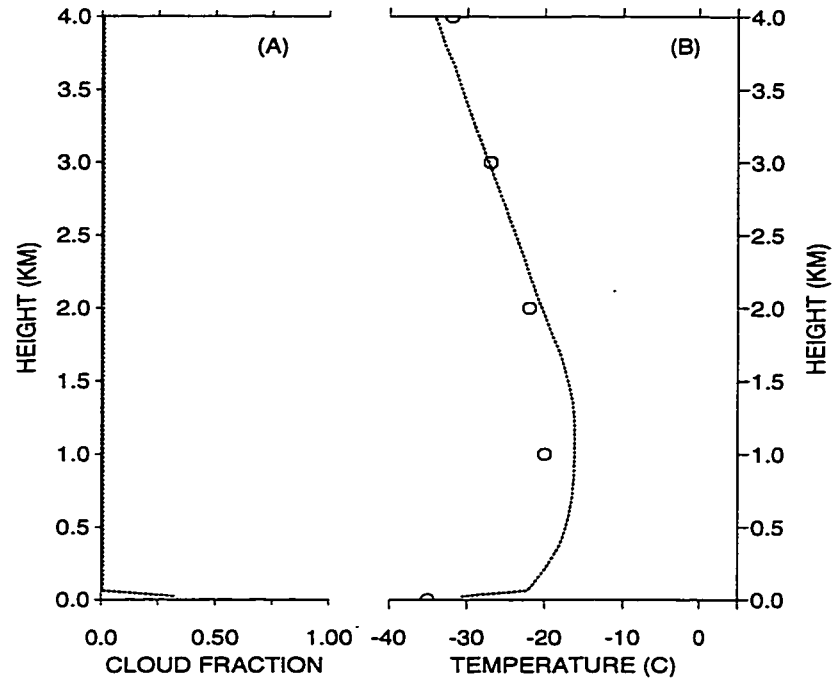

Figure 3.10: Mean profiles of (A) cloud fraction and (B) temperature from the standard winter simulation. Observed January and July air temperature (circles) are from Hare and Orvig (1959).

3.5.2 Summer

In stark contrast to the winter case, clouds are always present in the modeled summer climate. Figure 3.11 shows a robust cloud layer rising through the lower troposphere over a 5 day period and another taking its place after the first cloud has dissipated. The model frequently produces multiple cloud layers in the summer simulation, as observed over the Arctic Ocean (Herman and Goody 1976). Atmospheric ice is often present within the cloud layer and occasionally forms in clear air above the liquid clouds. The mean condensate content of the lower troposphere (75 g m^{-2}) is about seven times as large as in the winter simulation. The profile of mean cloudiness shown in Figure 3.12 has a maximum at the surface and decreases with height in qualitative agree-

ment with the analysis of Huschke (1969). However, the mean low-cloud amount of 100% is about 30% greater than observed from the surface. The lower troposphere of the summer simulation is cooler than observed (Figure 3.12) and the downward flux of solar radiation at the surface is too low by about 50 W m^{-2}. Both of these differences appear to be related to the persistence of cloud, which increases the emissivity and reflectivity of the lower atmosphere.

One possible explanation for the over-prediction of low-cloud amount is that vigorous vertical motions and large variations in the advection of moisture and temperature are required to clear the atmosphere, and the lateral boundary conditions used to drive the model do not represent this variability at full strength. Inaccuracies in the representation of shortwave absorption by clouds also may contribute the exaggerated longevity of individual cloud layers. The parameterization used in this model tends to underestimate shortwave cloud absorption when compared to estimates derived from aircraft measurements made in Arctic stratus (Slingo 1989). When short-

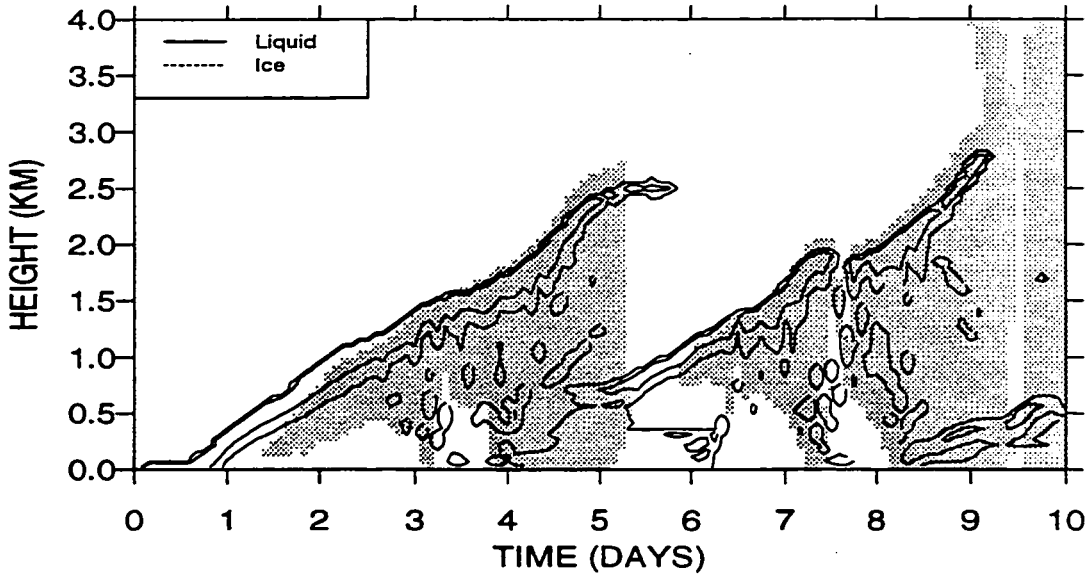

Figure 3.11: As in Figure 3.9, but for the standard summer simulation. The presence of ice from the surface to 4 km on day 10 is a transient feature.

wave cloud absorptivity is increased in the model, individual clouds are less persistent and hold less liquid water, which improves the agreement of lower-tropospheric temperatures and surface radiative fluxes with observations (see Section 3.5.3).

The standard cases demonstrate that the model simulates qualitatively the main features of the difference between summer and winter cloud regimes over the Arctic Ocean. The discrepancies between modeled and observed climates of each season are not surprising considering the simplicity of the lateral boundary conditions and uncertainty in the representation of physical processes. Experiments presented in Section 3.5.3 suggest that greater variability in the lateral boundary conditions would reduce these discrepancies and that the main climatic features of each season are not sensitive to uncertainties in physical parameters. That the model tends to exaggerate differences in the state of atmospheric condensate between the summer and winter suggests that the

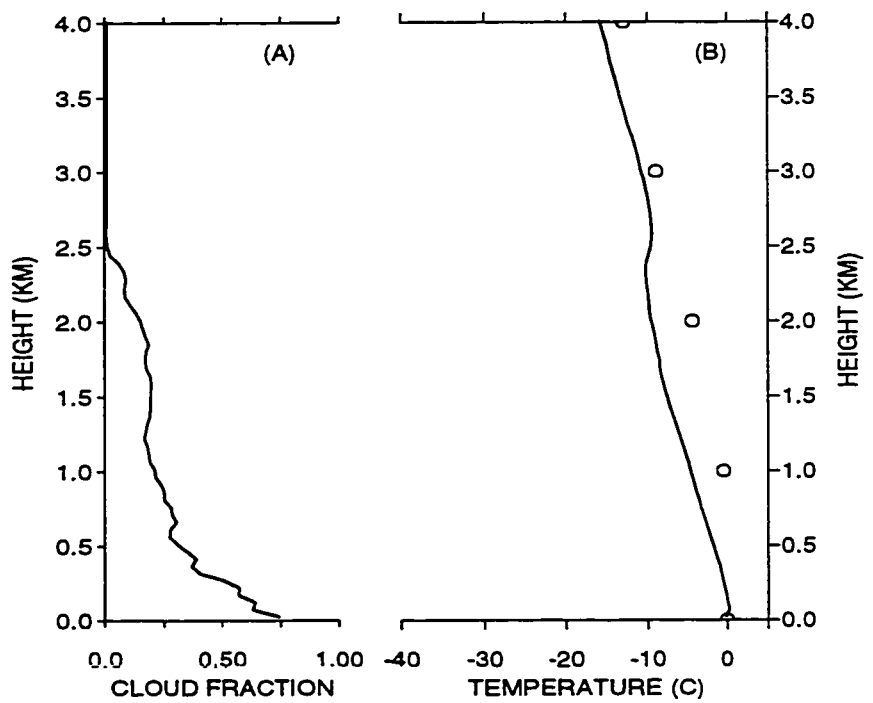

Figure 3.12: As in Figure 3.10, but for the standard summer simulation.

ingredients necessary to explain these differences may be contained in the model. The summer and winter standard cases offer good bases for testing hypotheses for the cause of the annual cycle of low cloud amount.

3.5.3 Sensitivity of model to lateral forcing and physical parameters

3.5.3.1 Lateral forcing

The lateral forcing terms (advection terms and vertical motion) represent the effects of atmospheric motions that occur on larger spatial scales than the assumed horizontal extent of the column model (~100 km). Each forcing profile is modeled as the sum of a mean profile and a perturbation profile that is multiplied by a randomly generated coefficient, as described in Section 3.4. This representation of lateral boundary conditions explains about half the variability present in the NASA/DAO reanalysis, but the results from Section 3.5.1 suggest that greater variability may be necessary to simulate the occasional occurrence of low cloud during the winter and absence of low cloud during the summer. To determine whether these discrepancies might be attributed to insufficient variance in the lateral boundary conditions, the model is integrated using forcing profiles obtained directly from the NASA/DAO reanalysis for the months of January, February, July, and August of 1989 at 74 N, 145 W. The atmospheric temperature in the model is relaxed to the reanalysis temperature using a timescale of 6 hours to prevent the simulation from departing significantly from the state of the reanalysis*, but moisture variables are allowed to evolve freely. The modeled evolution of liquid and ice water mixing ratio for the first 25 days of February is shown in

* It is not surprising that the state of the a column model should deviate from the reanalysis when forced using advection terms computed from the reanalysis since physical processes are represented differently in the column model and host model used for the reanalysis. The difference between the simulated and reanalyzed state of the atmosphere can become substantial in the absence of some form of relaxation if the time and height of cloud formation is different between the column model and the reanalysis host model.

Figure 3.13. Low-cloud amount in this simulation (37%) is greater than the observed average for February, which may be attributed to the relatively frequent incursions of warmer air. The simulated low-cloud amount is closer to the observed average during January, which was cooler and calmer than February in the reanalysis. The simulation of August (Figure 3.14) has more low cloud than the winter months, but the clouds are less persistent than in the standard summer simulation (Section 3.5.1). Low-cloud amount for the July and August simulations is very close to the observed summertime average. The results of these experiments suggest that the simplified lateral boundary conditions used in the standard cases may be responsible for the simulation of excessive cloud cover in summer and complete absence of cloud cover in winter. The model qualitatively reproduces the results of Section 3.6.2 and Section 3.6.3 when the experiments are repeated using direct forcing from the reanalysis (see Table 3.2).

3.5.3.2 Physical parameters

3.5.3.2.1 Ice particle fall speed

The terminal fall speed of an ice particle can range from about 10 cm s^{-1} to more than 100 cm s^{-1} depending on size and shape of the particle and on the properties of the air through which it falls (Heymsfield 1972). The bulk fall speed of a population of ice particles depends on the distribution of ice particle size and shape. In the model, the bulk fall speed of ice is related empirically to the amount of frozen condensate, such that the bulk fall speed increases with increasing ice mixing ratio. In air with a density of 1 kg m^{-3}, (3.7) yields bulk fall speeds of 31, 46, and 67 cm/s for ice water mixing ratios of 0.001, 0.01, and 0.10 g kg^{-1}, respectively. These fall speeds and the general relationship between bulk fall speed and ice mixing ratio are plausible, but there is no observational evidence that they are accurate in the arctic troposphere. The standard simulations are

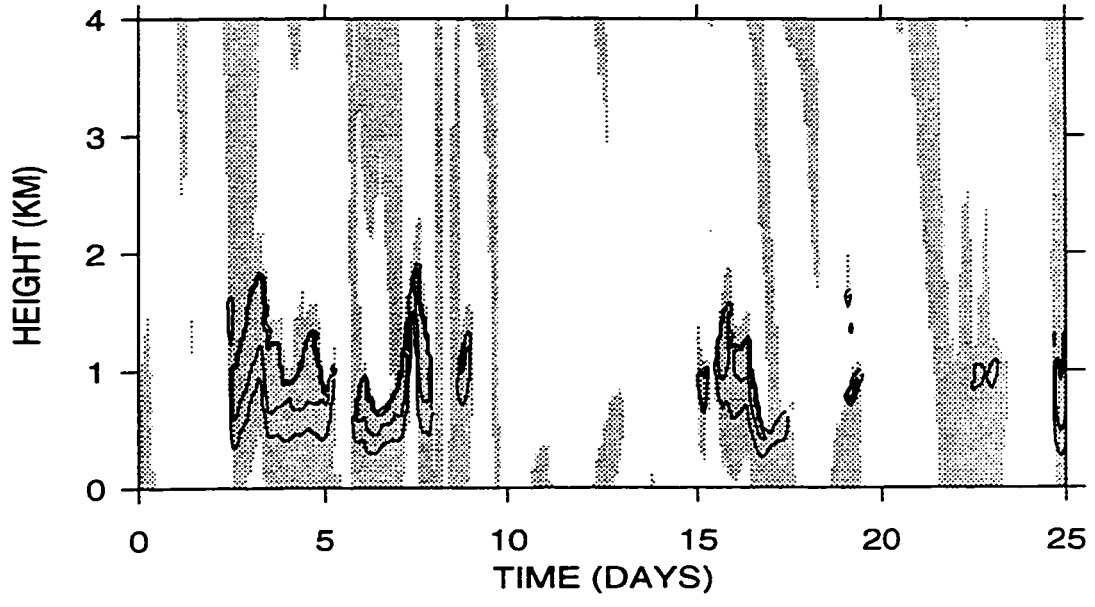

Figure 3.13: Time-height contours of liquid water mixing ratio for the first 25 days of the winter simulation using lateral forcing taken from the NASA/DAO reanalysis for February 1989 at 74 N, 145W. Contours are 0.01 and 0.10 g kg^{-1}, respectively, and shading indicates the presence of ice ($q_i > 0.005$ g kg^{-1}).

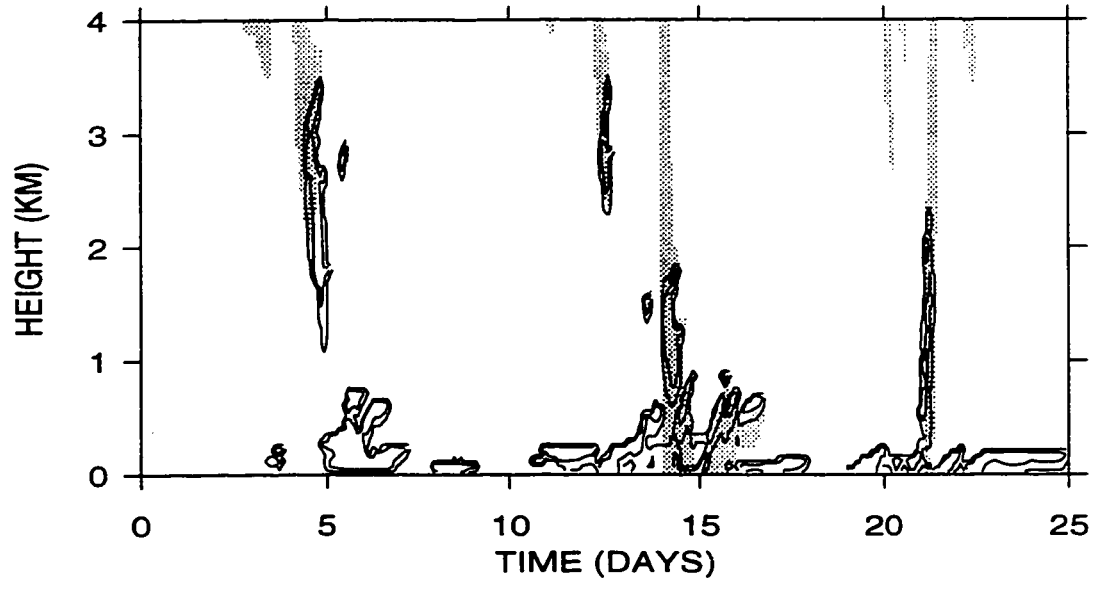

Figure 3.14: As in Figure 3.13, but for the summer using lateral forcing from August 1989.

repeated using fixed fall speeds of 20 and 70 cm/s to examine the sensitivity of the model to this uncertainty. The results shown in Table 3.2 indicate that lower fall speeds increase the mean ice water path of the lower troposphere by increasing the residence time of ice particles, and visa versa for larger fall speeds. These changes in ice water path affect the temperature profile by changing the radiative properties of the atmosphere. In the winter, for example, a decrease in fall speed (to 20 cm s^{-1}) increases the atmospheric ice water path and emissivity which results in a 6 C increase at the surface and a 1 C decrease at 900 mb. Aside from these modest effects, the major features of the summer and winter cloud regimes are unchanged by these rather drastic changes in ice particle fall speed.

3.5.3.2.2 Ice particle concentration

The concentration of ice particles is a specified model parameter that has a direct effect on the rate of vapor deposition onto ice particles. Equation (3.5) indicates that, for a given mass of ice particles in a supersaturated environment, the rate of deposition increases with increasing ice particle concentration (N_i). Summertime measurements of ice particle concentration by Hobbs and Rangno (1997) were typically in the range of 0.1 to 1 l^{-1}, but also exceeded 10 l^{-1} under some conditions. Microphysical measurements of lower tropospheric ice particles in colder conditions are described by Curry et al. (1990) and Hoff and Leaitch (1989). Curry et al. (1990) measured mean ice particle concentrations between 17 and 4210 l^{-1} on four flights during April; and Hoff and Leaitch (1989) reported typical concentrations of 10-20 l^{-1} during April.

The specified ice particle concentration is 10 l^{-1} in the winter case and 1 l^{-1} in the summer. Increasing N_i to 100 l^{-1} in the summer reduces the average liquid water content of low clouds by enhancing the effectiveness of water vapor deposition onto ice particles. When the summertime

ice particle concentration is reduced to 0.1 l^{-1}, the amount and phase of condensate does not change significantly from the standard case, but liquid clouds are able to persist longer at greater heights before being eliminated by ice phase processes (not shown). The mean low cloud amount in both summer experiments is still almost 100%. Reducing the ice particle concentration during the winter reduces the efficiency of water deposition onto ice particles. With N_i= 1 l^{-1}, the liquid clouds that form at the beginning of the simulation persist longer than in the standard winter case (Figure 3.8), but the mean amount of low cloud is only 1.8% once the atmosphere has settled into a steady state. The mean low-cloud amount increases to 54% when N_i is reduced to 0.1 l^{-1}, but these are limited to the lowest 500 m (unlike the summer simulation shown in Figure 3.11). The cloudiness in this case appears to be closely related to evaporation from open water within the ice pack, since the cloud amount and liquid water path decrease substantially in the absence of open water. There is little change from the standard case when the ice particle concentration is increased to 100 l^{-1}. These experiments demonstrate that the basic features of the summer and winter simulations are not very sensitive to the uncertainty in ice particle concentration. Seasonal variations in ice particles concentration (more in winter than in summer) do not appear to account for the difference in cloudiness between summer and winter, but they may enhance the amplify the negative correlation between of the deposition rate and temperature.

3.5.3.2.3 Shortwave absorption by clouds

Observational data analyses (e.g. Cess et al. 1994) suggest that shortwave absorption by clouds may be substantially greater than calculated by numerical models, such as the present model and GCM's. To examine the response of the CCM2 GCM to enhanced shortwave cloud absorption, Kiehl et al. (1995) tuned the shortwave cloud radiative parameterization so that the absorption was as large as suggested by the above observations. The sensitivity of the column

model to shortwave cloud absorption can tested by making the same adjustments to radiative parameters as by Kiehl et al., since the model employs the same radiative scheme as the CCM2. Figure 3.15 shows profiles of mean temperature and liquid water mixing ratio for the summertime simulation, with and without enhanced shortwave cloud absorption. Clouds above 1 km are significantly more tenuous when shortwave absorption is increased, which is consistent with the results of Herman and Goody (1976). Associated with this is a reduction in the mean amount of liquid condensate, which reduces the cooling effect of clouds and a increases the lower-tropospheric temperature. If the (untuned) column model is underestimating shortwave absorption by clouds, then this might explain some of the discrepancies between the standard summer simulation and observations.

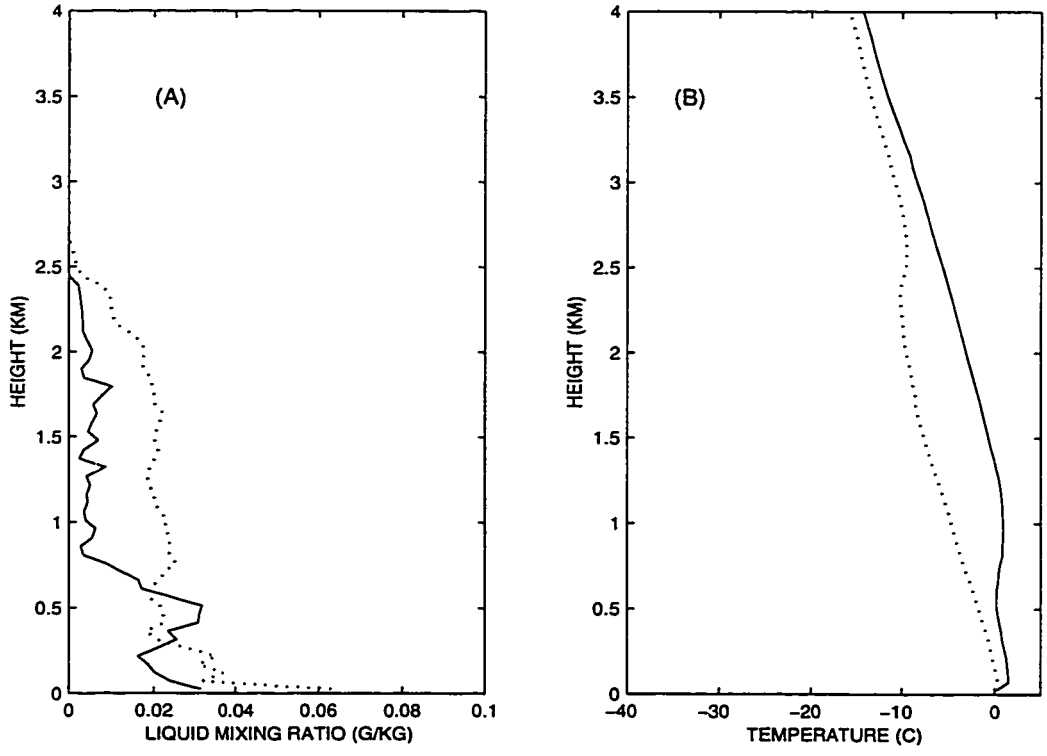

Figure 3.15: Mean profiles of (A) liquid water mixing ratio and (B) temperature for the summer simulation with enhanced shortwave cloud absorption following the approach of Kiehl et al. (1995). Enhanced shortwave absorption (solid); standard summer simulation (dotted).

Table 3.2: Results from model sensitivity tests (steady state averages)

case	low cloud fraction[a]	liquid water path[a]	ice water path[a]
winter			
standard	0.3%	0.003 g m^{-2}	10.6 g m^{-2}
Jan 1989 direct forcing[b]	17.2	1.3	8.8
same, but T_f= -20 C[b]	82.0	81.7	0.3
Feb. 1989 direct forcing[b]	37.2	22.7	52.0
$\overline{V}_i$ = 20 cm s^{-1}	0.6	0.03	29.5
$\overline{V}_i$ = 70 cm s^{-1}	0.9	0.009	8.6
N_i= 100 l^{-1}	0.0	0.0	8.4
N_i= 1.0 l^{-1}	1.8	0.04	8.6
N_i= 0.1 l^{-1}	54.0	8.9	9.8
N_i= 0.1 l^{-1} and no open water	33.2	2.7	10.2
summer			
standard	100.0	49.7	25.0
July 1989 direct forcing[b]	73.3	42.2	4.4
same, but no surface evaporation[b]	62.6	42.4	38.5
same, but T_f = 20 C[b]	1.9	0.5	68.9
August 1989 direct forcing[b]	69.1	26.6	6.1
$\overline{V}_i$ = 20 cm s^{-1}	99.8	45.2	71.9
$\overline{V}_i$ = 70 cm s^{-1}	100.0	47.8	71.9
N_i= 100 l^{-1}	96.6	26.4	23.1
N_i= 0.1l^{-1}	100.0	48.7	19.8
enhanced shortwave cloud absorption	98.0	25.8	4.1

a. Values defined for the lower troposphere, between approximately 50 and 2000 m.
b. Average of the first 25 days of the month. Lateral boundary conditions from the NASA/DAO reanalysis.

3.6 Experiments

3.6.1 Water vapor advection

To test the hypothesis that the annual cycle of stratus is caused by the annual cycle of moisture flux into the Arctic, the standard cases are repeated using the wintertime mean profile of water vapor advection in the summer case and the summertime mean profile in the winter case. According to the hypothesis, the greater amount of moisture advection in the winter experiment should produce larger amounts of clouds (as in summer) and the summer experiment should yield few low-level clouds. Temperature advection is adjusted in these experiments to compensate for the change in latent heat release that accompanies a change in moisture advection, but the following results are not sensitive to this detail.

The additional moisture advection in the winter produces virtually no effect on the vertical distribution or mean amount of low clouds, which is only 0.2%. The only changes resulting from the increase in moisture advection are proportionate increases in atmospheric ice content and precipitation and a slight reduction in lower tropospheric temperature due to enhanced radiative cooling caused by the additional atmospheric ice. Decreasing moisture advection during the summer has a modest effect on the mean profiles of cloud fraction, as shown in Figure 3.16. There is a slight increase near 2 km and a slight decrease below 1.5 km, but the mean low-cloud amount still exceeds 99%. The modeled total condensate path in the summer is about three times as large as in the winter, even though water vapor import from lower latitudes in summer is less than half of the winter value in these experiments. The results of these two experiments indicate that the summer and winter cloud regimes are virtually unaffected by the inter-seasonal variations in mean flux of water vapor into the Arctic.

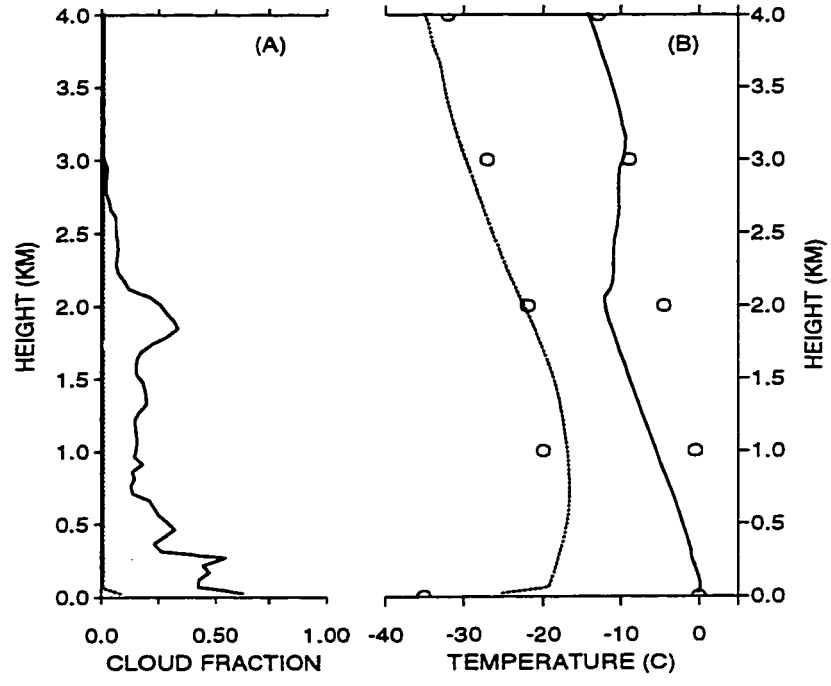

Figure 3.16: As in Figure 3.10, but for the vapor advection experiments: summer simulation with wintertime advection (solid) and winter simulation with summertime advection (short dotted).

3.6.2 Surface Evaporative Flux

According to the second hypothesis, isolating the atmosphere from a source of moisture at the surface should substantially reduce or eliminate low level clouds. To test the hypothesis that the annual cycle of low-level cloudiness is determined by the availability of moisture at the surface, the standard summer case is integrated using a transfer coefficient of zero in the equation for the surface moisture flux. The mean profile of cloud fraction (Figure 3.17) shows a slight decrease below 1 km, but the mean low cloud fraction is still almost 100%. The results of this experiment do not support the second hypothesis; instead, they suggest that the influence of surface evaporation on cloud amount is not significant during the arctic summer.

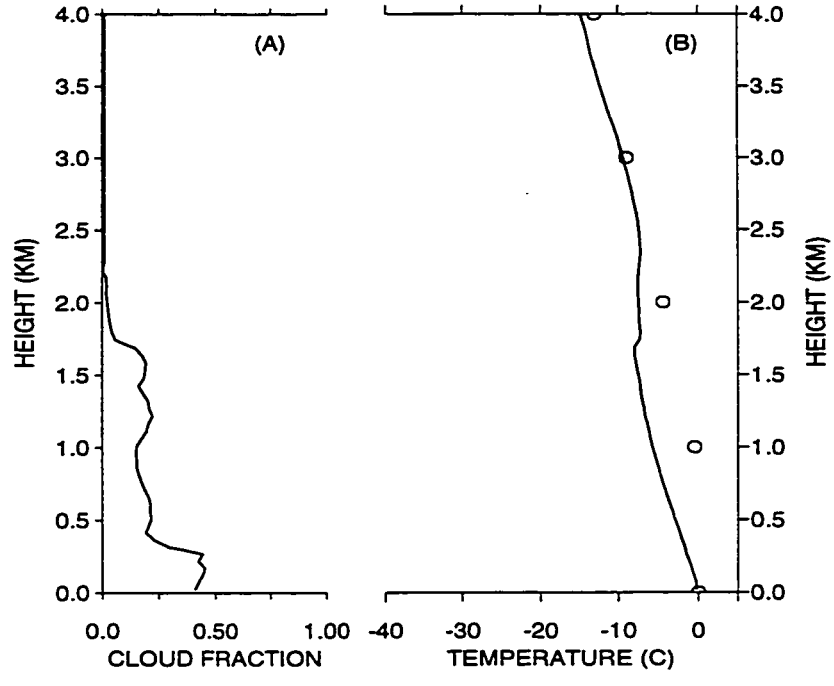

Figure 3.17: As in Figure 3.10, but for the surface evaporation experiment: evaporation is turned off in the standard summer simulation.

3.6.3 Atmospheric Ice Processes

A measure of the effectiveness of ice-phase microphysical processes in eliminating or preventing the formation of liquid water clouds is the rate at which the mixing ratio of atmospheric ice increases at the expense of other forms of atmospheric water in an environment that is saturated with respect to liquid water, such as a mixed phase cloud. The main processes responsible for this is vapor deposition onto ice ($-E_i$), which is given by (3.5). This process depends strongly on the number concentration of ice particles (N_i) and the supersaturation of the environment with respect to ice ($e_{sl}/e_{si} - 1$).

Experiments in Section 3.5.3 demonstrate that the effectiveness of deposition onto ice

increases as N_i increases; however, they do not support suggest that seasonal changes in N_i can explain the difference between summer and winter low-cloudiness. Low-cloud amount in the winter case increased to 95% when no ice was allowed to form the atmosphere (N_i= 0), which suggests that ice processes are essential in explaining the wintertime minimum in low-cloud amount.

Within a mixed-phase cloud, the supersaturation of the environment with respect to ice depends on the difference between the ambient air temperature and the freezing temperature of water, T_f. This value varies through the year as air temperature changes with respect to the fixed value of T_f. Hypothetically, if the freezing point of water were reduced by an amount equal to the temperature difference between the summer and winter lower troposphere (about 20 C), then vapor deposition would be as ineffective during the winter as it is in the summer. According to the third hypothesis, wintertime low-level cloudiness in such an environment should resemble the summer climate. Similarly, a freezing temperature of +20 C should strengthen the effect of vapor deposition and reduce or eliminate low-level cloud in the summer. To test the third hypothesis, the winter and summer standard simulations are repeated using temperature temperatures of -20 C and +20 C, respectively, for computing the saturation vapor pressure with respect to ice.

Mean low-level cloud amount in the winter experiment is 88.5%, and the time-averaged cloud fraction profile ($\bar{f}_c(z)$) decreases gradually with height (Figure 3.18). The mean lower-tropospheric condensate content in this experiment is more than three times greater than the standard winter simulation. Strong cloud-top radiative cooling enables the winter stratus to maintain convective mixing and to rise to greater heights before succumbing to dissipative processes than in the standard case. The abundance of condensate increases lower-tropospheric emissivity and virtually eliminates the temperature inversion. The mean surface temperature increases to -24 C in the winter experiment due to greenhouse trapping by the clouds.

There are no low clouds in the summer experiment. Without the radiative cooling of the stratus clouds, the lower troposphere is warmer and more stable than in the standard summer case (Figure 3.15). The presence of low-level clouds appears to be an important factor in shaping the mean temperature profile of the arctic lower-troposphere. The elimination of stratus increases downward shortwave and decreases downward longwave radiative fluxes at the surface; and the stable lower atmosphere produces net downward turbulent fluxes. Together, these changes increase the net downward energy flux by about 100 W m^{-2} over the standard winter simulation. The lower-tropospheric condensate content in the summer experiment is less than half as large in the winter experiment, even though the influx of moisture is twice as great. These experiments suggest that ice-phase microphysical processes can explain the difference in low-cloud amount between summer and winter.

3.7 Discussion and Application

The results from the experiments, summarized in Table 3.3, do not support the hypotheses that seasonal variations in low-level cloud amount are controlled by water vapor advection into the Arctic or by the evaporative flux from the ice pack. Instead, they suggest that microphysical processes related to ice are the dominant factor in determining the amount of low level clouds over the Arctic. It appears that the summer and winter weather regimes fall on either side of a threshold temperature that determines the dominant phase of condensate, where the 'dominant phase of condensate' is defined as frozen if, on average, the rate of ice formation by vapor deposition is greater that the rate of liquid formation by condensation. This produces a smaller amount of low cloud during the winter when ice is the dominant phase, since ice has a shorter residence time in the atmosphere than liquid condensate. An analogy may be drawn between the seasonal variation of

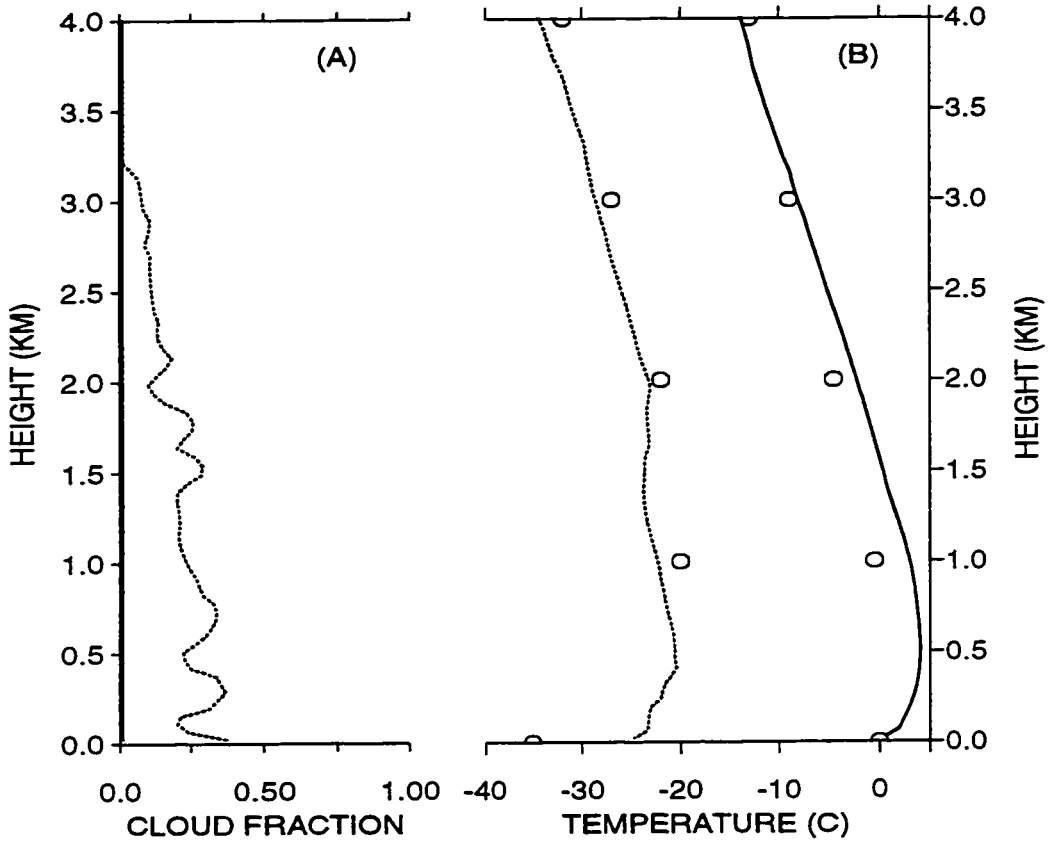

Figure 3.18: As in Figure 3.10, but for the ice-phase microphysics experiments in which the saturation vapor pressure with respect to ice is computed using an artificial values of the freezing point of water (T_f). Summer case with T_f= +20 C (solid) and winter case with T_f= -20 C (short dash). Note that liquid cloud fraction is zero at all heights in summer experiment.

Table 3.3: Results from model experiments (steady state averages)

case	low cloud fraction[a]	liquid water path[a]	ice water path[a]	surface temperature	downward LW irradiance	downward SW irradiance
winter						
observed	~ 20%	--[b] g m^{-2}	--[b] g m^{-2}	-35 C[c]	165 W m-2[d]	0 Wm^{-2}
standard	0.3	0.003	10.6	-31	169	0
summer $-\vec{\nabla} \cdot \nabla q$	0.2	0.006	20.7	-27	181	0
T_f= -20 C	88.5	25.8	8.1	-24	205	0
summer						
observed	~ 70	--[b]	--[b]	0	298[d]	220[d]
standard	100.0	49.7	25.0	0	311	169
winter $-\vec{\nabla} \cdot \nabla q$	99.6	40.0	22.7	0	307	149
no sfc. evap.	99.5	37.7	23.3	0	303	281
T_f= -20 C	0.0	0.0	18.9	0	268	281

a. Values defined for the lower troposphere, extending between approximately 50 and 2000 m.
b. Observations of average condensate water paths are not available.
c. From Gorshkov (1983).
d. As compiled by Fletcher (1965).

condensate phase in the lower Arctic atmosphere and the vertical variation in condensate phase through the troposphere (at temperate latitudes). In both cases the dominant phase of condensate is determined by the mean air temperature, which varies with time in the Arctic and with height through the troposphere.

3.7.1 GCM Simulation of Arctic Climate

The results of this study suggest that atmospheric ice processes should be included in GCM's to simulate the observed annual cycle of total cloud amount over the Arctic. Five of the nineteen GCM's examined by Tao et al. (1996) include ice-phase microphysical processes, typically by specifying the ice fraction within a cloud layer as a function of temperature and then allowing ice to fall out more rapidly than liquid. Total cloud amount is computed diagnostically in each model based on the cloud amount at each model layer and non-physical factors, such as the assumption of how clouds overlap and the number of layers in the model. Differences in these non-physical factors and in upper-level cloud amount can produce a bias in annually-averaged total cloud amount that is unrelated to a model's ability to simulate the annual cycle in low-cloud amount. These considerations suggest that the most meaningful quantity to examine is the departure of monthly total cloud amount from the *simulated* annual mean. Consistent with the hypothesis, the mean annual cycle of arctic cloudiness produced by GCM's with ice processes bears a qualitative resemblance to the observed annual cycle, in contrast to the mean of the fourteen models without ice processes (Figure 3.19). A probable explanation for excessive wintertime low-level cloudiness in models without ice-phase processes is the absence of an efficient mechanism to remove condensate from the lower-troposphere.

This result is not a statistically significant verification of the third hypothesis since the sample size is small (N= 5) and the standard deviation in monthly mean cloud amount among the

models is large (~18%). The next generation of models participating in AMIP will offer a new and possibly more significant test of the hypothesis, since it is likely that a greater number of these models will include ice processes and the variation among models will be smaller. However, statistical significance is not necessary to justify experimenting with simple ice-phase microphysics parameterizations in GCM's.

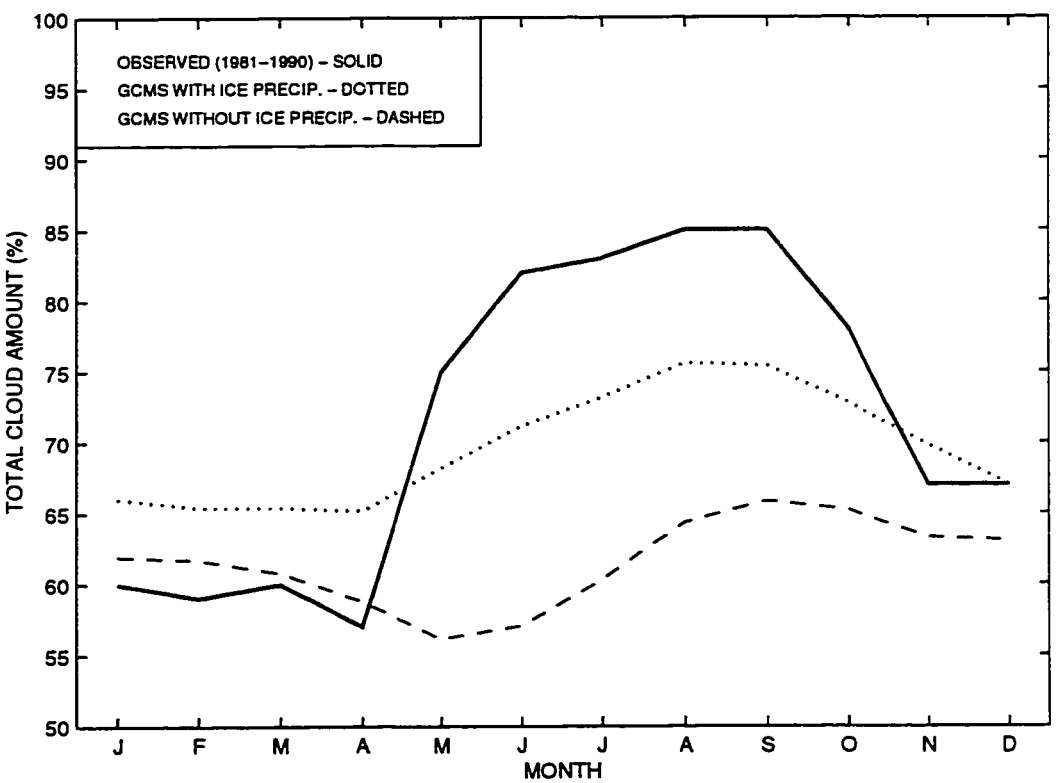

Figure 3.19: Annual cycles of total cloud amount over the Arctic Ocean: as observed with screening for adequate illumination (solid), and as simulated by GCM's with ice microphysics (dotted) and without (dashed). Observed amounts are from Hahn et al (1995) and AMIP GCM results are based on Tao et al. (1996). Model descriptions are obtained from AMIP (1997).

Chapter 4:

Conclusions

The overall goal of this dissertation is to contribute to the understanding of the effect of clouds on the sensitivity of the arctic climate. The goal of Chapter 2 is to estimate the effect of clouds on the steady state climate as measured by equilibrium ice thickness. In previous work, the direct effect of clouds on the surface energy balance (surface CRF) has been estimated, leading to the conclusion that clouds 'warm' the Arctic climate. In general, a change in clouds affects the atmospheric temperature profile, which may affect the surface energy budget on longer timescales. The results of Chapter 2 suggest that the equilibrium effect of clouds on the ice thickness, after the system has adjusted, cannot be predicted on the basis of the surface CRF. Instead, CRF measured at the top of the atmosphere provides a better indication of the effect of clouds on the ice thickness. This can be attributed to the fact that TOA CRF measures the effect of clouds on the ice-atmosphere system, whereas surface CRF only provides information about their effect on the surface. Given the uncertainties in the model estimate of the annually-averaged TOA CRF and in satellite estimates of TOA CRF, it is not certain whether the net effect of clouds is to increase or decrease ice thickness in the present climate. It was demonstrated in Chapter 2 that changes in sea ice thickness, in response to changes in clouds, can be predicted by estimating how the change in clouds affects TOA CRF. Improving the accuracy of satellite estimates of TOA CRF, as functions of cloud type and time of year, will improve the ability to predict the role of clouds in arctic climate

difference between the results of Chapter 2 and previous work demonstrates the importance of studying the arctic ice and atmosphere as a coupled system. The relevance of this coupling should be considered in future studies of arctic climate.

The goal of the research described in Chapter 3 is to understand the factors that control low-cloud amount over the Arctic Ocean. To explain the annual cycle of arctic low-cloud amount, it is necessary to know why there is so little cloud in the winter despite the strong stratification of the lower troposphere. Examination of climatological data on moisture flux convergence, surface evaporation, and the effect of air temperature on ice-phase microphysical processes does not allow us to rule out any of these factors as a potential explanation. Experiments with a one-dimensional model suggest that, of these factors, temperature dependent ice-phase processes are essential. These processes determine the partition of condensate between ice and liquid such that the residence time of lower-tropospheric condensate is shorter below a threshold temperature of about −10 to -15°C (258-263 K). This mechanism should apply anywhere the annual cycle of lower tropospheric temperature traverses the threshold temperature, such as the northern continents and the Weddell Sea in the Antarctic. The inclusion of ice-phase microphysical processes appears to improve the simulation of the annual cycle of total cloudiness over the Arctic Ocean among GCM's participating in the AMIP.

The conclusions of Chapter 3 must be qualified by the many uncertainties that continue to complicate the modeling of arctic clouds and precipitation. We might have greater confidence in the results after the hypotheses are tested using models that represent some of the physical processes differently than in the present model. Analyzing the relationships between observed cloud properties and other meteorological variables is another possible route. Surface-based cloud observations and temperature soundings have been recorded at drifting ice stations for more than 40 years. Another valuable source of data will become available in the next several years as detailed

measurements of temperature, humidity, cloud amount, cloud condensate content, and condensate phase are collected at sites in the Beaufort Sea and the North Slope of Alaska as part of the Atmospheric Radiation Measurement Program, the First ISCCP Regional Experiment III, and the Surface Heat Budget of the Arctic Ocean Experiment.

The conclusions from Chapters 2 and 3 can be applied to the problem of understanding how clouds affect the sensitivity of the arctic climate. The response of the arctic climate system to a perturbation in a climatic parameter, such as incoming solar radiation or carbon dioxide concentration, depends on the size of the perturbation and on feedback mechanisms acting within the Arctic. The formation of ice particles in the lower atmosphere constitutes a link in a feedback loop involving surface temperature, lower-tropospheric temperature, and low level clouds. Cloud properties (amount, height, condensate content, and condensate phase) affect surface temperature (except during the melt season) by influencing downward radiative fluxes and lower tropospheric mixing; surface temperature affects the temperature of the lower troposphere through upward radiative and turbulent energy fluxes; and lower-tropospheric temperature affects cloud properties through temperature dependent ice processes. To learn the sign and magnitude of the net cloud feedback requires knowledge of the interactions among three components of the feedback circuit.

We begin by asking how a uniform increase in air temperature might affect the annual cycle of low cloud amount. The results of Chapter 3 suggest that transitions between the summer and winter cloud regimes occur when the mean air temperature equals the transition temperature of the dominant phase of condensate. In a warmer climate, the mean air temperature would exceed the transition temperature earlier in the spring and later in the autumn. Based on Chapter 3, one might predict a greater amount of low-level clouds in early May and late September if the arctic climate is warmer*. The results of Chapter 2 suggests that cloud radiative forcing at the top of the atmosphere can be used to predict how a specific change in cloudiness will effect the mean ice thick-

ness which has a strong influence on the average temperature. Figure 2.10 indicates that CRF by low clouds is slightly negative in May and slightly positive in late September. Therefore, changes in low-level cloud amount produced by a general warming in the Arctic should not have a very large effect on mean ice thickness or average temperature. To the extent that the findings of this study can be applied to predicting cloud-climate feedback, they suggest that the feedback is small in magnitude. The accuracy of the estimated cloud feedback will improve as knowledge of other components of the arctic climate system incorporated. For example, the results of Chapter 2 suggest that a springtime increase in low cloud amount might trigger a strong surface albedo feedback, and thus modify the estimated feedback presented here.

---

* It may be possible to test this prediction by comparing mean annual cycles of low cloud amount at different regions within the Arctic Ocean, using existing archives of meteorological data obtained from drifting ice stations.

References:

Aagaard, K., L.A. Barrier, E.C. Carmack, C. Garrity, E.P. Jones,D. Lubin, R.W. Macdonald, J.H. Swift, W.B. Tucker, P.A. Wheeler,and R. H Whritner. U.S., Canadian Researchers Explore Arctic Ocean. *Eos Trans. AGU*, **77** (22), 1996, 209-213.

Albrecht, B.A., 1989: Aerosols, cloud microphysics, and fractional cloudiness. *Science*, **245**, 1227-1230.

Ambach, W., 1974: The influence of fractional cloud cover on the net radiation budget of a snow surface with high albedo. *J. Glaciol.*, **67**, 73-84.

Atmospheric Model Intercomparison Project, cited 1997: Summary documentation of the AMIP models. [Available on-line from http://www.pcmdi.llnl.gov/modeldoc/amip/01toc.html.]

Bechtold, P., C. Fravalo, and J.P. Pinty, 1992: A model of marine boundary-layer cloudiness for mesoscale applications, *J. Atmos. Sci.*, **49**, 1723-1744.

Bjerknes, J., 1925: Meteorologist's report. In *Our Polar Flight*, R. Amundsen and L. Ellsworth, Eds., Dodd, Mead and Company, 343-360.

Bretherton, C.S., and R. Pincus, 1995: Cloudiness and marine boundary layer dynamics in the ASTEX Lagrangian experiments. Part I: Synoptic setting and vertical structure. *J. Atmos. Sci.*, **52**, 2707-2723.

Bretherton, C.S., P.Austin, and S.T. Siems, 1995: Cloudiness and marine boundary layer dynamics in the ASTEX Lagrangian experiments. Part II: Cloudiness, drizzle, surface fluxes, and entrainment. *J. Atmos. Sci.*, **52**, 2724-2735.

Cess, R.D., and G.L. Potter, 1987: Exploratory studies of cloud radiative forcing with a general circulation model. *Tellus*, **39A**, 460-473.

Cess, R.D., and Coauthors, 1994: Absorption of solar radiation by clouds: Observations versus models. *Science*, **267**, 496-499.

Colony, R., and A.S. Thorndike, 1985: Sea ice motion as a drunkard's walk. *J. Geophys. Res.*, **90**, 965-974.

Crutcher, H.L., and J.M. Meserve, 1970: *Selected-Level Heights, Temperatures and Dew Point Temperatures for the Northern Hemisphere*. NAVAIR 50-1C-52. [Available from Chief, Naval Operations.]

Curry, J.A., 1983: On the formation of continental polar air. *J. Atmos. Sci.*, **40**, 2279-2292.

Curry, J.A., and Herman, G.F., 1985: Infrared radiative properties of summertime arctic stratus clouds. *J. Climate Appl. Meteor.*, **24**, 525-538.

Curry, J.A., and E.E. Ebert, 1992: Annual cycle of radiation fluxes over the Arctic Ocean: sensitivity to cloud optical properties. *J. Climate*, **5**, 1267-1280.

Curry, J.A., F.G. Meyer, L.F. Radtke, C.A. Brock, and E.E. Ebert, 1990: Occurrence and characteristics of lower tropospheric ice crystals in the Arctic, *Int. J. Climatol.*, **10**, 749-764.

Curry, J.A., J.L. Schramm, and E.E. Ebert, 1993: Impact of clouds on the surface radiation budget of the Arctic Ocean. *Meteor. Atmos. Phys.*, **51**, 197-217.

Curry, J.A., W.B. Rossow, D. Randall, and J. Schramm, 1996: Overview of arctic cloud and radiation characteristics. *J. Climate*, **9**, 1731-1764.

Ebert, E.E., and J.A. Curry, 1992: A parameterization of cirrus cloud radiative properties for climate models. *J. Geophys. Res.*, **97**, 3831-3836.

Ebert, E.E., and J.A. Curry, 1993: An intermediate one-dimensional thermodynamic sea-ice model for investigating ice-atmosphere interactions. *J. Geophys. Res.*, **98**, 10085-10109.

Fletcher, J.O., 1965, The heat budget of the Arctic Basin and its relation to climate. The Rand Corp., R-444-PR, 175 pp.

Fletcher, N.H., 1966: *The Physics of Rainclouds*. Cambridge University Press, 390 pp.

Gloersen, P., W.J. Campbell, D.J. Cavalieri, J.C. Comiso, C.L. Parkinson, and H.J. Zwally, 1992: *Arctic and Antarctic Sea-Ice: Satellite Passive Microwave Observation and Analysis. 1978-1987*. NASA SP-511, National Aeronautic and Space Administration, 290pp.

Gorshkov, S.G., 1983: *World Ocean Atlas, Volume 3: Arctic Ocean* (in Russian). Pergamon Press, 184 pp.

Hack, J.J., B.A. Boville, B.P. Briegleb, J.T. Kiehl, P.J. Rasch, and D.L. Williamson, 1993: Description of the NCAR Community Climate Model (CCM2). NCAR Tech. Note NCAR/TN-382+STR, 108 pp.

Hahn, C.J., S.G. Warren, and J. London, 1995: The effect of moonlight on observation of cloud cover at night, and application to cloud climatology. *J. Climate*, **8**, 1429-1446.

Hare, F.K., and S. Orvig, 1959: The arctic circulation. Arctic Meteorology Research Group Publication No. 12, McGill University, 211 pp.

Harrison, E.F. and coauthors, 1990: Seasonal variations of cloud radiative forcing derived from the Earth Radiation Budget Experiment. *J. Geophys. Res.*, **95**, 18,687-18,703.

Hartmann, D.L., 1994: *Global Physical Climatology*. Academic Press, 411 pp.

Hartmann, D.L., M.E. Ockert-Bell, and M.L. Michelsen, 1992: The effect of cloud type on Earth's energy balance: Global analysis. *J. Climate*, **5**, 1281-1304.

Herman, G.F., 1980:Thermal radiation in arctic stratus clouds. *Quart. J. Roy. Met. Soc.*, **106**, 771-780.

Herman, G.F., and R. Goody, 1976: Formation and persistence of summertime arctic stratus clouds. *J. Atmos. Sci.*, **33**, 1537-1553.

Heymsfield, A.J., 1972: Ice crystal terminal velocities. *J. Atmos. Sci.*, **29**,1348-1357.

Heymsfield, A.J. 1977: Precipitation development in stratiform ice clouds: A microphysical and dynamical study. *J. Atmos. Sci.*, **34**, 367-381.

Hobbs, P.V., and A. Rangno, 1985:Low and middle-level clouds in the Arctic Ice particle concentrations in clouds. *J. Atmos. Sci.*, **42**,2523-2549.

Hobbs, P.V., and A. Rangno, 1996: Low and middle-level clouds in the Arctic, submitted to *Q. J. Roy. Meteor. Soc.*

Hoff, R.M., and W.R. Leaitch, 1989: Ground-based cirrus clouds in the Arctic. *Preprints, Symp. on the Role of Clouds in Atmospheric Chemistry and Global Climate*, Anaheim, CA, Amer. Met. Soc., 324-327.

Holtslag, A.A.M., and B.A. Boville, 1993: Local versus nonlocal boundary-layer diffusion in a global climate model. *J. Climate*, **6**,1825-1842.

Houghton, J.T., G.J. Jenkins, and J.J. Ephraums (Eds.), 1990: *Climate Change. The IPCC Scientific Assessment.* Cambridge University Press, 365 pp.

Houze, R.A., 1993: *Cloud Dynamics.* Academic Press, 573.

Huschke, R., 1969: Arctic cloud statistics from "air-calibrated" surface weather observations. The Rand Corp. RM-6173-PR, 79 pp.

Kahl, J.D., 1990: Characteristics of low-level temperature inversions along the Alaskan Arctic coast. *Int. J. Climatol.*, **10**, 537-548.

Kiehl, J.T., J.J. Hack, M.H. Zhang, and R.D. Cess, 1995: Sensitivity of a GCM climate to enhanced shortwave cloud absorption. *J. Climate*, **8**, 2200-2212.

Klein, S.A., and D.L. Hartmann, 1993: The seasonal cycle of low stratiform clouds. *J. Climate*, **6**,1587-1606.

Lilly, D.K., 1968: Models of cloud-topped mixed layers under a strong inversion. *Quart. J. Roy. Meteor. Soc.*, **100**, 292-309.

Lindsay, R.W., and D.A. Rothrock, 1994: Arctic sea ice albedo from AVHRR. *J. Climate*, **7**, 1737-1749.

Lynch, A.H., W.L. Chapman, J.E. Walsh, and G Weller, 1995: Development of a regional climate model of the western arctic. *J. Climate*, **8**, 1555-1570.

McInnes, K.L., and J.A. Curry, 1995: Modelling the mean and turbulent structure of the summertime arctic cloudy boundary layer. *Bound.-Layer Meteor.*, **73**, 125-143.

Manabe, S, and R.T. Wetherald, Thermal equilibrium of the atmosphere with a given distribution of relative humidity. *J. Atmos.Sci.*, **24**, 241-259.

Maykut, G.A., 1978: Energy exchange over young sea ice in the Central Arctic. *J. Geophys. Res.*, **83**, 3646-3658.

Maykut, G.A., 1982: Large-scale heat exchange and ice production in the central Arctic. *J. Geophys. Res.*, **87**, 7971-7984.

Maykut, G.A., and N. Untersteiner, 1971: Some results from a time-dependent thermodynamic model of sea ice. *J. Geophys. Res.*, **76**,1550-1575.

Nakamura, N., and A.H. Oort, 1988: Atmospheric energy budgets of the polar regions. *J. Geophys. Res.*, **93**, 9510-9524.

Overland, J.E., and P.Turet, 1994: Variability of the atmospheric energy flux across 70 N computed from the GFDL data set. *Nansen Centennial Volume, Geophys. Monogr.*, **84**, Amer. Geophys. Union, 313-325.

Peixoto, J.P., and A.H. Oort, 1992: Physics of Climate. American Institute of Physics, 520 pp.

Petterssen, S., 1956: *Weather analysis and Forecasting, Volume 2*. McGraw-Hill, 266 pp.

Rockel, B., E. Raschke, and B.Weyers, 1991: A parameterization of broad band radiative transfer properties of water, ice, and mixed clouds. *Beitr. Phys. Atmosph.*, **64**, 1-12.

Rutledge, S.A., and P.V. Hobbs, 1983: The mesoscale and microscale structure and organization of clouds and precipitation in midlatitude cyclones. VIII: A model for the "seeder-feeder" process in warm-frontal rainbands. *J. Atmos. Sci.*, **40**, 1185-1206.

Schubert, S.D., R.B. Rood, and J. Pfaendtner, 1993: An assimilated dataset for earth science applications. *Bull. Amer. Meteor. Soc.*, **74**, 2331-2342.

Serreze, M.C., J.D. Kahl, and R.C. Schnell, 1992: Low-level inversions of the Eurasian Arctic and Comparisons with Soviet drifting station data. *J. Climate*, **5**, 615-629.

Shaw, G.E., 1995: The arctic haze phenomenon. *Bull. Amer. Meteor. Soc.*, **76**, 2403-2413.

Shine, K.P., and R.G. Crane, 1984: The sensitivity of a one-dimensional thermodynamic sea ice model to changes in cloudiness. *J. Geophys. Res.*, **89**, 10,615-10,622.

Slingo, A., 1989: A GCM parameterization for the shortwave radiative properties of water clouds. *J. Atmos. Sci.*, **46**, 1419-1427.

Smith, R.N.B., 1990: A scheme for predicting layer clouds and their water content in a general circulation model. *Quart. J. Roy. Meteor. Soc.*, **113**, 969-1009.

Smith, W.S., and C.-Y. Kao, 1996: Numerical simulation of observed arctic stratus clouds using a second-order turbulence closure model. *J. Appl. Meteor.*, **35**, 47-59.

Starr, D. O'C., and S.K. Cox, 1985: Cirrus clouds, Part II: Numerical experiments on the formation and maintenance of cirrus. *J.Atmos. Sci.*, **42**, 2682-2694.

Sundqvist, H., 1978: A parameterization scheme for non-convective condensation including prediction of cloud water content. *Quart. J. Roy. Meteor. Soc.*, **104**, 677-690.

Tao, X., J.E. Walsh and W.L. Chapman, 1996: An assessment of GCM simulations of arctic air temperature. *J. Climate*, **9**, 1060-1076.

Tsay, S.-C., and K. Jayaweera, 1984: Physical characteristics of Arctic stratus clouds. *J. Climate Appl. Meteor.*, **23**,584-596.

Untersteiner, N., 1961: On the mass and heat budget of arctic sea ice. *Arch. Meteorol. Geophys. Bioklimatol.*, **A, 12**, 4755-4766.

Vowinckel, E., and S. Orvig, 1970: The climate of the North Polar basin. In *Climates of the Polar Regions, World Survey of Climatology* (S. Orvig, Ed.), Vol. 14, Elsevier, pp. 129-252.

Walsh, J.E., X. Zhou, D. Portis, and M.E. Serreze, 1994: Atmospheric contribution to hydrological variations in the Arctic. *Atmosphere-Ocean*, **32**, 733-755.

Warren, S.G., C.J. Hahn, J. London, R.M. Chervin, and R.L. Jenne, 1988: Global distribution of total cloud cover and cloud type over the ocean. NCAR Tech. Note NCAR/TN-317+STR, 42 pp. plus 170 maps.

Zhang, T., K. Stamnes, and S.A. Bowling, 1996: Impact of clouds on surface radiative fluxes and snowmelt in the Arctic and subarctic. *J. Climate*, **9**, 2110-2123.

Appendix

Description of Variables

Chapter 2:

term	description
T	air temperature
T_i	ice temperature
h_i, h_s	ice and snow thickness
θ	potential temperature
q, q_{sat}	water vapor mixing ratio, q at saturation
ρ	air density
r,r^*	relative humidity, r of surface air
α	surface albedo
F_{rad}	radiative energy flux
U_1	windspeed at middle of lowest model level
A_i	ice concentration
T_m	oceanic mixed layer temperature (-1.9 C)
p,z,t	pressure, height, and time
C_p,C_i	heat capacity of air (1004 J kg^{-1} K^{-1}), ice (2106 J kg^{-1} K^{-1})
L_v,L_f	latent heat of vaporization (2.5 x 10^6 J kg^{-1}), fusion (0.33 x 10^6 J kg^{-1})
σ	Stefan-Boltzmann constant (5.67 x 10^{-8} W m^{-2} K^{-4})
ρ_i,ρ_s	density of ice (900 kg m^{-3}), snow (330 kg m^{-3})
k_i,k_s	conductivity of ice (2.1 W m^{-1} k^{-1}), snow (0.3 W m^{-1} k^{-1})

Chapter 3:

Term	description
θ_l	liquid water potential temp. = $\theta\left(1-\frac{Lq_l}{C_pT}\right)$
q_v	water vapor mixing ratio
q_l	cloud liquid water mixing ratio
q_w	'total' water mixing ratio = $q_v + q_l$
q_i	ice mixing ratio
q_r	precipitating liquid mixing ratio
A_l	autoconversion of q_l to q_r
C_l	collection of q_l by q_r
E_i	evaporation/deposition of q_i
E_r	evaporation of q_r
I_i	initiation of q_i from q_w
M_i	melting of q_i to q_r
L_s	latent heats of sublimation (2.83×10^6 J kg^{-1})
v, w	large-scale horizontal and vertical velocities
f_c	liquid cloud fraction
N_i	number concentration of ice particles

Vita

John A. Beesley

Born: 6 July 1966, Savona, Italy

Education: 1984, graduated from Mendham High School, Mendham, N.J.

1988, B.S. in Applied Mathematics at Columbia University, New York City